Isern, A.R., Anselmetti, F.S., Blum, P., et al., 2002
*Proceedings of the Ocean Drilling Program, Initial Reports* Volume 194

# 6. Site 1195[1]

Shipboard Scientific Party[2]

## INTRODUCTION

Site 1195 (proposed Site CS-10A) is located on the Marion Plateau, ~60 km northeast of the south central Great Barrier Reef margin, at a water depth of 420 m (Fig. **F1**). The main objective at this site was to recover a lower Miocene to Holocene sedimentary section that provides a complete chronostratigraphy of the Neogene Marion Plateau depositional succession. Site 1195 is located at the intersection of regional seismic lines MAR15 (shotpoint 3505) and MAR04 (shotpoint 3928), 70 km east of the northern carbonate platform and 60 km north of the southern platform (Figs. **F2, F3**). Drilling at this site penetrated 521.2 m of hemipelagic sediment. Unlike other Leg 194 sites that were drilled at platform or platform proximal locations, the sediments at Site 1195 record a distal shelf facies. This distal facies records the combined effects of changes in platform shedding, detrital input, and pelagic sedimentation, all of which can be linked to changes in sea level and paleoceanography.

Successfully drilling a conformable distal shelf section provides an accurate chronostratigraphic framework to date seismic reflections and seismic sequence boundaries. The ages for these horizons can be correlated with other sites in the seismic grid to refine the age constraints in environments with lower chronostratigraphic resolution. All of the Marion Plateau megasequences occur at Site 1195 in a mostly conformable succession (Fig. **F2**), indicating that sedimentation was continuous overall throughout the Neogene. This observation supports the assumption that Site 1195 sediments provide the most complete stratigraphic record of all Leg 194 sites. The depositional environment of the sediments at Site 1195, particularly in the upper part of the drilled section, is strongly controlled by currents, as indicated by drift geometries seen on seismic data (Fig. **F8,** p. 68, in the "Leg 194 Summary" chapter).

**F1.** Bathymetry map, p. 29.

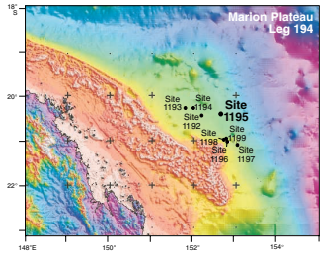


**F2.** Seismic line MAR04, p. 30.

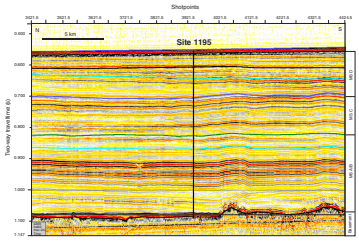


**F3.** Multichannel line MAR15, p. 31.

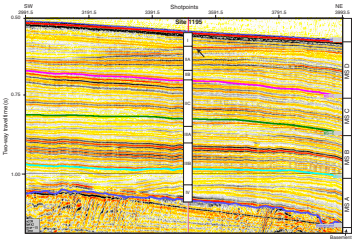


[1]Examples of how to reference the whole or part of this volume.
[2]Shipboard Scientific Party addresses.

In addition to calibrating the chronostratigraphy of the regional seismic sequences, Site 1195 will provide information on paleoceanographic changes recorded by variations in sedimentologic composition, physical properties, and geochemistry.

# OPERATIONS

Operations at Site 1195 (proposed site CS-10A) began when a beacon was dropped at 0700 hr on 26 January 2001. The corrected precision depth recorder reading indicted a water depth of 422.5 m.

## Hole 1195A

Hole 1195A was spudded with the advanced piston corer (APC) at 0905 hr on 26 January and established a water depth of 419.9 m (Table T1, p. 86, in the "Leg Summary" chapter; Tables T1, T2). When Core 9H was shot and advanced from 71.2 to 80.7 meters below seafloor (mbsf) with a full stroke and a normal pull of ~2.5 kilopounds (kips) was applied to the core barrel assembly as the driller picked up the drill string off bottom, all wireline weight was suddenly lost. The wireline was retrieved to the surface and found to have parted ~70 m above the wireline sinker bars. Attempts to fish the bottom-hole assembly with a wireline spear were unsuccessful and the drill string had to be recovered. The wireline had only nine runs on it since the last slip and cut of 150 m. A total of 620 m of wireline was removed from the aft winch as a result of the incident.

T1. Coring summary, p. 69.

T2. Expanded coring summary, p. 70.

The results of operations in Hole 1195A were 80.7 m cored with 79.27 m recovered (98.2% average recovery). The APC temperature tool was deployed at 33.2 and 71.2 mbsf. Cores were oriented starting with Core 194-1195A-4H.

## Hole 1195B

The vessel was offset 20 m east of Hole 1195A. In order to evaluate the magnetic overprint imparted by two drill bits, the standard 11 7/16 in APC/extended core barrel (XCB) bit used in Hole 1195A and a Russian-made 9.875 in APC/XCB polycrystalline diamond compact (PDC) bit, the latter was deployed in Hole 1195B. Hole 1195B was spudded with the APC at 2230 hr on 26 January. A water depth of 419.2 m was determined based on the drill string deployed and mudline recovered. Piston coring advanced to 207.9 mbsf, where 80 kips was required to retract a full-stroke core barrel. This was considered APC refusal depth. The Davis-Villinger temperature probe was deployed at 112.9 (following Core 12H) and 150.9 mbsf (following Core 194-1195B-16H). The cores were oriented starting with Core 194-1195B-3H. The average recovery for this portion of the hole was 101.1%.

XCB coring deepened the hole to a total depth of 521.2 mbsf. The XCB cored portion of the hole was 313.3 m with 189.29 m (60.4%) recovered. The total recovery for the hole was 399.5 m (76.7% of the cored interval).

Several attempts to lower the triple combination (triple combo) logging tool string out of the lower end of the pipe by gravity alone were unsuccessful. The tool string was finally pumped out of the pipe and subsequently lowered to within 2 m of the bottom of the hole without problems. For the second run, a successful check shot survey with the

well seismic tool (WST) was considered of highest priority. In order to minimize the risk to that objective, it was decided not to run the Lamont-Doherty Earth Observatory (LDEO) natural-gamma spectrometry tool in the string. The WST also had to be pumped out of the pipe, but it wouldn't descend into the hole. The drill pipe became stuck in the process, and the WST was recovered to allow the drill string to be worked. After the drill sting was freed, a partial wiper trip was run to 230 mbsf to clear the obstructions in the hole. During the wiper trip, the drill string became stuck again and was only freed with overpull as high as 210 kips. As the driller pulled back the bit to the initial logging depth, the pipe became stuck again in the sand-rich formation. The bit was then set at 79 mbsf and the WST was run back in the hole, but it could not be lowered below 121 mbsf. Three levels were shot at 118, 95, and 86 mbsf using the air gun. No further downhole logging was attempted.

The drill string and beacon were recovered and the vessel began the short transit to Site 1196 by 2100 hr on 29 January.

# LITHOSTRATIGRAPHY AND SEDIMENTOLOGY

Site 1195 penetrated a 521-m-thick lower Miocene to Pleistocene succession, overlying Eocene or lower Miocene carbonate buildup. The upper 130 m of sediments is unconsolidated, whereas the lower intervals are poorly to moderately lithified. The lithostratigraphy of Site 1195 comprises five units (Table **T3;** Fig. **F4**). Subdivisions are based upon sedimentary texture, glauconite content, color variations, noncarbonate constituents, and biotic associations. The sediments above the basal carbonates at Site 1195 consist of quartz-sandstone and grainstone with glauconite, representing a proximal periplatform environment (Unit IV), clay-rich carbonates deposited in a distal periplatform paleoenvironment (Unit III), and carbonates indicative of a hemipelagic environment (Units II and I).

## Lithologic Units

### Unit I (0.0–34.5 mbsf; Pleistocene–Late Pliocene)

Unit I consists of a 36.9-m-thick succession of skeletal packstone and grainstone (Fig. **F4**). It differs from underlying units by its high content of bioclasts and low content of carbonate mud. The sediment is usually well sorted, fine- to medium-grained, and pale yellow in color. Several 10- to 40-cm-thick layers of coarse and poorly sorted skeletal-rich floatstone or grainstone are present. Some of the layers show a sharp basal contact with the underlying finer-grained sediment. Fining-upward trends are observed in these layers. Skeletal components are dominantly planktonic foraminifers. Other bioclasts mostly appear within coarser layers and include benthic foraminifers, bivalves, gastropods, scaphopods, echinoids, arthropods, and rare bryozoans and solitary corals.

The contact with Unit II was positioned at the basal surface of the lowermost coarse layer, which is a skeletal floatstone at 34.5 mbsf (Fig. **F5**). This layer contains abundant light brown–stained phosphatized foraminifers and up to 5-mm-sized partly phosphatized lithoclasts.

**T3.** Lithologic units, p. 78.

**F4.** Lithologic summary, p. 32.

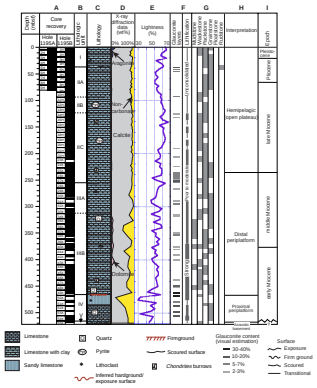

**F5.** Close-up photograph of a coarse and poorly sorted skeletal-rich floatstone, p. 33.

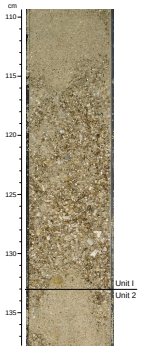

## Unit II (36.9–255.9 mbsf; Pliocene–Late Middle Miocene)

Unit II consists of a 219-m-thick interval of skeletal wackestone and packstone (Fig. F4). It differs from Unit I in its reduced biotic diversity (dominantly planktonic foraminifers) and darker color (light greenish olive-gray). Unit II is topped by a 10-m-thick interval composed of medium sand-sized skeletal grainstone with glauconite. Glauconite is rare and mostly present within foraminifer chambers. Two 30-cm-thick layers at 36 mbsf and 38.3 mbsf have glauconite contents between 10% and 20% (Fig. F6). Unit II is divided into three subunits based on the occurrence of glauconite-rich intervals, textural variations, and pyrite content.

F6. Close-up photograph showing a glauconite-rich layer from Subunit IIA, p. 34.

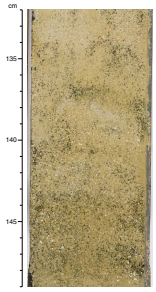

## Subunit IIA (36.9–93.9 mbsf; Pliocene–Latest Miocene)

Subunit IIA consists of 57 m of very fine sand to fine sand–sized, poorly bioturbated foraminifer packstone and grainstone with clay. This subunit is defined by the absence of pyrite and textural alternations, which are abundant in Subunits IIB and IIC. Near the bottom of Subunit IIA at 90.4 mbsf, a 1.7-m-thick glauconite-rich layer occurs. The 20-cm-thick interval at its base has a glauconite content of ~10%.

## Subunit IIB (93.9–123.9 mbsf; Latest Miocene)

Subunit IIB is a 30-m-thick silt-sized to very fine sand–sized skeletal packstone. It is characterized by a finer grain size than Subunit IIA and by common burrows that are stained black from finely disseminated pyrite. The boundary between Subunits IIA and IIB coincides with the first downcore appearance of silt-sized wackestone with a higher clay content, which is overlain by a fine sand–sized skeletal grainstone. This boundary occurs between Cores 194-1195B-10H and 11H and coincides with a marked downcore decrease of magnetic susceptibility values (see "Core Physical Properties," p. 16).

## Subunit IIC (123.9–255.9 mbsf; Late Miocene–Latest Middle Miocene)

In the upper part of Subunit IIC, the lithologies mainly consist of alternations between silt- and very fine sand–sized wackestone and very fine to fine sand–sized packstone. In the lower part, alternations of silt- to fine sand–sized packstone and fine to medium sand–sized grainstone occur. The grainstone layers frequently show a fining-upward trend. Scoured surfaces were observed at the bottom of some coarser layers (Fig. F7). Alternations of lithologies with different grain sizes occur every 0.2 to 1.5 m. The silt- to very fine sand–sized fraction is dominated by broken planktonic foraminifers. Compared to Subunit IIB, this subunit has a higher content of carbonate mud, a higher variability in grain size, and common *Chondrites*. Glauconite preferentially occurs in coarse layers within the uppermost 3 m and the lowermost 20 m of Subunit IIC.

F7. Close-up photograph showing a scoured surface from Subunit IIC, p. 35.

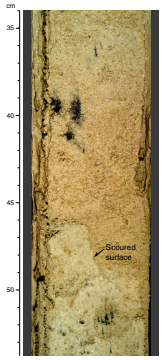


## Unit III (255.9–463.3 mbsf; Middle–Early Miocene)

Unit III, a 211.4-m-thick interval of skeletal mudstone to grainstone, differs from Unit II mainly in its higher benthic foraminifer content, lower planktonic foraminifer content, and finer grain size. An overall downhole decrease in color reflectance occurs at the transition between

Unit II and Unit III, with the latter showing common dark olive-gray to greenish gray colors (Fig. F4) reflecting a higher noncarbonate fraction (mostly clay). This conclusion is supported by X-ray diffraction (XRD) data (see "Geochemistry," p. 12). Unit III is divided into two subunits based on clay and quartz content.

### Subunit IIIA (255.9–313.5 mbsf; Middle Miocene)

Subunit IIIA consists of 57.6 m of silt- to fine sand–sized wackestone to grainstone with glauconite occurring below 275 mbsf. Skeletal grains, particularly planktonic foraminifers, are mostly recrystallized. Benthic foraminifers are common. Alternations between wackestone and packstone occur but at a lower frequency than in Subunit IIC.

### Subunit IIIB (313.5–463.3 mbsf; Early Middle–Early Miocene)

Subunit IIIB, a 153.8-m-thick interval of skeletal mudstone to grainstone, differs from Subunit IIIA in having a higher content of noncarbonate components and a higher content of total organic carbon (see "Geochemistry," p. 12). Within the 20-m-thick upper part of Subunit IIIB, quartz grains are common, coinciding with a noticeable peak in noncarbonate content (up to 50%) estimated from XRD measurements (Fig. F4). Downcore, alternations between mudstone, silt- to very fine sand–sized wackestone and very fine to fine sand–sized packstone occur. Toward the base of the subunit, alternations between silt- to very fine sand–sized packstone and fine to medium sand–sized grainstone are observed, similar in those of Subunit IIC. Mudstone and wackestone layers are always darker than packstone layers and show well-preserved *Chondrites* burrows (Fig. F8). As with Subunit IIC, a scoured surface overlies some of the finer layers. All layers are bioturbated. The lowermost 15 m of Subunit IIIB consists mainly of light gray grainstone with rare quartz grains. The color reflectance curve indicates a sharp decrease in lightness between this grainstone and a greenish gray wackestone with high glauconite content and quartz grains representing the top of Unit IV.

### Unit IV (463.3–517.5 mbsf; Early Miocene)

Unit IV consists of greenish gray, well-sorted, fine to medium sand–sized grainstone and quartz siltstone to sandstone (Figs. F4, F9, F10). Subordinate wackestone and packstone texture is also observed. Rounded glauconite and angular quartz grains are abundant. Pebble-sized sandstone and carbonate lithoclasts, as well as silt-sized foraminifer fragments are also present. Well-preserved *Chondrites* burrows are common (Fig. F9).

### Unit V (517.5–517.7 mbsf; Eocene)

Unit V, the lowermost 20-cm core recovered at Site 1195, consists of a light yellowish brown skeletal grainstone with abundant nummulitids, mollusk fragments, coralline algae, and lithoclasts (Fig. F4). This dense limestone is capped along an irregular sharp surface by a centimeter-thick dark skeletal grainstone of Miocene age with lepidocyclinids (see "Biostratigraphy and Paleoenvironments," p. 6).

F8. Close-up photograph showing alternation of skeletal packstone and mudstone, p. 36.

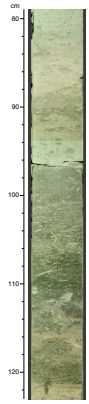

F9. Close-up photograph showing greenish gray sand with glauconite, p. 37.

F10. Photomicrograph of a siltstone to sandstone with pitted quartz, p. 38.

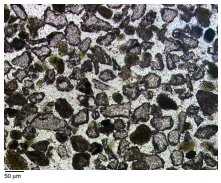

### Discussion

Because Unit V is only 20 cm thick and heavily disturbed from drilling, an uncertainty remains about its origin. It could be the top of an Eocene platform, as bioclastic components and texture suggest a high-energy shelf. Alternatively, this nummulitid grainstone could also be a component of an early Miocene breccia.

Most sediment grains from Unit IV are reworked and generally well sorted. Rare *Chondrites* burrows, presence of planktonic foraminifers and calcareous nannofossils, and silt-sized reworked neritic foraminifers mixed with coarser sediment suggest a proximal periplatform setting (see "**Biostratigraphy and Paleoenvironments,**" p. 6). Episodic periods of high terrigenous input are indicated by the occurrence of angular quartz sand. In addition, the well-sorted silt-sized to very fine sand–sized detrital material indicates significant sediment transport by bottom currents.

Unit III, with its higher content of planktonic foraminifers, represents a distal periplatform setting subject to the input of fine neritic carbonate components, especially benthic foraminifers. The higher abundance of coarse terrigenous layers in Subunit IIIB indicates a more proximal environment with respect to the platform, whereas Subunit IIIA with fewer benthic and more planktonic foraminifers, was deposited in a more distal setting.

Overall deepening continues upsection. As shown by its higher content of planktonic foraminifers and its low content of benthic foraminifers, Unit II reflects a deeper setting than Unit III. Larger benthic foraminifers (see **"Biostratigraphy and Paleoenvironments,"** p. 6) from Subunit IIC and the lower part of Subunit IIB record neritic input and were deposited in a periplatform setting. Above that interval, evidence of neritic input is minor, and a hemipelagic setting is indicated for the remainder of Unit II (see **"Biostratigraphy and Paleoenvironments,"** p. 6). Textural evidence indicates an overall upsection decrease in energy through Subunits IIC and IIB, which could reflect further deepening. Within Subunit IIA, textures show a reverse trend with less mud and coarser material, which could indicate the onset of strong bottom currents during the Pliocene. The dominance of planktonic foraminifers and grainstone texture suggest that the sediments of Unit I were deposited by strong bottom currents in a high-energy hemipelagic setting.

## BIOSTRATIGRAPHY AND PALEOENVIRONMENTS

Nannofossils and foraminifers (planktonic and benthic) were examined from core catcher samples at Site 1195 for age assignments (Table **T4**) and paleoenvironmental interpretation (Table **T5**). In addition, a number of samples from within selected cores were also studied. Core catcher samples from Hole 1195A generally contained well-preserved calcareous microfossils ranging in age from late Pleistocene to late Miocene. Hole 1195B (cored to a depth of 521.2 mbsf) contained a mixture of poorly to well-preserved calcareous microfossils ranging in age from late Pleistocene to early Miocene.

**T4.** Biostratigraphic datums, p. 79.

**T5.** Summary of paleoenvironmental interpretations, p. 80.

### Calcareous Nannofossils

Calcareous nannofossils are generally abundant for the entire sequence recovered at Site 1195. Preservation of nannofossils is good in

the upper 10 cores and gradually deteriorates downhole. A succession of Neogene nannofossil datums (Table T4) was recognized throughout the sediment sequence, providing the best biostratigraphic resolution among the sites cored during Leg 194. The biostratigraphy also shows that, unlike other sites, the sequence cored at Site 1195 is virtually complete, with no apparent hiatuses. Detailed shore-based studies of samples from Site 1195 have the potential for recognizing most of the global Neogene nannofossil datums and providing a valuable reference section and possibly detailed biomagnetostratigraphic calibration for the tropics.

## Hole 1195A

The first core catcher sample (Sample 1H-CC) contains abundant *Gephyrocapsa,* which includes *Gephyrocapsa oceanica* and various small species of the same genus. *Emiliania huxleyi* and *Pseudoemiliania lacunosa* were absent. This suggests that the sample has an age of 0.26–0.46 Ma. Sample 194-1195A-2H-CC contains *P. lacunosa* but no *Calcidiscus macintyrei* and can be assigned an age of 0.46–1.7 Ma. *C. macintyrei* was first encountered in Sample 194-1195A-3H-CC. This sample does not contain discoasters or any large *Gephyrocapsa* and was dated as 1.7–2.0 Ma.

Two late Pliocene datums (last occurrences [LOs] of *Discoaster brouweri* = 2.0 Ma and *Discoaster pentaradiatus* = 2.5 Ma) are located between Samples 194-1195A-3H-CC and 4H-CC. The apparent hiatus is most likely an artifact resulting from the large sample spacing (9.5 m). Similarly, both the LOs of *Discoaster surculus* (2.6 Ma) and *Discoaster tamalis* (2.8 Ma) are located between Samples 194-1195A-4H-CC and 5H-CC. Smaller sample spacing may show the sequential occurrences of the two datums, eliminating the appearance of a hiatus within this interval.

The late Pliocene/early Pliocene boundary, generally approximated by the LO of *Reticulofenestra pseudoumbilica,* is located between Samples 194-1195A-5H-CC and 6H-CC. Both *R. pseudoumbilica* and *Sphenolithus abies* are common in the latter sample.

The Miocene/Pliocene boundary, as approximated by the LO of *Discoaster quinqueramus,* is placed between Samples 194-1195A-8H-CC and 9H-CC, based on the presence of the index species in the latter sample. *D. surculus* is also present in the latter sample, constraining the sample to an age of 5.6–7.5 Ma.

## Hole 1195B

Nannofossil biostratigraphy for the upper nine cores from Hole 1195B is similar to Hole 1195A. Minor differences observed can be attributed to (1) depth offsets of the cores from the two holes and (2) large sample spacing (9.5 m).

A series of nannofossil datums below Core 194-1195B-9H (Table T4) provides a relatively large number of age-control points for the rest of the sequence. Significant hiatuses are not apparent. More remarkable is that all the Miocene nannofossil datums fall near a straight line when plotted against depth (see "Age Model," p. 12, for age vs. depth and sedimentation rate plots), further indicating the general stratigraphic completeness of the Miocene interval.

A sample from interval 194-1195B-55X-CC, taken 0.5 cm above the sharp boundary between Units IV and V within the semilithified glauconitic packstone, yielded a few specimens of *Cyclicargolithus floridanus* and small *Reticulofenestra* and a specimen that resembles *Sphenolithus*

*belemnos* or *Sphenolithus disbelemnos* (a clear identification to either species was not possible because a detrital grain partially blocked the specimen). Either species can constrain the age of the sample to the early Miocene. In the absence of either species, the assemblage can be described as similar to an impoverished middle to lower Miocene assemblage. Another possibly displaced, semilithified sediment sample was taken from the very bottom of the core catcher in Section 194-1195B-55X-CC beneath a piece of limestone defining Unit V, although there is uncertainty as to whether the semilithified sediment was in situ. That sample yielded rare specimens of *C. floridanus* and small *Reticulofenestra,* an assemblage that most resembles an impoverished middle to lower Miocene assemblage.

## Planktonic Foraminifers

Hole 1195A penetrated through Pliocene sediment to a sufficient depth to reach the Pliocene/Miocene boundary. This interval was repeated in Hole 1195B with a complete sequence of lower Miocene to Pleistocene sediments. The shipboard planktonic foraminifer biostratigraphy is largely founded on Hole 1195B. Planktonic foraminifer abundance and preservation are good downcore to Sample 194-1195B-37X-CC, at which point biostratigraphic resolution becomes less certain as preservation deteriorates.

### Hole 1195A

Sample 194-1195A-1H-CC contains *Globorotalia truncatulinoides* and *Pulleniatina finalis,* which places the sample in the middle of Zone N22 and younger. *Globorotalia tosaensis* was absent; thus, the sample must represent an age younger than its LO datum at the base of Pt 1b. Sample 194-1195A-4H-CC contains *Globigerinoides fistulosus, Globigerinoides extremus,* and *G. tosaensis*. *Globorotalia miocenica* is absent, and *G. truncatulinoides* is present; however, there is a marked decline in species number from Samples 194-1195A-3H-CC to 4H-CC. This may indicate some downhole contamination in Sample 194-1195A-4H-CC rather than it being placed within the datum range of *G. truncatulinoides*. In summary, Sample 194-1195A-4H-CC most likely represents the interval between the first occurrence (FO) of *G. truncatulinoides* and the LO of *G. miocenica* (i.e., a zonal assignment at the N21/N22 boundary); thus, the Pleistocene/Pliocene boundary occurs between Samples 194-1195A-3H-CC and 4H-CC.

Samples 194-1195A-6H-CC through 8H-CC contain *Sphaeroidinella dehiscens, Globigerina nepenthes, Globorotalia margaritae, Globorotalia cibaoensis,* and *Dentoglobigerina altispira,* which places these samples in Zones N20 and N19. Sample 194-1195A-9H-CC was assigned to Zone N18 based on the absence of *S. dehiscens* and the continued presence of *Globorotalia tumida*. The Pliocene/Miocene boundary, therefore, lies between these two core catcher samples.

### Hole 1195B

Samples 194-1195B-1H-CC and 2H-CC contain *G. truncatulinoides, G. tosaensis,* and *P. finalis,* confining the samples to Pt 1a. *G. extremus* is absent in Sample 194-1195B-2H-CC and present in Sample 3H-CC, which places the Pleistocene/Pliocene boundary between these samples. The continued presence of *G. fistulosus* in Sample 194-1195B-4H-CC places this sample in Zone N21. Sample 194-1195B-9H-CC was placed within

the lower part of Zone N19 based on the occurrence of *G. nepenthes* and *S. dehiscens,* even though specimens of *G. tumida* were present. Sample 194-1195B-10H-CC contains *G. cibaoensis* but no *S. dehiscens* or *G. tumida* and represents, therefore, the uppermost Zone N17. Therefore, the base of Zone N18, which approximates the Pliocene/Miocene boundary, must occur within Sample 194-1195B-9H-CC or 10H-CC.

Samples 194-1195B-10H-CC through 25X-CC were assigned to the extensive Zones N17 and N16 that comprise the late Miocene. These zones can be largely assigned using a combination of the occurrences of *Globorotalia plesiotumida* (FO datum lies in the middle of Zone N16) and *Neogloboquadrina acostaensis* (FO marks the base of Zone N16). Sample 194-1195B-26X-CC is assigned to Zones N14–N15 based on the presence of the *Globorotalia siakensis-mayeri* lineage. The late/middle Miocene boundary bisects Zone N15 and thus probably lies within Core 194-1195B-26X. The LO datum of *Globorotalia peripheroacuta* occurs between Samples 194-1195B-28X-CC and 29X-CC, thus marking a possible Zone N12/N11 boundary. Although this lineage would be used to define the late middle Miocene, this group is rare in abundance, and in many cases, surface denudation precludes accurate identification. The *Orbulina* taxa share a common FO datum marking the Zone N8/N9 boundary, which can be placed between Samples 194-1195B-35X-CC and 36X-CC. *Globigerinoides sicana, Praeorbulina curva,* and *Praeorbulina transitoria* occurrences were also used to assign a number of samples, such as 194-1195B-35X-CC through 40X-CC, to Zones N8–N9. The exact position of the early/middle Miocene boundary at the base of Zone N8 could not be defined.

Planktonic foraminifers identified in Samples 194-1195B-43X-CC through 57X-CC were not diagnostic for establishing an early Miocene biostratigraphic framework. As with previous sites during Leg 194, abundances were very low and test alteration levels were high. Within these samples, index species (*G. sicana, Catapsydrax dissimilis,* and *Globorotalia birnageae*) were either tentatively identified, or more commonly, samples would contain nonindex species of extended ranges (e.g., *Globoquadrina dehiscens, Globoquadrina venezuelana,* and *Globorotalia bella*). *Globigerina ciperoensis* was also cautiously identified at the base of the hole in Sample 194-1195B-57X-CC. This may indicate a sample age (in the upper portion of its range Zones P20–N5) of Zones N4–N5. This datum is not included in the age vs. depth plot (see **"Age Model,"** p. 12) because the identification is not certain.

## Benthic Foraminifers

Microscopic analysis of biogenic constituents, particularly the diverse and often abundant benthic foraminifers, provide data for paleoenvironmental interpretation of the sediment sequence at Site 1195 (Table **T5**).

### Hole 1195A

The sand-sized fraction of Samples 194-1195A-1H-CC (4.70 mbsf) through 9X-CC (80.9 mbsf) are overwhelmingly dominated by planktonic foraminifers (Table **T5**). Benthic foraminifers are rare to common and often include conspicuous *Cibicidoides,* nodosarids, and agglutinated specimens, indicating a bathyal depositional environment. Fifty percent or fewer of the grains were brown in color. The relative proportions of coarser and finer planktonic fractions varies among samples, possibly indicating changes in current winnowing. These samples rep-

resent lithologic Unit I and Subunit IIA (see "Lithostratigraphy and Sedimentology," p. 3) and indicate a hemipelagic, current-influenced environment.

### Hole 1195B

Samples 194-1195B-1H-CC (8.4 mbsf) through 10H-CC (94.1 mbsf) represent lithologic Unit I and Subunit IIA (see "Lithostratigraphy and Sedimentology," p. 3) and are very similar to those described for this interval in Hole 1195A (Table T5). Samples 194-1195B-11R-CC (103.5 mbsf) and 21H-CC (198.9 mbsf) (lithologic Subunits IIB and IIC) are also overwhelmingly dominated by planktonic foraminifers but differ somewhat in that brown and black grains are generally rare to occasionally common but never as abundant as higher in the section. Benthic foraminifers indicate that all of these samples represent hemipelagic sediments deposited at upper bathyal water depths.

In Samples 194-1195B-22H-CC (207.4 mbsf) through 47X-CC (446.2 mbsf), planktonic foraminifers continue to be abundant in the coarse sand fractions but neritic debris becomes increasingly important, particularly very fine bioclastic material with minor quartz and occasionally slightly larger reworked bioclasts that include small specimens of larger benthic foraminifers. Glauconite grains and infill are rare to common in most samples. Based on these neritic components, a distal periplatform depositional environment at outer neritic depths is interpreted.

Beginning in Sample 194-1195B-48X-CC (458.0 mbsf), glauconite, quartz, and neritic debris substantially increase downcore. In Sample 194-1195B-49X-CC (463.5 mbsf), glauconite, quartz, and blackened grains predominate and remain important through Sample 194-1195B-54X-CC (513.1 mbsf). These samples, which are part of lithologic Unit IV (see "Lithostratigraphy and Sedimentology," p. 3), are interpreted as representing a proximal periplatform depositional environment in outer neritic water depths. Sample 194-1195B-55X-CC (517.7 mbsf) contains a gold-colored limestone, which contains abundant larger benthic foraminifers. These foraminifers are tentatively identified as nummulitids, discocyclinids, and *Heterostegina* spp., which may be late Eocene in age. This gold-colored limestone has a lithified contact with a black grainstone that contains abundant *Lepidocyclina,* which, along with nannofossils in the surrounding sediment, indicate lower Miocene deposition. Confirmation of the age and depositional environment of the gold limestone will require detailed thin section analysis.

## PALEOMAGNETISM

Paleomagnetic analyses were performed on the archive sections of cores recovered at Site 1195 using the three-axis pass-through cryogenic magnetometer. The core sections were first measured for natural remanent magnetization (NRM), and then were subjected to 5-mT and 30-mT field demagnetizations in the alternating-field coils of the cryogenic magnetometer to measure their successive magnetization. The maximum destructive field used was 30 mT.

In order to reduce the magnetic overprint from drilling, the APC cores from Hole 1195B were collected with a nonmagnetic Russian-made PDC bit, whereas a standard C3RBI bit was used for Hole 1195A. Comparing the APC records from Hole 1195A and 1195B (Figs. F11, F12A), we can see the downward overprinting effect of the drill bits on

F11. Long-core measurements from Hole 1195A, p. 39.

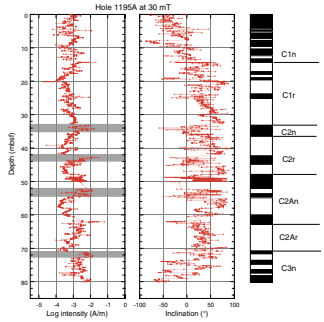


F12. Long-core measurements from Hole 1195B, p. 40.

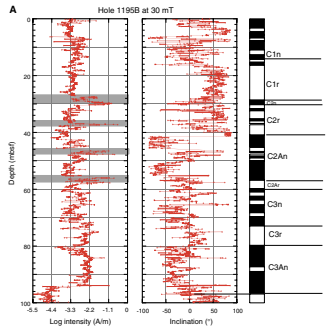

the paleomagnetic record. As seen at the previous sites, magnetostratigraphic data in Hole 1195A are all shifted toward positive inclinations, an indication of the downward overprint of the drilling process (Fig. F11). This effect can result in misinterpreting a normal polarity event to be a reversed one. Results from Hole 1195B (Fig. F12A) have no downward magnetization overprint, and most of the values are only slightly offset toward the negative side of the axis. Surprisingly, some of the normal polarity intervals seem to be unresolved, possibly because of an uncleaned modern-day magnetic field overprint, which, in fact, should not affect the reversal record at Site 1195.

## Results

### Natural Remanent Magnetization

The NRM intensity generally varies between $10^{-3}$ and $10^{-2}$ A/m with an average intensity of $10^{-2.5}$ A/m for the top 100 mbsf (Figs. F11, F12). Average intensity decreases to $10^{-3.5}$ A/m between 100 and 400 mbsf and slightly increases to a mean value of $10^{-3}$ A/m below 400 mbsf. These intensity variations appear to be a function of the quantity of magnetic mineral input rather than core-top anomalies, as observed in the previous sites. When all of the core sections are demagnetized to 30 mT, which is the minimum considered necessary to remove the effects of viscous remanent magnetization (VRM), the intensity drops approximately one order of magnitude throughout the section. The low intensity levels suggest the dominance of diamagnetic and paramagnetic minerals, whereas high-intensity levels indicate the presence of strongly magnetic materials. We have identified ten levels of high intensity; four are found within the first 80 mbsf and occur in Holes 1195A and 1195B (Figs. F11, F12). The equivalent depths of these high intensity zones in Hole 1195B are systematically 6 m shallower than in Hole 1195A. Most high-intensity levels appear to correlate well with glauconite-rich layers (see "Lithostratigraphy and Sedimentology," p. 3). Comparison of results with sedimentological descriptions indicate that other minor intensity increases are also linked with glauconite occurrences. Glauconite is a family of sheet silicate (mica) minerals resembling muscovite with high proportions of paramagnetic ions such as $Fe^{3+}$ and $Fe^{2+}$ in its two structural sites. Whether the glauconite is authigenic or transported, it suggests higher concentration of magnetic minerals like magnetite and hematite. However, other sections further downcore do not show a one-to-one relation between glauconite occurrence and magnetic susceptibility (see "Core Physical Properties," p. 16, and "Downhole Measurements," p. 21).

### Magnetostratigraphy

Although there are indications of VRM, the magnetization measured at 30 mT represents predominantly the primary NRM. Results for the top 100 mbsf (late Miocene to Pleistocene) in Holes 1195A and 1195B (Figs. F11, F12A) record a sequence of magnetic polarity reversals. The correlation of the observed pattern of normal and reversed polarity interval with the geomagnetic polarity timescale (GPTS) was assigned based on the preliminary age estimates from calcareous nannofossils. In this correlation, the prominent polarity intervals are easily matched, but some short polarity intervals are masked and cannot be unambiguously identified. Some of the observed magnetostratigraphic intervals

show a shorter duration than expected, indicating temporarily reduced or interrupted sedimentation. These intervals are sometimes found to coincide with the location of anomalous intensity increases, lending support to the presence of a hiatus. Between 100 and 200 mbsf (Fig. F12B), the prominent late Miocene chrons have been identified. Between 200 and 300 mbsf (Fig. F12C), low recovery hindered correlation with the GPTS. Despite this difficulty, the prominent Chrons C5n, C5r, C5An, and C5Ar have been assigned to the observed polarity intervals. Below 300 mbsf (Fig. F12D, F12E), in the lower Miocene section, coring gaps preclude magnetostratigraphic interpretation. Nevertheless, an attempt was made to identify some magnetic polarity zones (Fig. F12E) based on the distinctive C6n Chron (Table T6). The five short normal intervals observed between 500 and 530 mbsf are tentatively assigned to the C6Ar, C6Aan, and C6Aar (early Miocene) (Fig. F12F). The overall magnetostratigraphic interpretation is shown in Figure F13. The resulting age-depth curve is plotted in Figure F14 (see "Age Model," below).

T6. Magnetic polarity transitions, p. 82.

F13. Comparison of the observed magnetic stratigraphy with the geomagnetic polarity timescale, p. 46.

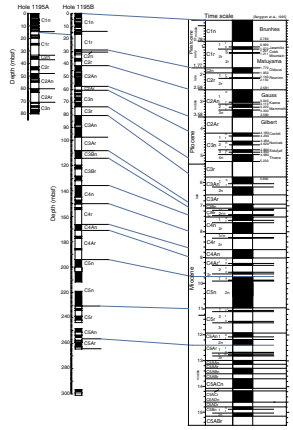

F14. Age-depth model and sedimentation rates, p. 47.

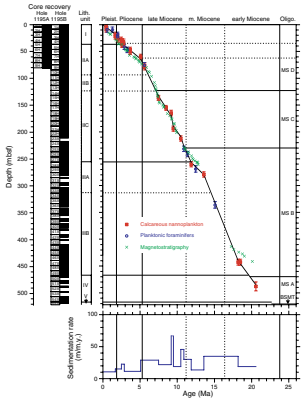

## AGE MODEL

Site 1195 was selected to provide a chronostratigraphy for Leg 194 that was more complete than one that could be obtained at locations proximal to carbonate shedding. The Site 1195 chronostratigraphy will be used to refine the chronostratigraphy from other Leg 194 sites through the correlation of seismic sequences through the regional seismic grid. A total of 27 calcareous nannofossil datums and 11 planktonic foraminifer datums were established for the 521-m-thick sequence of early Miocene to Pleistocene age drilled at Site 1195 (Fig. F14; Table T7) (see "Biostratigraphy and Paleoenvironments," p. 6). The magnetostratigraphy obtained at this site is in agreement with the biostratigraphic datums for the middle Miocene and early late Miocene intervals (see "Paleomagnetism," p. 10). However, the late Miocene to Pleistocene magnetostratigraphy suggests ages of up to 1 m.y. younger than the biostratigraphy (Fig. F14). The age model is constructed based on the biostratigraphic control points.

Given the larger benthic foraminifer assemblage, a piece of limestone in Unit V (518 mbsf), presumed to represent the top of the acoustic basement, may be late Eocene in age. However, the sample is surrounded with sediment containing nannofossils of early Miocene age, and the exact age of this horizon remains uncertain.

Miocene interval sedimentation rates vary between 13 and 67 m/m.y. (average 31 m/m.y.); Pliocene–Pleistocene rates vary between 10 and 23 m/m.y. (average 15 m/m.y.) (Fig. F14). No hiatuses were observed at the resolution of shipboard sampling.

Age picks for lithologic and seismic unit boundaries are summarized in Table T8.

T7. Age-depth control points, p. 84.

T8. Age picks, p. 85.

## GEOCHEMISTRY

### Volatile Hydrocarbons

Concentrations of volatile hydrocarbon gases were measured from every core using the standard ODP headspace sampling technique and gas chromatographic analysis. Methane only occurred in very minor concentrations (1.8–10 ppmv) (Table T9).

T9. Headspace gas composition, p. 86.

The low gas content at Site 1195 is likely a function of appreciable pore water $SO_4^{2-}$ concentrations, which limit methanogenesis, and the lack of mature organic matter to provide a thermogenic component to the gas fraction.

## Interstitial Water Chemistry

A total of 49 pore water samples were recovered from Site 1195 sediments. Samples were taken approximately every 10 m from 9.1 to 517 mbsf. Analyses from Holes 1195A and 1195B are discussed together (Fig. **F15;** Table **T10**).

Pore water chloride concentration increases slightly downhole from a value of ~563 mM in the upper few tens of mbsf to ~569 mM at 360 mbsf (Fig. **F15A**). The data show considerable scatter about this trend. From 360 mbsf to the bottom of the hole at 517 mbsf, the chloride concentration varies between 571 and 564 mM, with no clear trend in the data.

Pore water alkalinity shows little variation in the upper 80–90 mbsf, remaining near 2 mM (Fig. **F15B**). Over the interval from 80 to 362 mbsf, alkalinity increases steadily to a maximum of 4.62 mM at 362 mbsf. Below that depth, the alkalinity decreases almost linearly to a minimum of 0.65 mM at the bottom of the cored section.

Pore water sulfate concentration shows little change in the upper 100 mbsf, remaining near the seawater value of ~29 mM (Fig. **F15C**). The concentration decreases by only 1–2 mM to a depth of 175 mbsf, then continues to decrease more rapidly downhole. By the bottom of the cored interval in Hole 1195B, sulfate has decreased to ~13 mM. The change in slope of the sulfate profile at 175 mbsf marks the initiation of sulfate reduction. The first visible evidence of diagenetic iron sulfides are also found at approximately this depth (see **"Lithostratigraphy and Sedimentology,"** p. 3).

As observed at other sites, ammonium values at Site 1195 show a negative correlation to sulfate values as a response to organic carbon remineralization through sulfate reduction (Fig. **F15D**). The ammonium concentration remains almost constant, varying between 62 and 77 µM, from 9.1 to 77.5 mbsf. Below 77.5 mbsf, the ammonium concentration rises linearly to just over 800 µM at 350 mbsf. From 350 mbsf to the bottom of the cored interval, the ammonium concentration is fairly constant.

Magnesium and calcium concentrations are also relatively constant in the upper 70–80 mbsf (Fig. **F15E, F15F**); thereafter, they have opposing downhole trends. Magnesium decreases to 23.5 mM and calcium increases to 36.5 mM near the bottom of Hole 1195B. The two constituents are highly correlated (Fig. **F16**), with $r^2 = 0.95$. It is not certain whether the linear correspondence between magnesium and calcium results from a 1:1 exchange during low-temperature alteration of basaltic basement rocks that underlie the cored interval or from authigenic dolomite formation. The low alkalinity in Site 1195 pore waters supports the latter mechanism (Fig **F15B**).

Pore water strontium concentration increases significantly above seawater values in the upper few tens of mbsf, reaching a local maximum of 209 µM at 29.6 mbsf (Fig. **F15G**). The concentration then decreases to 127 µM at 67.6 mbsf. Thereafter, pore water strontium increases steadily to a concentration of 962 µM at 442.97 mbsf. The value remains near 900 µM to the bottom of the cored interval. The increase

**F15.** Interstitial water chemistry, p. 48.

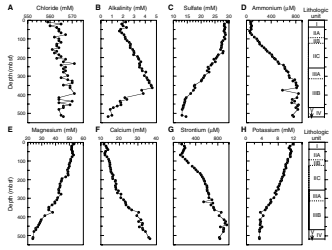


**T10.** Interstitial water chemistry, p. 87.

**F16.** Dissolved magnesium vs. calcium, p. 49.

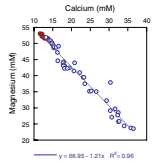

suggests fairly constant calcite recrystallization throughout the sedimentary interval.

Potassium concentration is also relatively constant in the upper 80 mbsf, around 11 mM (Fig. F15H). Over the interval from 80 to 360 mbsf, potassium values decrease to ~3.5 mM and remain close to that value to the bottom of the hole.

Perhaps the most interesting feature of Site 1195 pore fluid chemistry is the nearly constant concentration of all constituents in the upper ~80 mbsf. The unchanging concentrations imply either a lack of chemical reaction or a constant renewal of the pore fluids with seawater. The former explanation seems unlikely in light of the fact that there is little difference in lithology between the sediments of the upper 80 m and the underlying units. The latter explanation, however, requires some mechanism by which pore fluid in an 80-m-thick sequence of sediments can be exchanged with overlying seawater. One possibility is that the strong bottom currents that characterize the Marion Plateau might be able to entrain water from within the sediments or cause pressure differences, hydraulic head in effect, from one area to another.

## X-Ray Diffraction Carbonate Mineralogy

Ninety-three sediment samples were analyzed for carbonate mineralogy from Site 1195 (Fig. F17; Table T11). In the upper 30 mbsf, lithologic Unit I contains ~10% aragonite. Below 30 mbsf, aragonite is absent. Through the base of lithologic Subunit IIIA at 310 mbsf, the sediments are composed almost entirely of calcite, with a few samples at 80–90 and 200–230 mbsf containing 3–5 wt% dolomite. Traces of dolomite were found in many samples, however. In the upper 90 m of lithologic Subunit IIIB, dolomite content increases to ~10%. In the lower 50 m of lithologic Subunit IIIB and in Unit IV, only calcite is present.

## Sedimentary Geochemistry

### Results

$CaCO_3$ content at Site 1195 ranges from ~18 to 95 wt% and generally covaries inversely with total organic carbon (TOC) content, which ranges from 0.01 to 0.51 wt%. Note that TOC values from Rock-Eval pyrolysis and CNS analyses provide somewhat similar downsection profiles although values differ greatly (Fig. F18; Tables T11, T12). The peak in CNS-determined TOC content at ~145 mbsf is anomalous, and the reason has not yet been determined.

Hydrogen index (HI) values at Site 1195 range from 60 to 500 mg HC/g TOC (Fig. F18; Table T13), but the low TOC values of some intervals limit the reliability of these results. We performed duplicate and triplicate analyses on these samples, and the results were within 10% of the mean value. Oxygen index (OI) values vary from 0 to 52,980 mg $CO_2$/g TOC (Table T13). In general, high OI values are attributed to the thermal degradation of carbonate minerals during pyrolysis and are not considered in this interpretation. $T_{max}$ values range from 302° to 450°C (Table T13), although the most reliable values cluster between 400° and 420°C.

Total S content in Site 1195 sediments ranges from 0 to ~2.22 wt% (Fig. F18; Table T12) and its distribution is similar to that of TOC. C/N

F17. Carbonate and noncarbonate mineral percentages, p. 50.

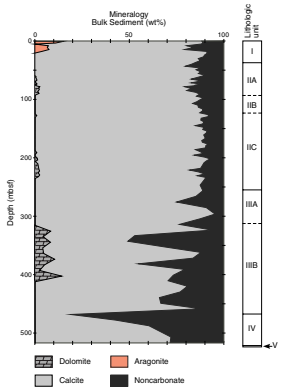


T11. Aragonite, calcite, dolomite, and noncarbonate mineral percentages, p. 88.

F18. Carbon, HI, and sulfur plots, p. 51.

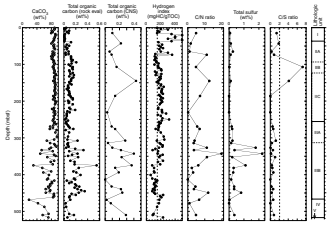

T12. Carbon, nitrogen, sulfur, and hydrogen results, p. 89.

T13. Rock-Eval pyrolysis results, p. 91.

and C/S ratios (Fig. F18; Table T11) reflect deposition in a marine environment.

## Discussion

Variations in the generally high $CaCO_3$ content (average = ~82 wt%) of sediments at Site 1195 mostly reflect fluctuations in the ratio of biogenic carbonate and its dilution by terrigenous sedimentation through time. $CaCO_3$ content exhibits an overall decrease from 88 wt% at 0.6 mbsf to 79 wt% at 15 mbsf, an interval containing relatively elevated TOC content and corresponding to the upper half of lithologic Unit I (see "Lithostratigraphy and Sedimentology," p. 3). Little to no organic carbon exists in the lower half of Unit I, whereas up to 91 wt% $CaCO_3$ was measured. The base of lithologic Unit I was placed at a phosphatized scour surface (see "Lithostratigraphy and Sedimentology," p. 3), which appears to roughly coincide with a slight increase in TOC content to ~>0.1 wt%.

Average $CaCO_3$ contents of 87 wt% and TOC contents of 0.1 wt% were measured in sediment samples from ~40 to 270 mbsf, an interval that corresponds to lithologic Unit II. Much of the $CaCO_3$ content in this interval is attributed to the dominance of planktonic foraminifers in the sediment (see "Biostratigraphy and Paleoenvironments," p. 6). In this unit, a relative increase to >0.2 wt% TOC at ~95 mbsf roughly marks the base of lithologic Subunit IIA (see "Lithostratigraphy and Sedimentology," p. 3). Lithologic Subunit IIB does not appear to be geochemically distinguishable from Subunit IIC, although C/S ratios in Subunit IIB and the top of Subunit IIC are possibly indicative of the presence of brackish conditions during or shortly after deposition. The base of lithologic Unit II is marked by a relative decrease in $CaCO_3$ content and an increase in TOC content at ~270 mbsf, a horizon that corresponds to scour surfaces and glauconite in the sediment (see "Lithostratigraphy and Sedimentology," p. 3).

Lithologic Unit III (~256–467 mbsf) is notable for a broad range in inversely covarying $CaCO_3$ and TOC values (Fig. F18) and repeated intervals of thin glauconitic and grainstone layers alternating with meter-thick bioturbated packstone (see "Lithostratigraphy and Sedimentology," p. 3). Portions of this geochemical record are similar to conspicuously low $CaCO_3$ and high TOC content horizons observed at Sites 1193 and 1194. At those sites, the horizons also contained elevated total S content. Subunit IIIB also contains high total S contents, relatively elevated TOC, elevated HI, and elevated C/N ratios (~19) that approach the terrestrial C/N field (~25–35) in the upper half (from ~320 to 380 mbsf) and consistently low HI values with relatively elevated TOC values in the lower half (from ~373 to 453 mbsf). These parameters may be indicative of a downsection shift to more oxic conditions in Subunit III. Toward the base of Subunit IIIB at ~450 mbsf, an increase in TOC and total S content is observed immediately overlying a >20% increase in $CaCO_3$ content between ~450 and 460 mbsf. Through all of lithologic Unit III, these geochemical data, collectively considered with observations of higher mud and clay content in this unit (see "Lithostratigraphy and Sedimentology," p. 3), are interpreted to reflect more neritic and terrigenous input to the distal periplatform setting of Site 1195.

A decrease to the lowest $CaCO_3$ content (~18%; ~468 mbsf) measured at Site 1195 coincides with a firmground and marks the top of lithologic Unit IV (see "Lithostratigraphy and Sedimentology," p. 3).

Lithologic Unit IV also displays an overall relative drop in TOC content. The low $CaCO_3$ horizon corresponds to a glauconitic sandstone (see "Lithostratigraphy and Sedimentology," p. 3) and overlies a unit with relatively elevated $CaCO_3$ (~72% at ~507 mbsf) and lower TOC content.

# CORE PHYSICAL PROPERTIES

Evaluation of physical properties at Site 1195 included nondestructive measurements of bulk density, bulk magnetic susceptibility, natural gamma radiation, and *P*-wave velocity on whole cores using the multisensor track (MST). *P*-wave velocity (x-, y- and z-direction) and moisture and density (MAD) were measured on split cores and plug samples. Color reflectance was measured on the archive halves of split cores. Thermal conductivity was measured on whole cores and semilithified core samples.

## Density and Porosity

Bulk density at Site 1195 was computed from gamma ray attenuation (GRA) using unsplit cores, and from MAD measurements on plug samples. Bulk density decreases from 1.70 to 1.45 g/cm³ in the upper 56 m of Hole 1195A and Hole 1195B (Fig. F19). Bulk density abruptly increases to 1.7 g/cm³ at 90 mbsf, below which it generally increases down to ~345 mbsf. Between 345 mbsf and the base of the hole (521 mbsf), bulk density is rather uniform, with an average of 2.07 g/cm³. Small-scale variations in density occur down the entire hole. Composite profiles of independently derived MAD bulk density estimates have similar trends and amplitude ranges (Fig. F19). With the exception of a few outliers, the GRA bulk density agrees well with the MAD values between 0 and 210 mbsf. Cores from this interval were recovered using the APC. After 210 mbsf, cores were cut using the XCB. The discrepancy in bulk density values in this section could be a function of core diameter variations produced by XCB coring, problems with the GRA calibration, excessive drying of the core prior to sampling for MAD measurements, and/or mass loss during the sample drying and pycnometer measurements. Nevertheless, the repeatability of the MAD measurements suggests that the consistent difference between GRA and MAD densities most likely arises because of the variability in core diameter.

Grain density averages 2.89 g/cm³ but shows large scatter, ranging from 2.4 to 3.6 g/cm³ between 0 and 380 mbsf (Fig. F20A, F20B). Below this interval, the grain density is approximately constant at 2.7 g/cm³. Given that the density of calcite and dolomite is 2.710 and 2.866 g/cm³, respectively, grain density values approaching 3.6 g/cm³ are problematic. The abrupt change and tight grouping of grain density at depths greater than 380 mbsf (Fig. F20B) relate to the replacing of a dysfunctional pycnometer. This pycnometer apparently compromised the quality of dry volume estimates and thus the grain density between 0 and 380 mbsf. The replacement pycnometer was used to determine the volume estimates of cube samples between 380 and 450 mbsf. The suspicion concerning a dysfunctional pycnometer has been confirmed by remeasuring grain densities between 300 and 400 mbsf (Fig. F20B) using the replacement pycnometer. Good agreement exists between the repeat measurements of beaker samples between 300–400 mbsf and the

F19. GRA and MAD bulk density, p. 52.

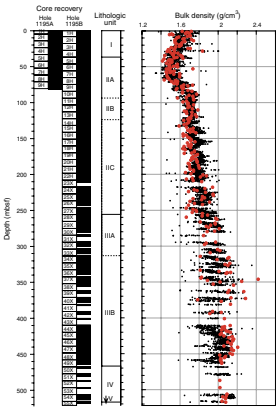


F20. Bulk density, grain density, porosity, and comparison of original and remeasured grain density and residual porosity, p. 53.

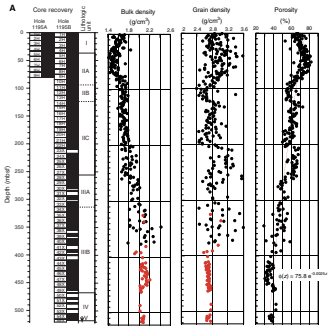

tightly grouped cube sample density values determined for the 380- to 450-mbsf interval.

A quick analysis explains how an erroneous dry volume measurement leads to an incorrect grain density even though the MAD bulk density agrees with the GRA bulk density (Fig. F19). Bulk density, $\rho_{wet}$, is determined using the bulk mass, $M_{wet}$, and volume, $V_{wet}$. The bulk density can be expressed as (assuming $V_{pw} \approx V_{water}$)

$$\rho_{wet} = M_{wet}/V_{wet} = (\rho_{pw}V_{pw} + \rho_{solid}V_{solid})/V_{wet},$$

where $V_{solid}$ is the dry (solid) volume and $V_{pw}$ is the fluid volume (including salt).

The differential change in bulk density relative to the grain density is

$$\partial\rho_{wet}/\partial\rho_{solid} = V_{solid}/V_{wet},$$

and given that $(1 - \phi)V_{wet} = V_{solid}$, where $\phi$ is porosity, then the above equation can be written as

$$\partial\rho_{wet} = (1 - \phi)\partial\rho_{solid}.$$

From this relationship, it is clear that for large porosity (i.e., shallow within the section), the changes in bulk density are relatively insensitive to the changes in grain density. Such a relationship explains the observed agreement between GRA bulk density and MAD bulk density, even though the MAD-derived grain densities are clearly incorrect. As porosity decreases, however, the bulk density will increasingly be affected by volume measurement errors just like the grain density, which helps to explain the increasing scatter in the MAD bulk density and porosity with depth (<380 mbsf; Fig. F20A).

For homogeneous sediments that are not overpressured, porosity may be approximated by an exponential function of depth (e.g., Athy, 1930). For Site 1195, the porosity is relatively low at the seafloor (60%–65%) and initially increases to ~80% at ~52 mbsf (Fig. F20A). The low surface porosity may reflect surficial reworking, sorting and efficient grain packing by oceanographic currents. This porosity trend may reflect increased current activity starting at ~3.8 Ma (52 mbsf; see "Age Model," p. 12). Below 52 mbsf, the porosity generally decreases downhole. The general behavior of the porosity as a function of depth is broadly consistent with Athy's relationship (see "Core Physical Properties," p. 21, in the "Explanatory Notes" chapter). A least-squares estimation of these parameters gives a surface porosity ($\phi_o$) of 75.8% and a compaction decay constant (k) of 0.0025 $m^{-1}$ (Fig. F20A; correlation coefficient of 0.88). The inverse of the decay constant (400 m) can be physically interpreted as the depth over which porosity is halved with respect to the surface or initial value.

Porosity profiles generally reflect a combination of stress history and sedimentologic and diagenetic effects, such as variability in compressibility, permeability, sorting, grain fabric and cementation. Porosity is calculated from the pore water content of soft sediment samples and cubes of lithified sediment, assuming complete saturation of the wet sediment sample (Blum, 1997) (see "Core Physical Properties," p. 21, in the "Explanatory Notes" chapter). The porosity curve mirrors that of the bulk density, with minor differences caused by variations in grain size, sedimentary facies and grain density (Fig. F20A). Porosity at Site

1195 shows a general decrease with depth. Superimposed on this trend are shorter wavelength variations over a length scale of 80–100 m. Because of the pycnometer problems, it is difficult to be confident about the geological significance of these trends. Nevertheless, it is interesting to note that abrupt changes in the downhole trend correlate approximately with lithologic unit boundaries and grain size distribution. Comparison of the porosity residuals, obtained by removing the least-squares porosity trend from the observed porosity, with the grain size distribution (see "Lithostratigraphy and Sedimentology," p. 3) indicates, to first-order, a dependence of porosity on carbonate texture and/or grain size. For example, the change in grain size from wackestone to grainstone and back to wackestone between 0 and 100 mbsf correlates with the porosity residual variations shown in Figure F20C. Similarly, abrupt offsets in the porosity residuals, for example at 100, 125, 205, 265, 300 and 450 mbsf, are approximately coincident with both lithologic unit and subunit boundaries (e.g., 105 mbsf is coincident with Subunit IIA/IIB boundary; 125 mbsf is coincident with Subunit IIB/IIC boundary; and 265 mbsf is coincident with Subunit IIC/IIIA boundary).

The compaction properties of carbonate sediments contrast with those of siliciclastic systems. Compaction of sand siliciclastic systems is dominated by the deformation of the matrix. In contrast, shale compaction occurs initially by the dewatering of the clays followed by the deformation of the matrix, after which sand and shale systems eventually compact in a similar way at depths ≥1000 m. The carbonate equivalent of siliciclastic sands and shales are mudstones/wackestones and grainstones/rudstones. It is suggested that the micritic mud supporting the matrix of mudstones and wackestones, because it does not have an intracrystalline porosity, responds to increasing overburden pressure by directly deforming the matrix. This behavior is analogous to siliciclastic sand systems. In contrast, grainstones and rudstones are grain or clast supported sediments such that during compaction, the generally high porosity clasts (e.g., rhodoliths) need to deform first in order for the matrix to deform. This compaction behavior is thus analogous to shale compaction. Alternatively, the relatively higher porosity of grainstones may reflect a high initial porosity that is maintained during the early compaction process. This analogy for carbonate compaction helps to explain the correlation of residual porosity with carbonate facies (Fig. F20C).

## Compressional Wave Velocity

Compressional wave velocity was measured using the PWS1 (z-direction) and PWS2 (y-direction) insertion probe system on split cores (within the core liner), and the PWS3 contact probe system on both split cores (within the core liner) and ~9.5-cm³ cube samples of semilithified and lithified sediments. The cubes were used to measure velocity in the transverse (x and y) and longitudinal (z) directions. Continuing problems with the transducer-liner coupling of the MST *P*-wave logger forced its discontinuation during Site 1195 drilling.

Velocity obtained using the PWS3 contact probe, irrespective of the direction measured, shows abrupt shifts, for example between 0 and 35 mbsf, 85 and 113.5 mbsf, and 208 and 245 mbsf (Fig. F21). Similar problems were experienced at other sites (e.g., "Core Physical Properties," p. 19, in the "Site 1194" chapter). These abrupt velocity steps appear to be caused by a pressure gauge linked to the PWS3 sensor. When activated, the acquisition software does not correct for movement of

F21. *P*-wave velocity, p. 56.

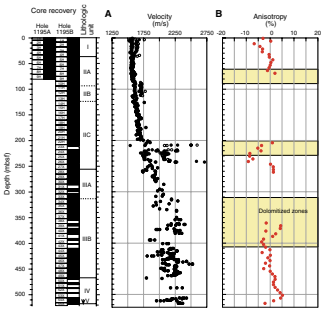

the gauge, thereby overestimating the calculated velocity. To correct the various shifts, all PWS3 x-direction data between 0–35 mbsf and 85–113.5 mbsf were decreased by 100 m/s, whereas the x-, y-, and z-direction data were decreased by 310 m/s between 208 and 245 mbsf (Fig. F21).

Corrected velocity values increase gradually from ~1558 to a maximum of 2250 m/s at a depth of 360 mbsf, after which the velocity is scattered around a mean of 2100 m/s (Fig. F21). This general behavior correlates with carbonate content (see "Geochemistry," p. 12), which is ~80% over a depth range of 0–300 mbsf. From 300 mbsf to the base of the hole, the carbonate content is characterized by large fluctuations superimposed on an overall decreasing trend toward basement. No simple relationship between the lithologic units and the velocity trends is observed (see "Lithostratigraphy and Sedimentology," p. 3).

Velocity anisotropy is significant and ranges from –10% to 5% (Fig. F21) (see "Core Physical Properties," p. 21, in the "Explanatory Notes" chapter). In general, positive anisotropy is more common in layered sediments, where sound transmission is relatively more efficient parallel to bedding rather than across. Dolomitization, since it represents chemical modification of the sediment structure, should be conducive to an isotropic velocity distribution. At Site 1195, most of the anisotropy is negative, indicating that the fast direction is vertical. Seismic anisotropy shows no obvious relationship with either dolomitization or lithologic units (Fig. F21; see "Lithostratigraphy and Sedimentology," p. 3).

A crossplot of velocity vs. porosity for Site 1195 shows a general inverse relationship (Fig. F22). For the time-average empirical equation of Wyllie et al. (1956), the travel time of an acoustic signal through rock is the sum of the traveltime through the solid matrix and the fluid phase. However, the porosity and velocity data from Site 1195 do not match the time-average equation but can be described with a power law relation,

$$V_P(\phi) = a\phi^{-b},$$

where $V_P$ is the compressional wave velocity, and a (63,119 m/s) and b (1.55) are empirical constants determined from a least-squares regression (correlation coefficient = 0.87; Fig. F22). Deviations from the velocity-porosity model do not show any simple relationship with either dolomitization or lithologic units.

## Thermal Conductivity

Thermal conductivity values at Site 1195 show an overall increase with depth, ranging from ~0.8 W/(m·K) near the seafloor to ~1.4 W/(m·K) at the base of Hole 1195B (Fig. F23). Scatter tends to increase downsection, which is broadly consistent with the porosity data (Fig. F20A). A direct inverse relationship should exist between porosity and thermal conductivity because of the power law dependence of bulk thermal conductivity on the solid matrix grain thermal conductivity and the thermal conductivity of the interstitial fluid (see "Core Physical Properties," p. 21, in the "Explanatory Notes" chapter) (Keen and Beaumont, 1990).

The variation in bulk thermal conductivity for the observed porosity range obtained at Site 1195 is shown in Figure F24. Except for a small number of outliers, the majority of the measured thermal conductivi-

F22. Crossplot of velocity vs. porosity, p. 57.

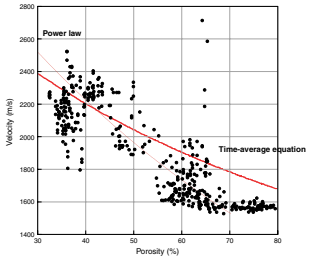


F23. Average thermal conductivity, p. 58.

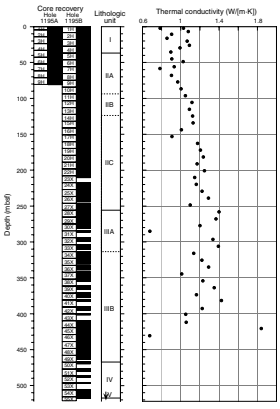


F24. Crossplot of porosity and thermal conductivity, p. 59.

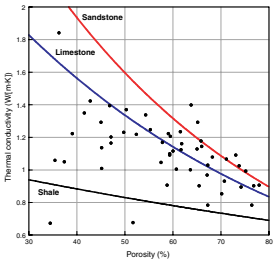

ties lay between the shale and sandstone power law relationship, giving confidence in the viability of the observations. Given the predominance of carbonate through most of the section at Site 1195 (see "Geochemistry" p. 12), the observed thermal conductivity is consistent with the carbonate sediment facies mixed with clays and siliciclastics.

## Magnetic Susceptibility, Natural Gamma Radiation, and Color Reflectance

Magnetic susceptibility (MS) and natural gamma radiation (NGR) contain independent information concerning terrigenous sediment source and magnetic mineral derivation. In general, for Site 1195, NGR correlates with the MS and inversely correlates with the lightness (L*) parameter of color (Fig. F25). The MS and NGR can be divided into four main zones with distinct patterns (Fig. F25):

1. 0–98 mbsf, where the data are characterized by high frequency, relatively large amplitude variations;
2. 98–210 mbsf, where the data are nearly constant with almost zero amplitude;
3. 210–462 mbsf, where the data shows modest variability and amplitude; and
4. Below 462 mbsf, where the MS and NGR values again have a large amplitude.

Carbonate content slowly decreases below ~220 mbsf (see "Geochemistry," p. 12), more or less as the MS and NGR values increase. The general decrease in lightness as both the MS and NGR increase between 0 and 80 mbsf and below 230 mbsf indicates increased terrigenous clay content (lithologic Units IIIA and IIIB; see "Lithostratigraphy and Sedimentology," p. 3).

MS and NGR can be used to estimate the depth offset between Holes 1195A and 1195B by matching characteristic features in the data sets (Fig. F26). For example, the NGR shows a prominent peak at 36 mbsf in Hole 1195B (Fig. F25). The interpreted counterpart in Hole 1195A is at 36.3 mbsf, suggesting a minor 30-cm offset between the holes at this depth. This offset will not apply to other cores or necessarily to other sections in these cores. However, it represents the typical margin of uncertainty in depth measurements with the drill string. In contrast, the high-amplitude MS peak at 26–30 mbsf in Hole 1195B is not reflected in Hole 1195A although both holes contain the high-amplitude peak at 48–50 mbsf. Caution should be exercised if these MS data are to be used for cyclicity studies.

An important component of lithologic Subunits IIA, IIC, and IIIB, and Unit IV is the presence of glauconite, in places approaching 40% (see "Lithostratigraphy and Sedimentology" p. 3). Glauconite, rich in ferro- and ferric-ions, is potentially susceptible to induced magnetization. Glauconite is essentially a member of the mica and illite clay families and is thus a phyllosilicate. Consequently, glauconite may be able to scavenge radioactive minerals much in the same way as other clays and fine-grained micas. In order to examine the NGR and MS correlation with glauconite, the high-concentration glauconite zones straddling the lithologic Subunits IIC and IIIA (236–257 and 293–304 mbsf; Fig. F27A) were plotted with the MST-NGR and the Schlumberger hostile environment natural gamma ray sonde (HNGS) logging data (see

F25. Comparison of magnetic susceptibility, carbonate content, natural gamma radiation, and color reflectance, p. 60.

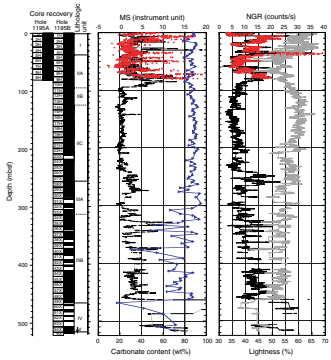


F26. Depth offset between Holes 1195A and 1195B, p. 61.

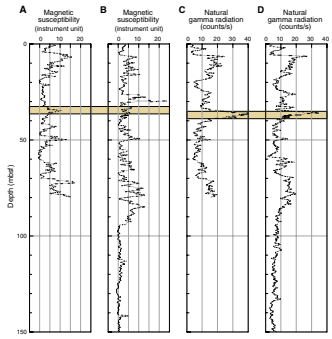


F27. Comparison between the color reflectance parameter a*, the MST-NGR, the HNGS gamma radiation data, magnetic susceptibility, and glauconite-rich units, p. 62.

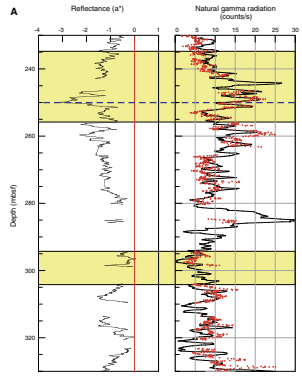

"Downhole Measurements," p. 21). Superimposed onto the lithologic units is the a* color reflectance parameter (green-red value; Fig. F27A). The HNGS data are characterized by a number of peaks occurring between 234 and 256 mbsf. A local minimum in the a* occurs at 250 mbsf, superimposed on a broad low in the a* values between 230 and 290 mbsf. In detail, the a* local minimum does not correlate well with any of the NGR-HNGS peaks, although the general MST-NGR high is coincident with the general green emphasis of a* (Fig. F27A). In contrast, the high-glauconite zone recognized from the lithostratigraphy at 294–304 mbsf is not represented in either the a* or NGR-HNGS data. Furthermore, the maximum HNGS peak at 285 mbsf is associated with neither a local minimum in a* nor with a conspicuous glauconite layer in the core. A similar correlation problem exists with the MS (Fig. F27B). For the entire 235–320 mbsf section, the MS ranges in amplitude from 0 to $7 \times 10^{-6}$ SI units and shows no clear correlation with either the a* data or the location of the glauconite zones. It is concluded that glauconite does not show an appreciable MS effect, despite its potential as a strong paramagnetic mineral. Further, the association of the broad NGR-HNGS peak between 240 and 253 mbsf and the a* local minimum may reflect the existence of glauconite, but clearly, not every natural gamma radiation peak is necessarily associated with glauconite (see "Paleomagnetism," p. 10).

# DOWNHOLE MEASUREMENTS

## Logging Operations

Logging operations in Hole 1195B were shortened as a result of deteriorating hole conditions. Only one run with the triple combo and three check shots with the WST in shallow depths were completed (Table T14). Operations began at 0315 hr on 29 January with the rigging of the triple combo with the LDEO temperature, acceleration, pressure tool at the bottom and the LDEO multisensor gamma ray tool (MGT) at the top. The tools reached total depth (TD) at 517.5 mbsf, which was ~2 m above TD cored. A successful first pass retrieved excellent logging data (Fig. F28). Already recognizing two narrow spots on the caliper in the upper part of the hole, it was decided to abandon the second run with the MGT in favor of running the WST because an accurate time-depth conversion was crucial for achieving the objectives at this site. In a first attempt of deployment, the WST did not pass the bottom of the pipe and the pipe became stuck. Despite a subsequent wiper trip, hole conditions worsened. In a second attempt, the WST could only be lowered to a newly developed tight spot at ~150 mbsf. Three check shots were completed using the 300-in³ air gun above this depth (Table T15). At 1745 hr, it was decided to abort further logging in this hole.

## Log Quality

During the first run, the almost smooth borehole yielded high-quality logging data (Fig. F28). The exception is the interval above 185 mbsf, where the caliper shows a maximum aperture of 17 in, causing the tool to loose contact with the borehole wall. In these intervals, the quality of the density and porosity measurements are somewhat degraded, whereas natural gamma ray (HSGR) and deep resistivity are little affected.

T14. Summary of logging operations, p. 92.

F28. Downhole logging data, p. 64.

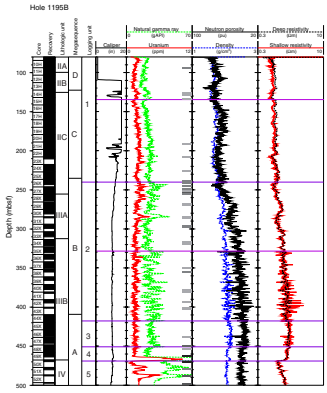


T15. Stations of the check shot survey, p. 93.

The air gun produced a sharp high-amplitude signal that allowed easy picks of the first arrivals captured by the WST. In contrast, shots with the water gun used at the previous site had a precursor signal that severely hindered the picking of the first arrivals on the seismograms, resulting in unreliable data.

Comparison of logs with core data (Fig. F29) shows a good correlation of the data profiles. In the upper 170 m of the logged section (80–250 mbsf), the absolute values of GRA densities are slightly higher than the log values because the density measurements downhole were affected by an enlarged hole. Between 250 and 370 mbsf, the two data sets match well. However, below 370 mbsf, the core values are slightly lower than the downhole log values. The absolute values of natural gamma radiation are not comparable, as they have different units.

F29. Comparison of core measurements and downhole logs, p. 65.

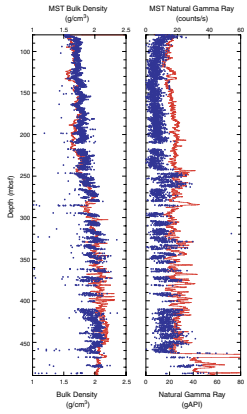


## Results

The logged interval of Hole 1195B is divided into five logging units (Fig. F28). Logging Unit 1/2 and 4/5 boundaries correspond roughly with lithologic Unit II/III and III/IV boundaries, respectively. In the lower part of the drilled interval, the logs suggest the possibility of additional lithologic subdivisions. In general, log values display little variability down to 240 mbsf, which is in concert with the rather homogeneous lithology of unconsolidated skeletal wackestone to packstone in this interval (see "Lithostratigraphy and Sedimentology," p. 3). Below 240 mbsf, the logs have a cyclic appearance, which again correlates well with the alternations of light gray and greenish gray sediments observed in the cores (see "Lithostratigraphy and Sedimentology," p. 3).

### Logging Unit 1 (80–240 mbsf)

Logging Unit 1 shows relatively low resistivity and HSGR (~20 gAPI) values with generally minor variations in all log values (Fig. F28). A small log change occurs at 134.5 mbsf that is characterized by an excursion to higher HSGR and lower resistivity values. Below 134.5 mbsf, log responses are similar to the interval above. Logging Unit 1 roughly coincides with lithologic Unit II, consisting of unconsolidated skeletal wackestone to packstone (see "Lithostratigraphy and Sedimentology," p. 3). Sediments in lithologic Subunit IIC are progressively more consolidated downhole. They are separated from the more unconsolidated sediments above by glauconite-rich beds at the base of lithologic Subunit IIB that might be the cause of the high HSGR values at 134.5 mbsf. These beds also mark the seismic Megasequence C/D boundary (see "Seismic Stratigraphy," p. 24).

### Logging Unit 2 (240–418 mbsf)

The boundary of logging Unit 2 (240 mbsf) is marked by an increase in density, resistivity, and HSGR values (Fig. F28). In this logging unit, the log curves display more variability. Below 328 mbsf, the frequency of log peaks is much higher and the amplitude of the HSGR log increases (20 to 40 gAPI), as does the amplitude in the resistivity log (from 2 to 4 Ωm).

The upper boundary of logging Unit 2 is ~15 m above that of the lithologic Unit III boundary (Fig. F28). This boundary also coincides with the seismic Megasequence B/C boundary (see "Seismic Stratigraphy," p. 24, and "Lithostratigraphy and Sedimentology," p. 3). The

transition from lithologic Unit II to Unit III is one of the major changes in sedimentation; Unit III is characterized by alternations of light gray and darker greenish gray layers that also have textural variations. The dark layers are related to increased terrigenous input, as shown by the increased quartz and clay content of the sediment (see "Lithostratigraphy and Sedimentology," p. 3). The HSGR variations between 240 and 328 mbsf are predominantly related to variations in uranium content, whereas those between 328 and 418 mbsf are mainly caused by changes in thorium and potassium concentration (Fig. F30). Glauconite-rich layers occur in the upper portion of lithologic Unit III and appear to be correlated with increased uranium concentrations. Light layers, which are enriched in neritic material and show lower HSGR, also have lower porosity and higher resistivity values, indicating increased cementation. The thorium and potassium enrichment, however, correlates with an increased terrigenous input (see "Lithostratigraphy and Sedimentology," p. 3).

F30. Log spectral gamma ray data showing potassium, thorium, and uranium concentrations, p. 66.

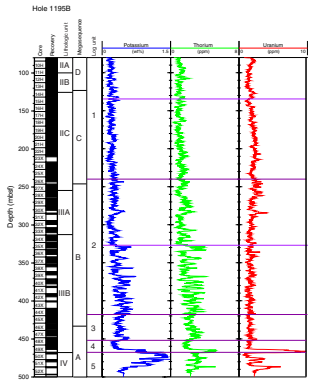


## Logging Unit 3 (418–451 mbsf)

The boundary between logging Units 2 and 3 is marked by an increase in density and resistivity values, which are generally above 2.2 g/cm³ and 3.4 Ωm, respectively, and a decrease in variability in all neutron porosity and HSGR values to ~35 pu and 25 gAPI, respectively (Fig. F28). Toward the bottom of logging Unit 3, HSGR and resistivity amplitudes increase. This pattern of high variation in the lower part of the interval and less variation in the upper part is similar to logging Unit 2, suggesting a repetition of the sedimentation pattern, although with reduced thickness.

No lithologic boundary is recognized at the upper boundary of logging Unit 3 (418 mbsf), but the boundary correlates well with seismic Megasequence Boundary A/B at ~408 mbsf (Fig. F28) (see "Seismic Stratigraphy," p. 24). Logging Unit 3 occurs within the lower part of lithologic Subunit IIIB, which is composed of fining-upward sequences of skeletal packstone with well-preserved burrows (see "Lithostratigraphy and Sedimentology," p. 3).

## Logging Unit 4 (451–468.5 mbsf)

Logging Unit 4 shows generally lower variability in all measured physical properties with overall slightly lower density (2.05 g/cm³), resistivity (3 Ωm) and HSGR values (22 gAPI) (Fig. F28). The lower boundary of this logging unit is placed at 468.5 mbsf, where resistivity sharply decreases. A HSGR peak at the bottom of this unit, with the highest uranium values (~10 ppm) measured in Hole 1195B (Fig. F29), correlates to a glauconite-rich layer observed in the sediments (see "Lithostratigraphy and Sedimentology," p. 3).

Logging Unit 4 corresponds to the lowermost 15 m of lithologic Subunit IIIB, which consists mainly of grainstone with rare quartz grains and a glauconite-rich layer at the base (see "Lithostratigraphy and Sedimentology," p. 3).

## Logging Unit 5 (468.5–517.5 mbsf)

At 468.5 mbsf, the resistivity drops to 1 Ωm, marking the boundary to logging Unit 5 (Fig. F28). Within the unit, the logs are characterized by high HSGR values up to 78 gAPI; uranium values peak at 3–6 ppm,

and potassium is generally high with maximum values of 1.5 wt% (Fig. F30). The upper boundary of logging Unit 5 coincides with the lithologic boundary from Unit III to Unit IV. Lithologic Unit IV consists of greenish gray, well-sorted fine- to medium-grained packstone, grainstone, and quartz sandstone with abundant rounded glauconite (see "Lithostratigraphy and Sedimentology," p. 3).

### Temperature Data

Temperature data were recorded from the seafloor to 517.5 mbsf (Fig. F31). The temperature curve shows an unusual shape. The downgoing temperature gradient is rather steep, as the tool was lowered rapidly (>4000 ft/hr) and the sensor did not have time to stabilize. At the bottom of the hole, the tool had several minutes to get into equilibrium with the surrounding water and to measure the borehole temperature of 26°C at that time. After beginning to log uphole, the temperature increased slightly. When the tools were lowered a second time because of software problems, the temperature at the bottom of the hole reached 29°C (Fig. F31). The increase of 3.0°C occurred within 12 min and 43 s, indicating that high formation temperatures cause the heating of the borehole water at the bottom of the hole.

F31. Temperature profile, p. 67.

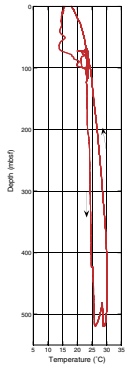


## SEISMIC STRATIGRAPHY

Site 1195 penetrated 521.2 m of sediment through seismic Megasequences D, C, B, A, and a previously unmapped carbonate sequence (possibly Eocene in age) at the base of the section (Fig. F3). This site was chosen for the continuous nature of the seismic reflections, which indicate a nearly complete Neogene sedimentary section. This section is expected to provide a higher resolution chronostratigraphy than what could be produced from locations proximal to the Marion Plateau carbonate platforms (Fig. F7, p. 67, in the "Leg 194 Summary" chapter). Site 1195 is located at the intersection of multichannel seismic lines MAR15 (shotpoint 3505) (Fig. F3) and MAR04 (shotpoint 3928) (Fig. F2), located ~70 km east of the Northern Marion Platform and 60 km north of the Southern Marion Platform (Fig. F2, p. 62, in the "Leg 194 Summary" chapter).

### Time-Depth Conversion

Three check shots between 70 and 120 mbsf provide an accurate traveltime-depth link between the seafloor and the upper section of the hole. No further check shots are available below because deteriorating conditions did not allow lowering the tool further downhole (see "Downhole Measurements," p. 21). Consequently, the time-to-depth conversion for the lower section of this site was partly calculated by integrating shipboard velocity data collected from cores using the *P*-wave sensor method (see "Core Physical Properties," p. 16). The resulting traveltime to depth conversion was fixed at the depth of the basal carbonate unit at 521 mbsf, which corresponds to a strong reflection just above basement at 1076 ms two-way traveltime (TWT). Using shipboard velocity data and bulk density from a first successful logging run, a synthetic seismogram was calculated that is superimposed and compared to line MAR15 and displayed at the right on Figure F32. A normal

F32. Synthetic seismogram plotted on line MAR15, p. 68.

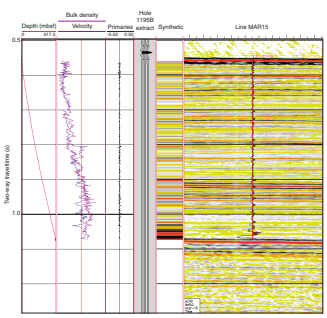

polarity zero-phase wavelet of 80 ms length was statistically extracted from the seismic data of line MAR15 to generate the seismogram.

## Megasequence D

### Seismic Facies and Geometries

The seismic facies of Megasequence D (550–712 ms TWT; 0–123 mbsf) (Fig. F3) is characterized by laterally continuous low to moderate amplitude reflections showing large-scale convex-upward mounded geometry that is typical for drift geometries. A relatively strong reflection near 602 ms TWT marks the top of a drift package, which thickens to the northeast. Above 602 ms TWT, the drift package, which potentially migrated from the southwest, is onlapping onto this reflection, indicating a hiatus across this unconformity (Fig. F3). The reflections in Megasequence D have low to moderate amplitude differences that are weaker than those below 602 ms TWT. The Megasequence C/D boundary, at the base of Megasequence D, occurs at 123 mbsf (712 ms TWT) and is marked by a conformable low-amplitude reflection (Fig. F3). The age model for this site provides an age of 7.22 Ma for the base of Megasequence D (see "Age Model," p. 12).

### Correlation with Cores

Megasequence D correlates well with the late Miocene to Pleistocene hemipelagic sediments of lithologic Units I, IIA, and IIB (0–123.9 mbsf) (see "Lithostratigraphy and Sedimentology," p. 3). The sediments within these units are predominantly unconsolidated packstone and grainstone. Physical properties data from Site 1195 show a shift to less variable velocity values downcore at the base of lithologic Unit I, which correlates well with the prominent reflection at 602 ms TWT. The base of Megasequence D (lithologic Unit II/III boundary) corresponds to the presence of a 15-m-thick interval of glauconite-rich layers indicative of low sedimentation rates. In addition, this horizon can be seen in physical properties data as a shift to lower *P*-wave velocity.

## Megasequence C

### Seismic Facies and Geometries

Megasequence C (712–824 ms TWT; 123–230 mbsf) is characterized by laterally continuous, generally low-amplitude reflections that dip gently to the northeast (Fig. F3). To the southwest of the site, two higher amplitude reflections can be seen at 719 and 730 ms TWT. These reflections decrease in amplitude to the northeast. The Megasequence B/C boundary at the base of Megasequence C is present at 230 mbsf and is characterized as a conformable low-amplitude reflection that has been dated as 11 Ma (see "Age Model," p. 12).

### Correlation to Cores

Megasequence C correlates with the upper part of lithologic Subunit IIC, which is a skeletal wackestone to packstone/grainstone deposited in a hemipelagic environment. Physical properties data from the Megasequence C interval show reduced variability in density, magnetic susceptibility, and natural gamma radiation (see "Core Physical Properties," p. 16) that are reflected in the seismic data by the low-amplitude

nature of the reflections. An exception to the reduced variability data set is the prominent velocity peak that appears near 210 mbsf. This peak correlates well with a relatively high-amplitude reflection that can be seen on the seismic profiles at 796 ms TWT. The horizon marking the base of Megasequence C coincides with the top of a glauconite-rich interval at the base of lithologic Subunit IIC (230–255 mbsf). It also corresponds to the upcore change in facies from a distal periplatform to a hemipelagic depositional environment.

## Megasequence B

### Seismic Facies and Geometries

Megasequence B (824–983 ms TWT; 230–408 mbsf) consists of laterally continuous reflections, which show a gradual dip to the northeast. Reflections in Megasequence B have low amplitudes in the interval above 827–909 ms TWT and higher amplitudes below. Megasequence Boundary B/A at the base of Megasequence B occurs at 408 mbsf and is seen as a conformable, low-amplitude reflection with an age of 19.8 Ma (see "Age Model," p. 12).

### Correlation with Cores

Megasequence B encompasses the lower part of lithologic Subunits IIC, IIIA, and the upper portion of IIIB. The sediments deposited in this interval are predominantly skeletal mudstone to grainstone characterized by a downcore increase in terrigenous concentration. A scoured horizon that marks the base of lithologic Unit II does not correlate to a significant reflection in the seismic data. However, physical properties data from this megasequence show increased variability in most data sets relative to the intervals above. The depth at which a change in reflection amplitude occurs (827 m) correlates well with the base of Subunit IIIA that marks a change from a greater amount of terrigenous sediments in Subunit IIA to a more carbonate-rich depositional system with increased dolomite concentration.

## Megasequence A

### Seismic Facies and Geometries

Megasequence A (983–1076 ms TWT; 408–517 mbsf) is characterized by low-amplitude reflections within two packages showing mounded drift geometries. At Site 1195, these packages are separated by a prominent unconformity within Megasequence A at 1040 ms TWT. The amplitude of this reflection increases to the northeast of the site.

### Correlation with Cores

Megasequence A encompasses the lower part of lithologic Unit III and all of Unit IV. The boundary between these two units is correlated with the prominent seismic unconformity between two sediment drift packages in Megasequence A (Fig. F3). Sedimentologically, this boundary is characterized by a downcore change from a light gray grainstone with rare quartz deposited in a distal periplatform environment (Unit III) to a greenish gray wackestone with high glauconite and quartz content deposited in a proximal periplatform environment (Unit IV) (see "Lithostratigraphy and Sedimentology," p. 3, and "Biostratigraphy

and Paleoenvironments," p. 6). This change in depositional environment between the two drift sequences may reflect a change in sedimentation source.

## Base Carbonate Unit

At the base of Site 1195 (517.5 mbsf), 20 cm of well-indurated, yellowish brown skeletal grainstones of possibly Eocene age were recovered. This sequence is observed on the seismic data to be a thin veneer of sediment overlain by a high-amplitude reflection at 1081 ms TWT and underlain by acoustic basement (Fig. F3). This reflection can be traced laterally for a short distance before it onlaps onto a basement high to the southwest of the site. To the northeast, this horizon continually thins below seismic resolution and merges with the basement (Fig. F3).

# REFERENCES

Athy, L.F., 1930. Density, porosity, and compaction of sedimentary rocks. *AAPG Bull.,* 14:1–24.

Berggren, W.A., Kent, D.V., Swisher, C.C., III, and Aubry, M.-P., 1995. A revised Cenozoic geochronology and chronostratigraphy. *In* Berggren, W.A., Kent, D.V., Aubry, M.-P., and Hardenbol, J. (Eds.), *Geochronology, Time Scales and Global Stratigraphic Correlation*. Spec. Publ.—Soc. Econ. Paleontol. Mineral. (Soc. Sediment. Geol.), 54:129–212.

Blum, P., 1997. Physical properties handbook: a guide to the shipboard measurement of physical properties of deep-sea cores. *ODP Tech. Note,* 26 [Online]. Available from World Wide Web: <http://www-odp.tamu.edu/publications/tnotes/tn26/INDEX.HTM>. [Cited 2001-01-10]

Keen, C., and Beaumont, C., 1990. Geodynamics of rifted continental margins. *In* Keen, M.J., and Williams, G.L. (Eds.), *Geology of the Continental Margin of Eastern Canada*. Geol. Soc. Am., 1:391–472.

Wyllie, M.R.J., Gregory, A.R., and Gardner, L.W., 1956. Elastic wave velocities in heterogeneous and porous media. *Geophysics,* 21:41–70.

**Figure F1.** Bathymetry map showing location of Leg 194 sites.

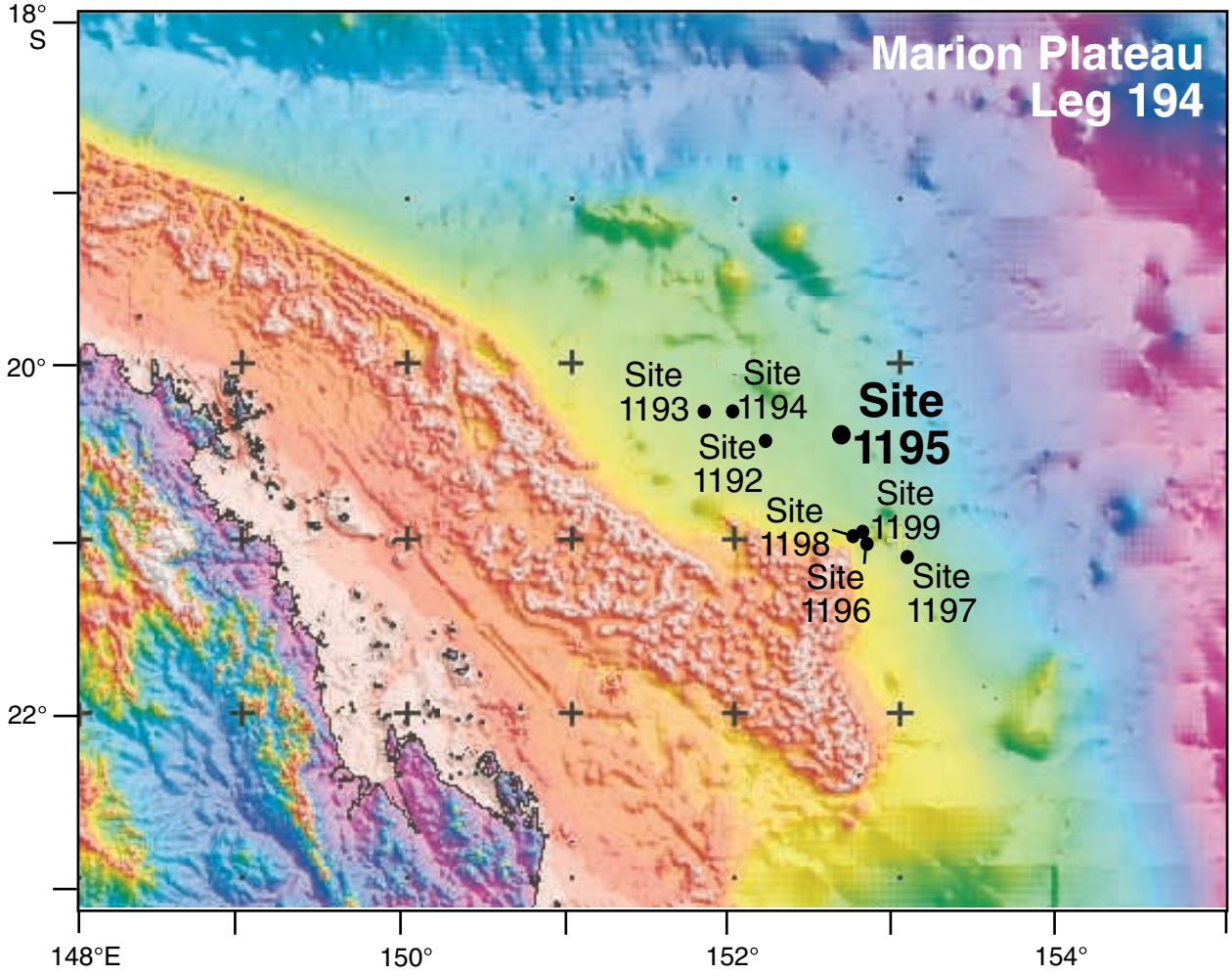

**Figure F2.** Seismic line MAR04 with location of Site 1195. This site is positioned at the intersection with line MAR15, which provides subsurface information in a dip direction. MS = Megasequence.

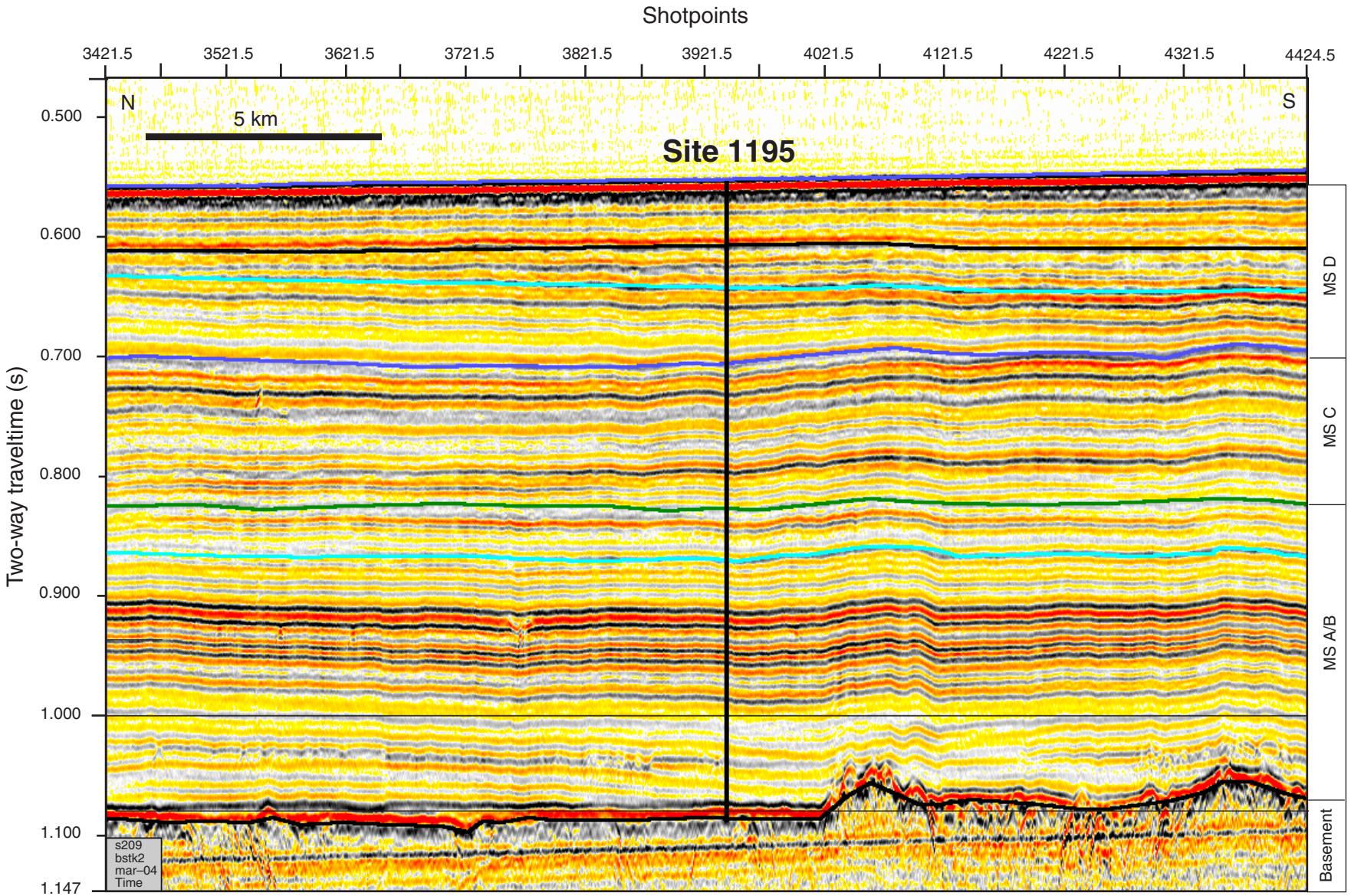

**Figure F3.** Multichannel line MAR15, with the location of Site 1195 (shotpoint 3505) and the penetration depth with lithologic units superimposed (see **"Lithostratigraphy and Sedimentology,"** p. 3). The seismic megasequences and the basement are marked and traced along the section. The arrow points to a prominent reflection and unconformity at 602 ms. MS = Megasequence.

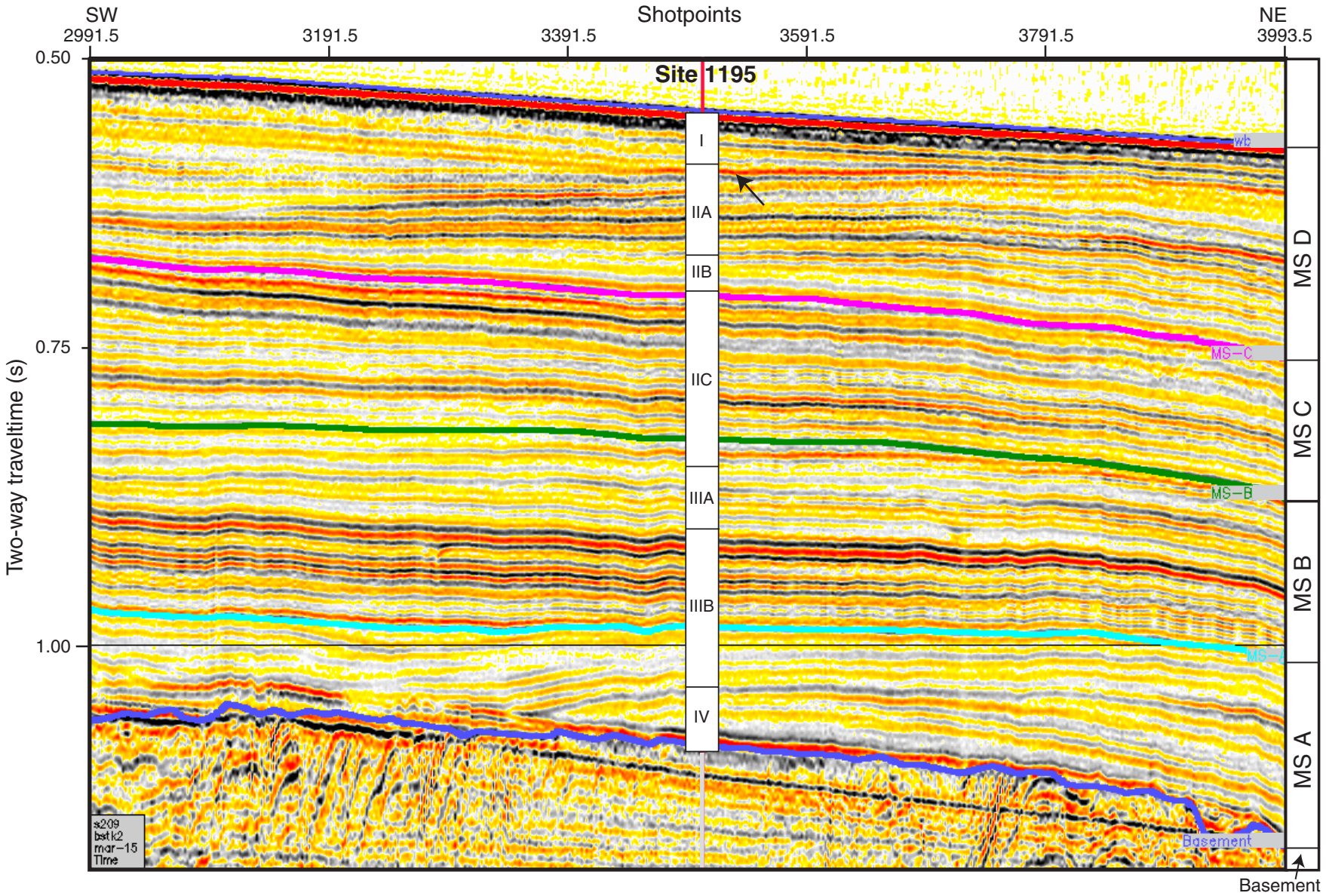

**Figure F4.** Lithologic summary for Site 1195. **A.** Core recovery for Holes 1195A and 1195B. Black = recovered, white = gap. **B.** Lithologic unit boundaries. **C.** Graphic representation of the major sedimentary rocks encountered. **D.** Carbonate and noncarbonate concentrations from XRD. **E.** Lightness measured at 5-cm intervals and smoothed for Hole 1195B. **F.** Degree of lithification. **G.** Sedimentary texture. **H.** Sedimentary environment. **I.** Ages (see "Age Model," p. 12).

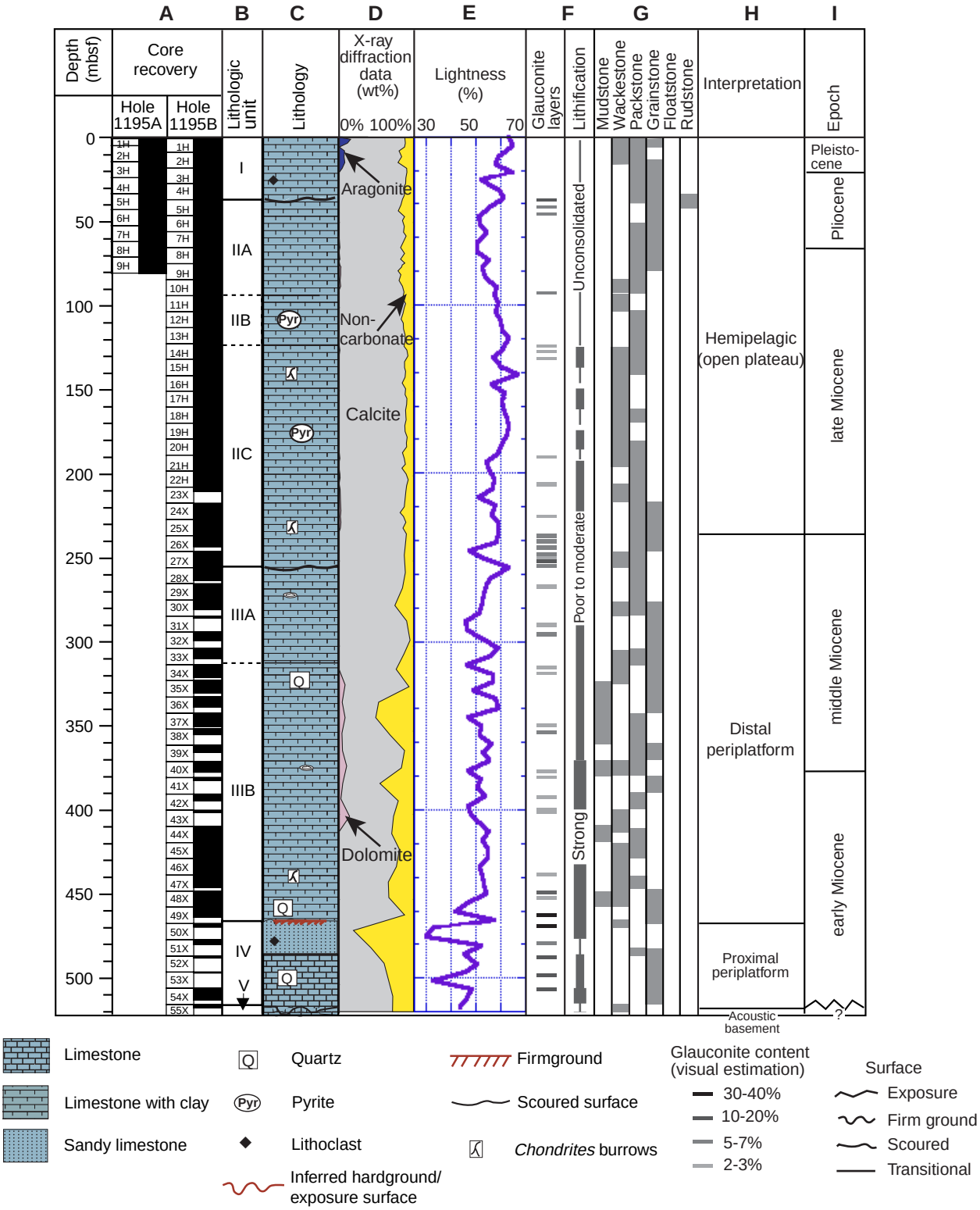

**Figure F5.** Close-up photograph of interval 194-1195A-5H-1, 110–138 cm, showing a coarse and poorly sorted skeletal-rich floatstone with light brown phosphatized lithoclasts, interlayered with foraminiferal grainstone. The base of the floatstone layer at 34.5 mbsf represents the boundary between Units I and II at Site 1195A.

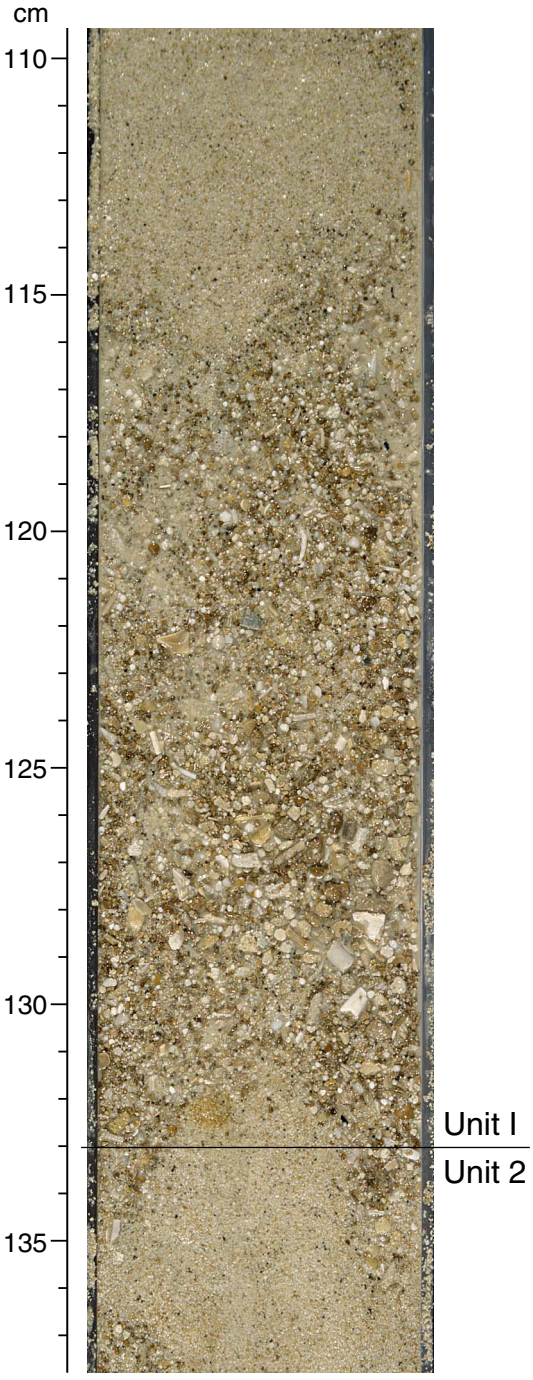

**Figure F6.** Close-up photograph of interval 194-1195A-5H-2, 132–149 cm (39.62–39.79 mbsf), showing a glauconite-rich layer from Subunit IIA.

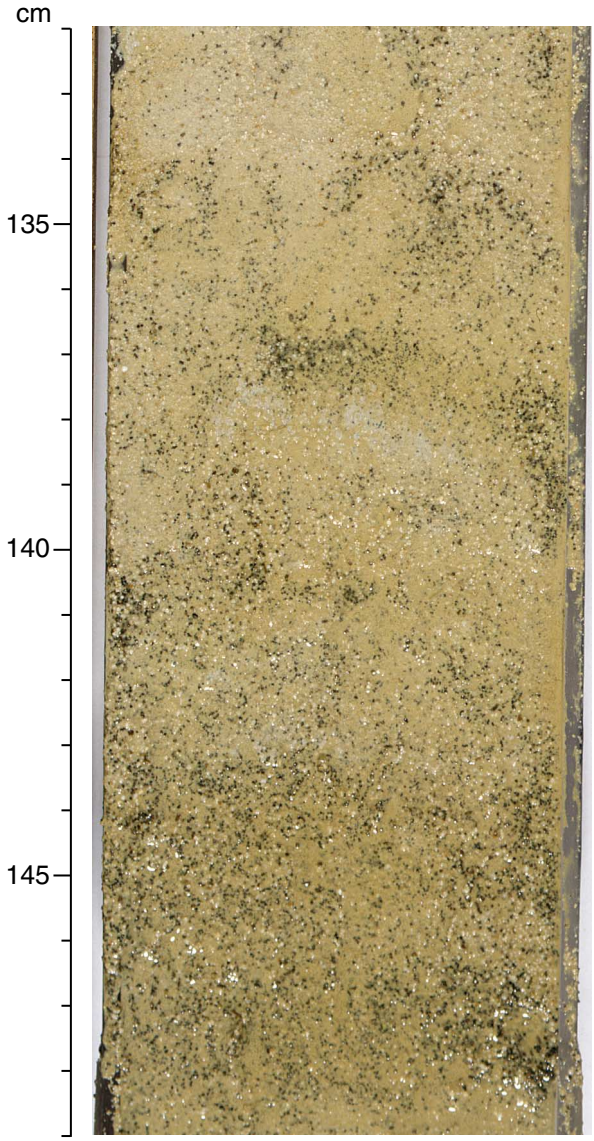

**Figure F7.** Close-up photograph of interval 194-1195B-21H-5, 34–54 cm (195.11 mbsf), showing a scoured surface at 46 cm (Subunit IIC). A light gray, fine sand–sized skeletal wackestone/packstone overlies and cuts into a light greenish gray wackestone below. Black stains are pyrite-filled burrows.

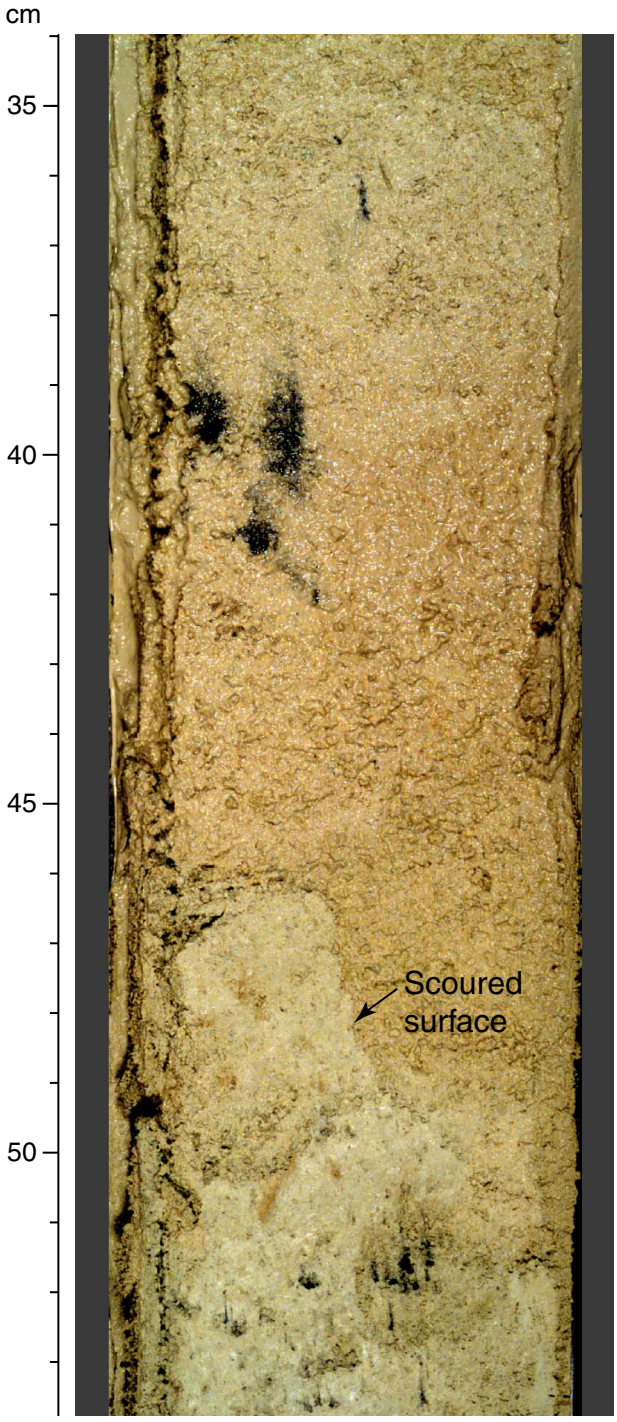

**Figure F8.** Close-up photograph of interval 194-1195B-44X-1, 80–121 cm (410.69 mbsf; Subunit IIIC), showing alternation of silt-sized light gray skeletal packstone and greenish gray mudstone with *Chondrites*. The top and basal surfaces of the mudstone layer (89 cm and 120 cm respectively) are sharp curved-scoured surfaces.

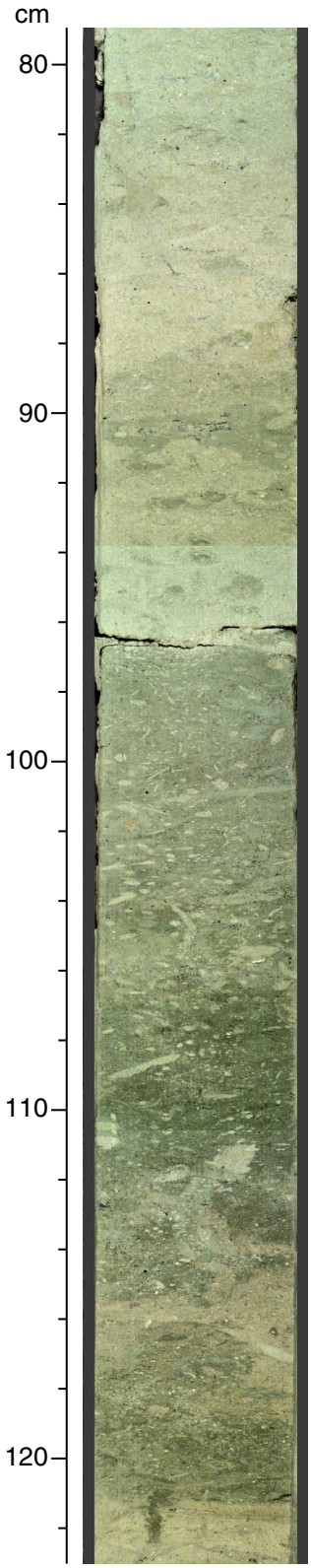

**Figure F9.** Close-up photograph of Sample 194-1195B-50X-1, 42–62 cm (468.12 mbsf; Unit IV), showing medium-sized, well-sorted greenish gray sand with glauconite. *Chondrites* appear as common white burrows.

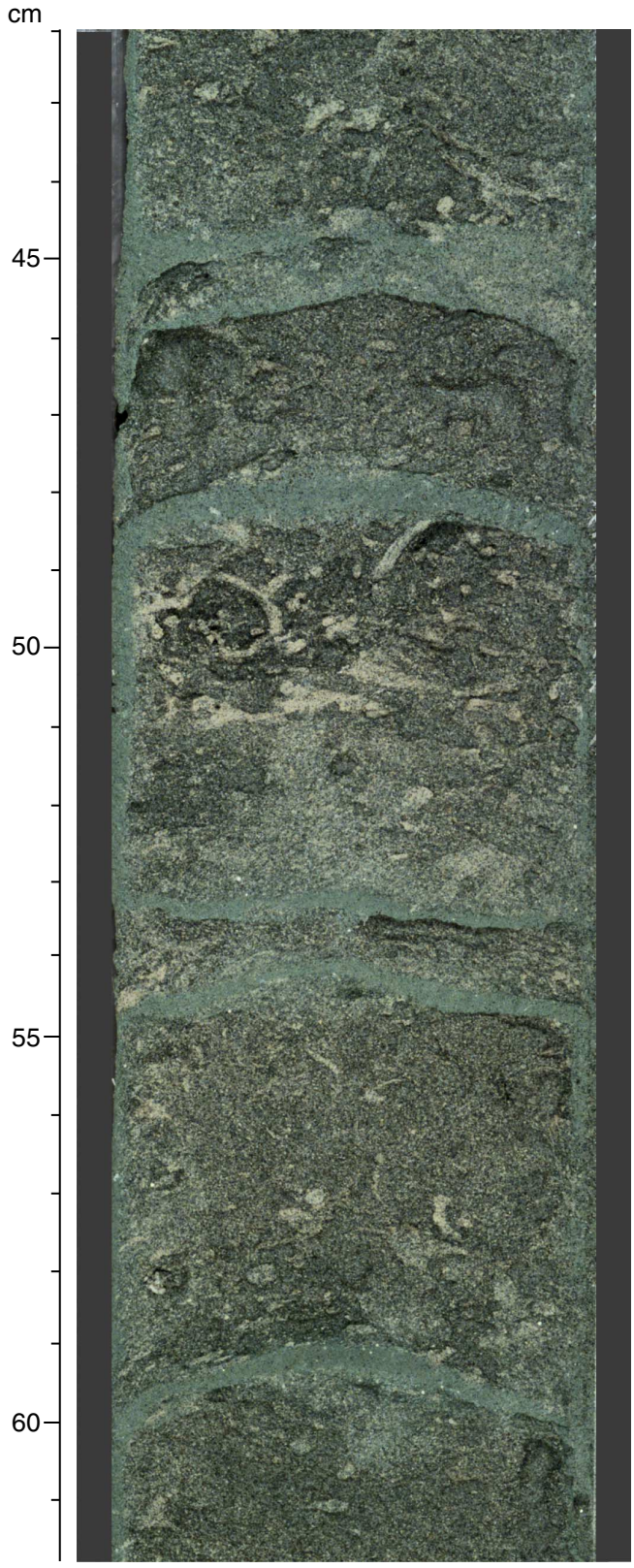

**Figure F10.** Photomicrograph of Sample **194-1195B-50X-2, 12–16 cm** (469.32 mbsf; Unit IV), showing a moderately sorted siltstone to very fine sandstone with pitted quartz, rounded glauconite, and rare broken planktonic foraminifers.

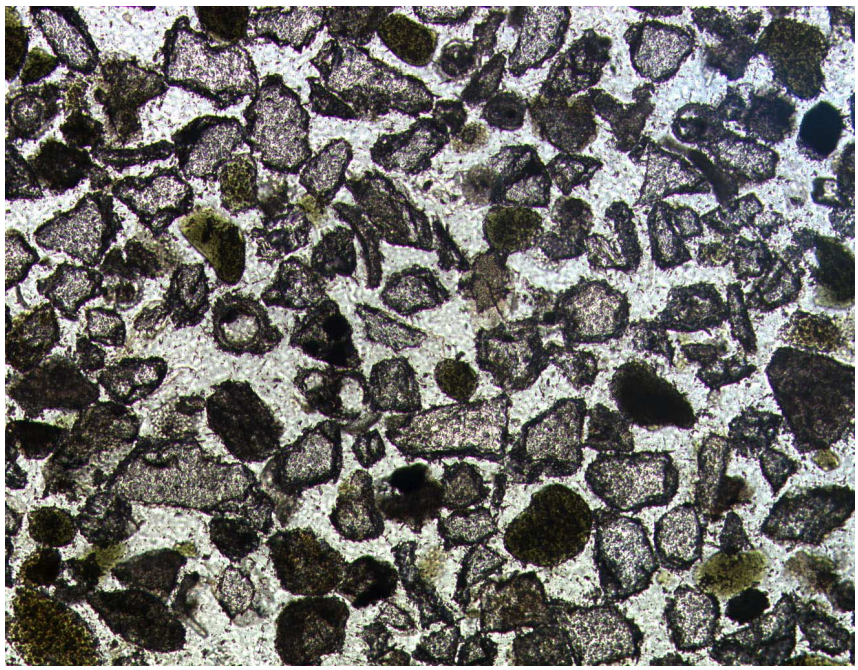

**Figure F11.** Long-core measurements from Hole 1195A, showing NRM intensity and inclination as a function of depth. Intervals of high intensities are shown by light gray boxes across the plot. This hole was drilled with the standard C3RBI bit.

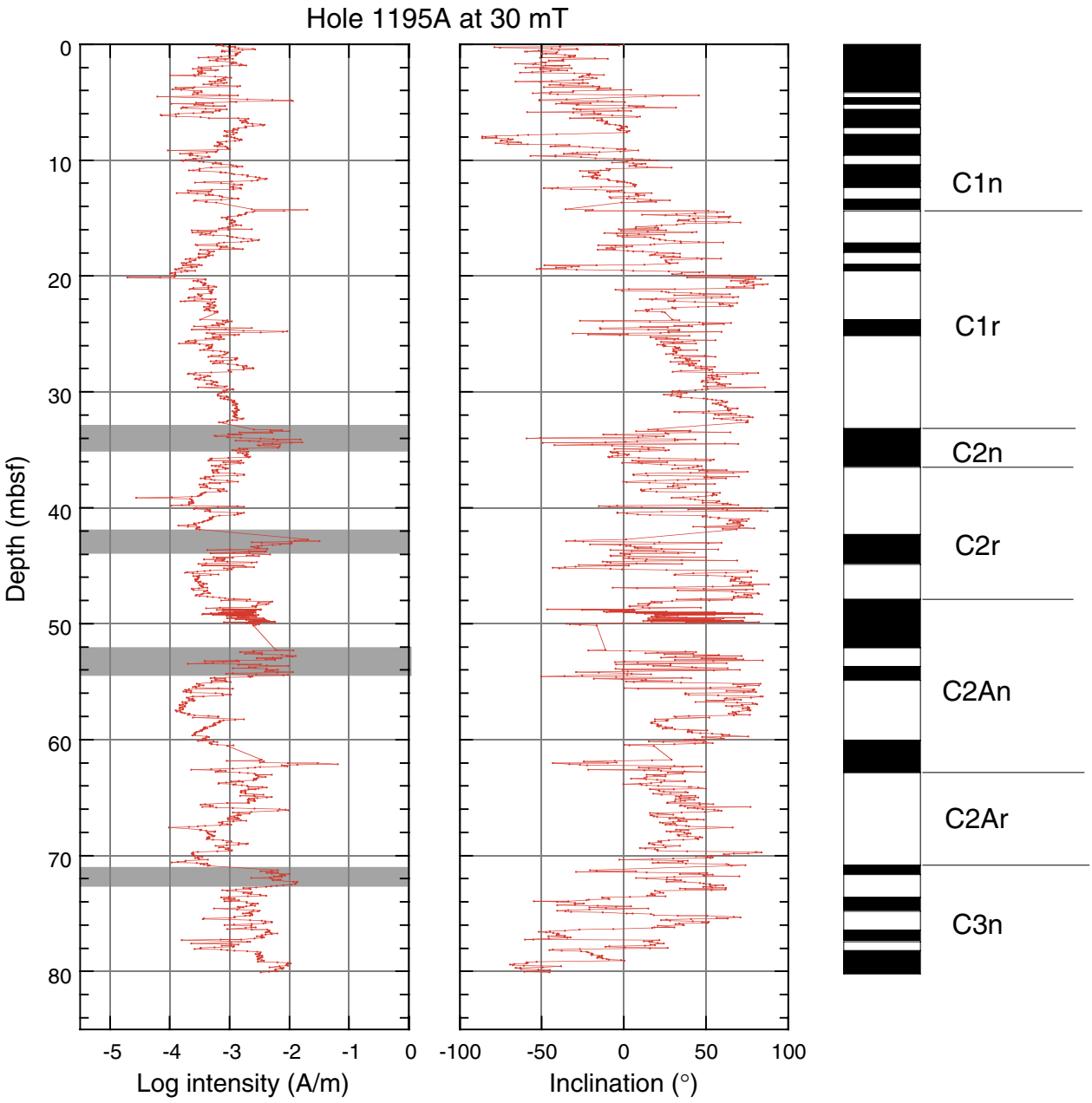

**Figure F12.** Long-core measurements from Hole 1195B showing NRM intensity and inclination as a function of depth. Intervals of high intensities are shown by light gray boxes across the plot. This hole was drilled with a Russian-made PDC bit, which is less magnetic than a standard bit. **A.** 0–100 mbsf. (Continued on next five pages.)

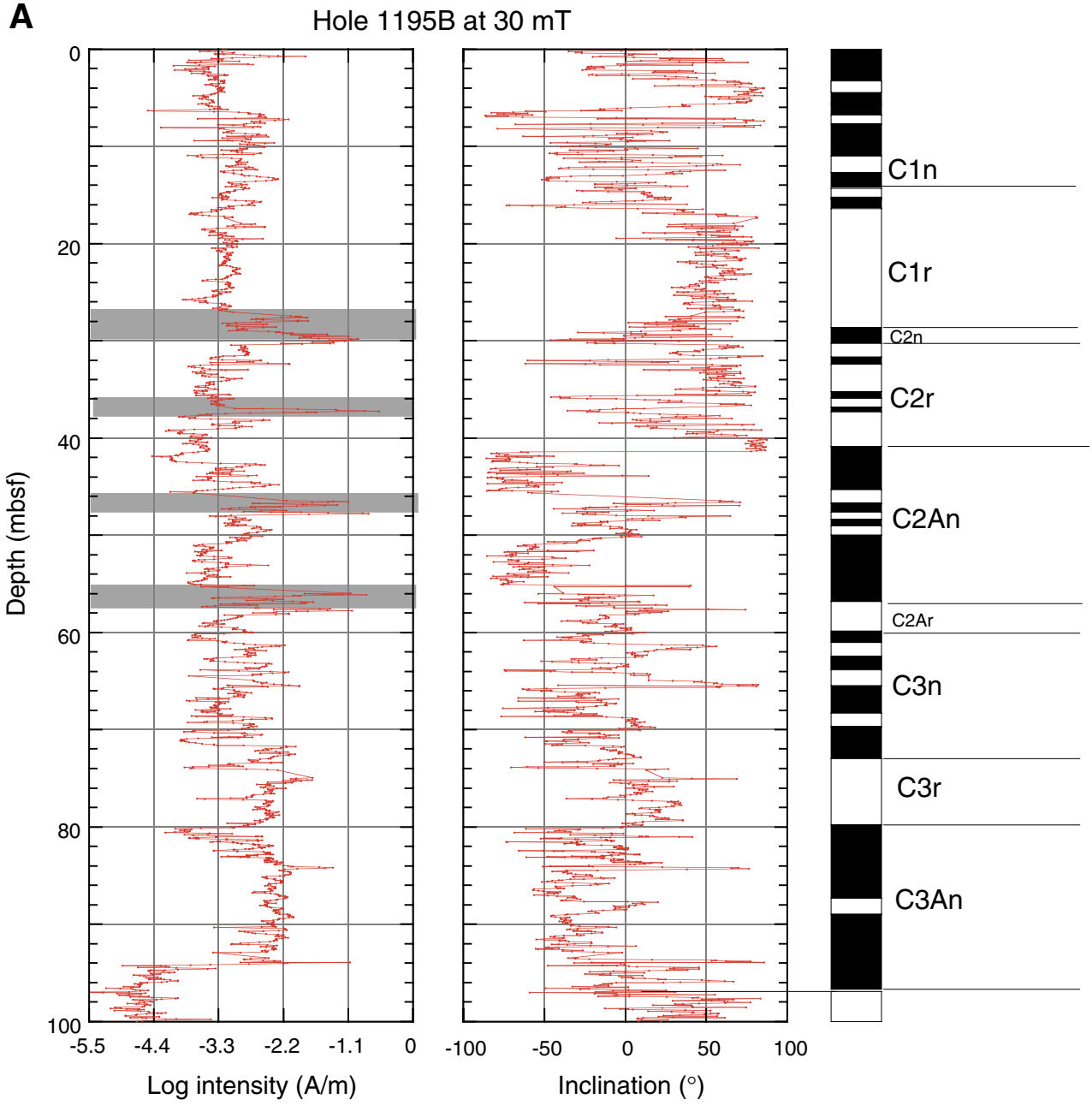

**Figure F12 (continued). B.** 100–200 mbsf.

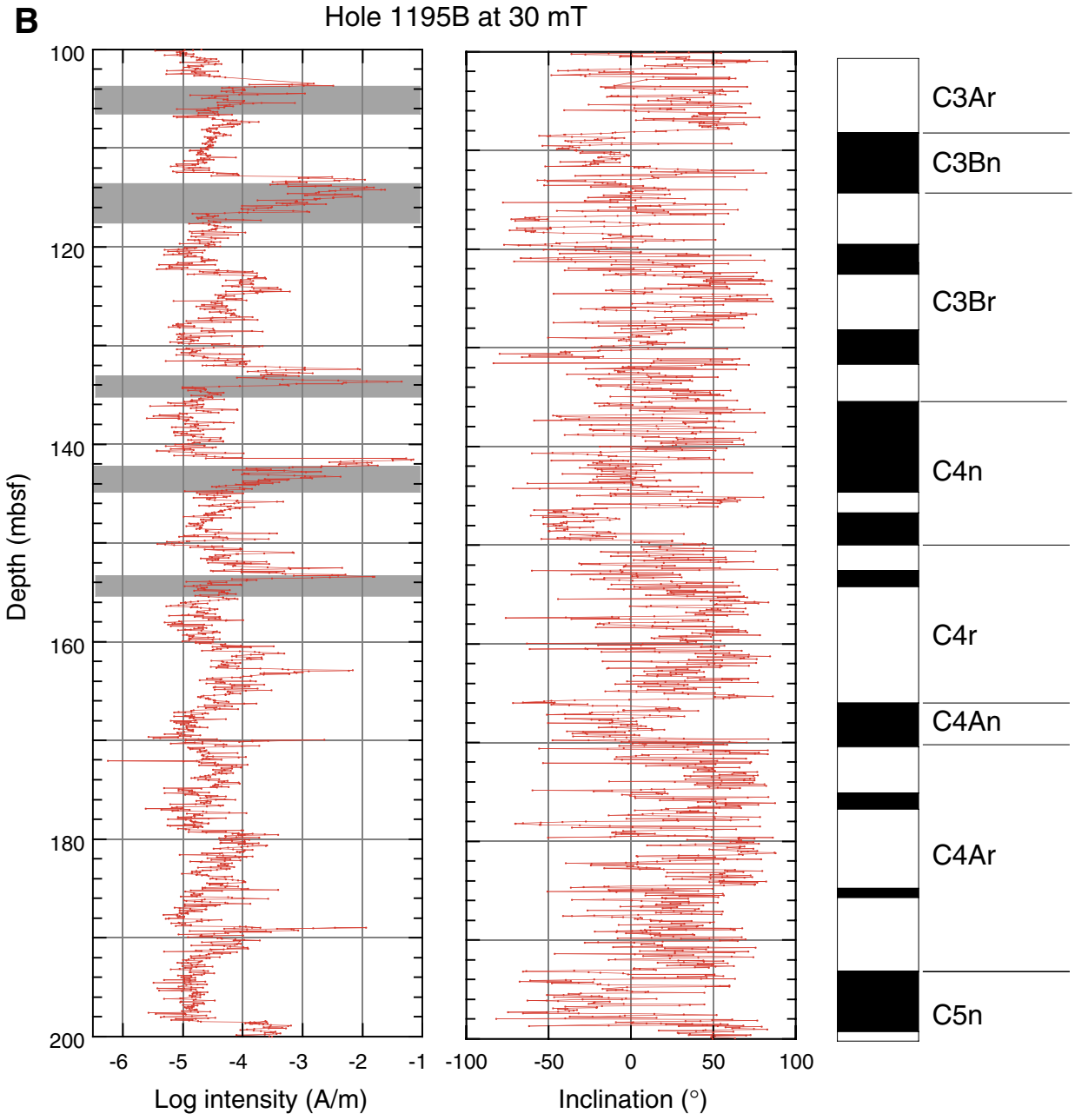

**Figure F12 (continued).** C. 200–300 mbsf.

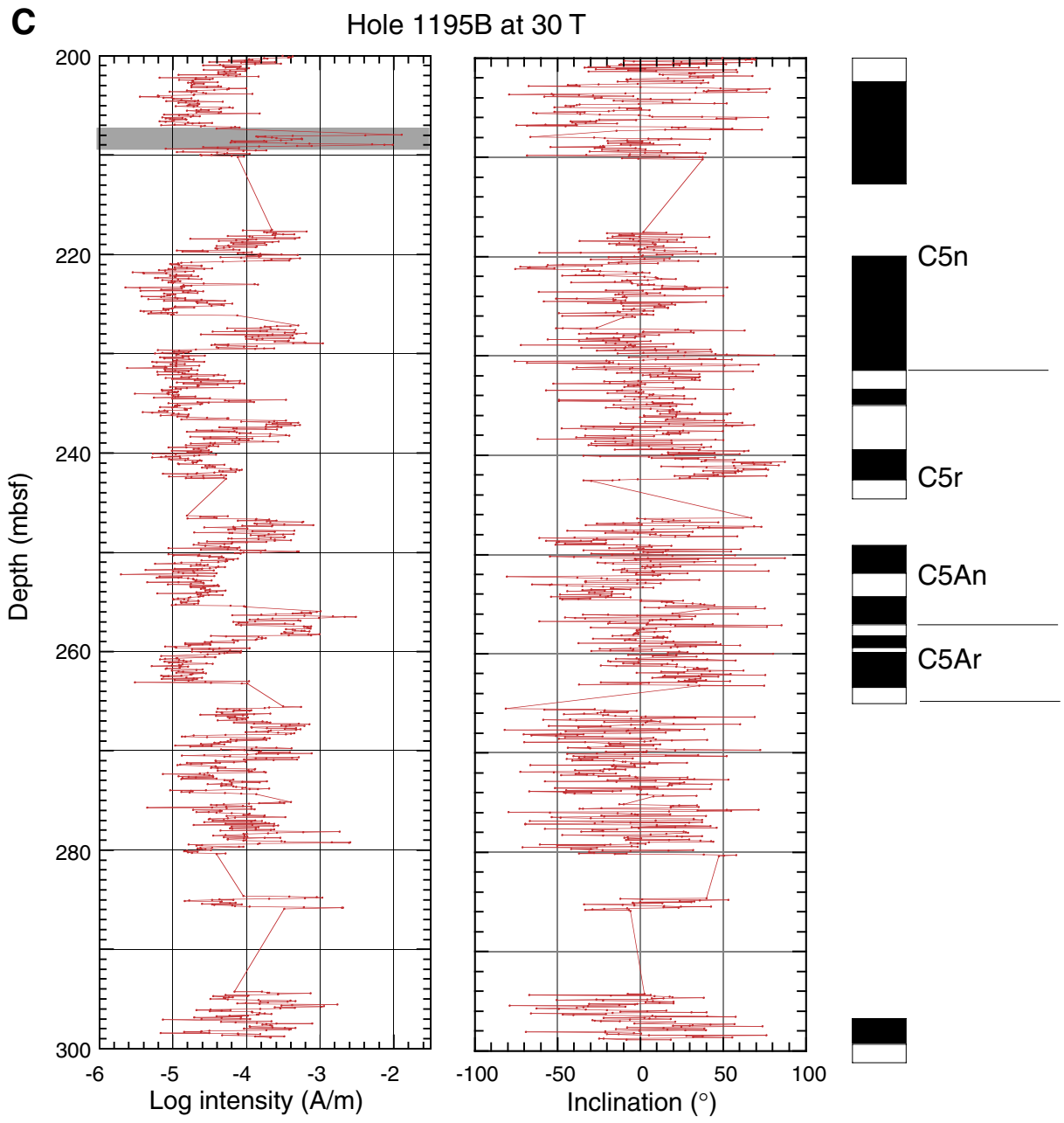

**Figure F12 (continued).** D. 300–400 mbsf.

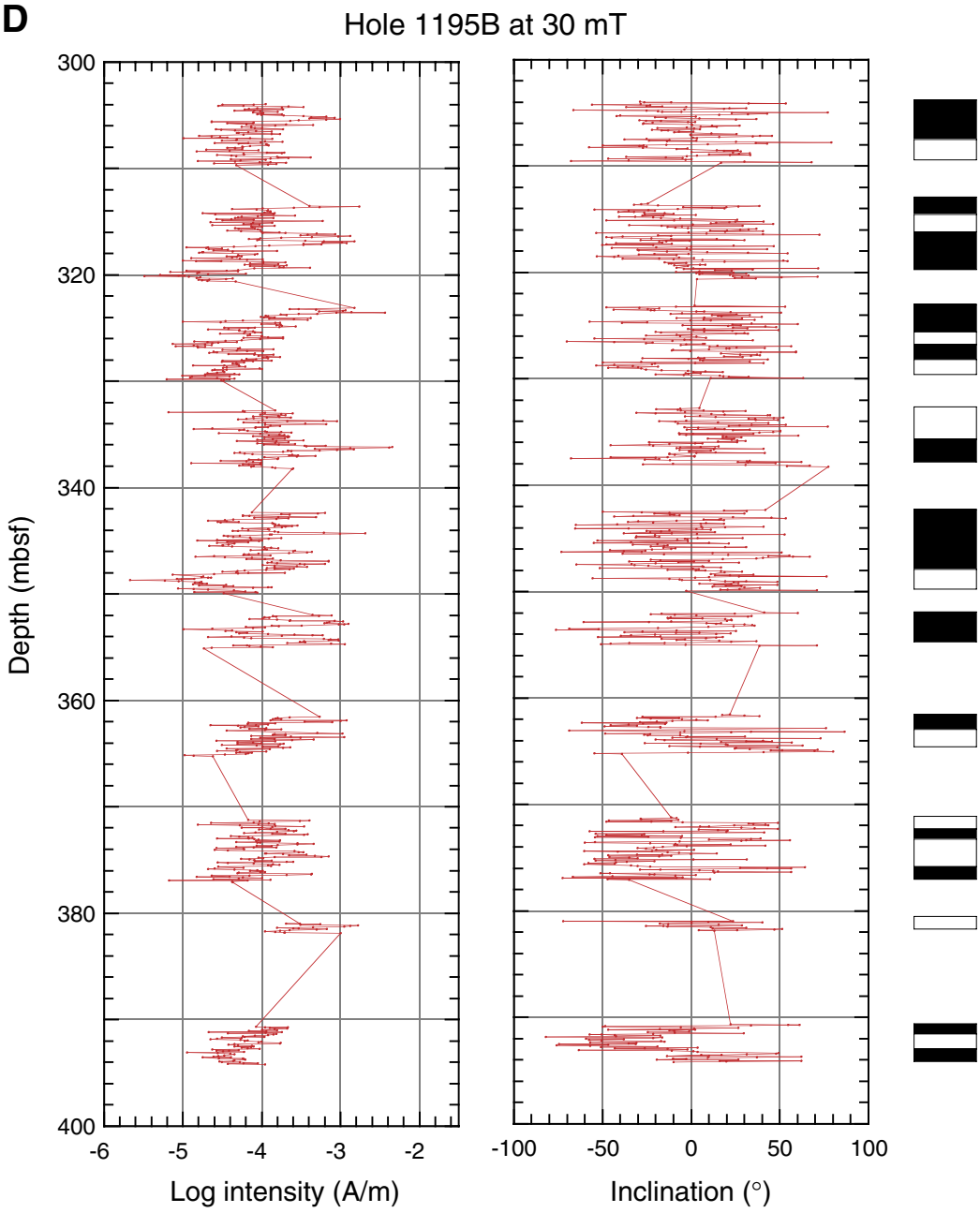

**Figure F12 (continued).** E. 400–500 mbsf.

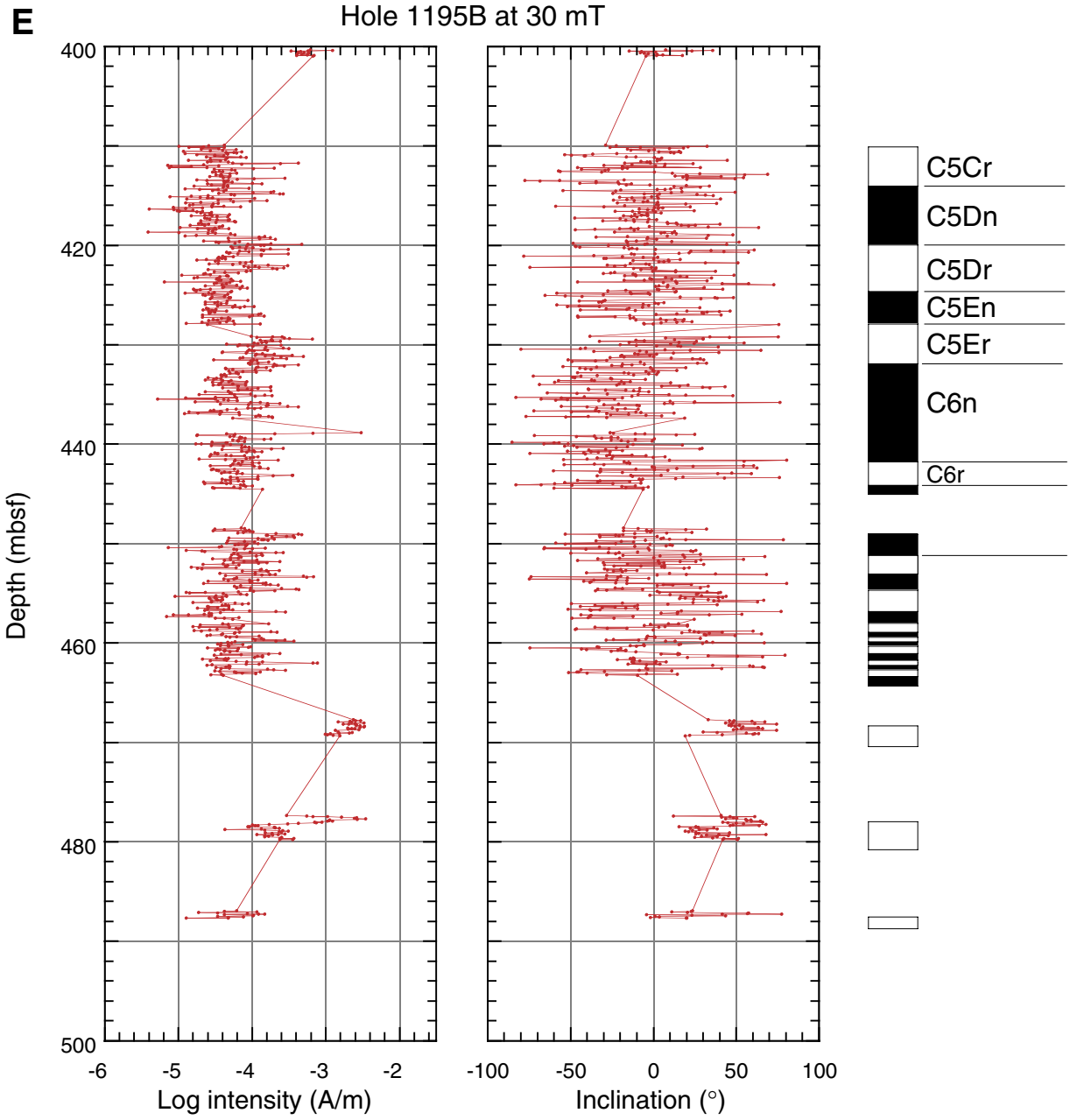

**Figure F12 (continued).** F. 500–520 mbsf.

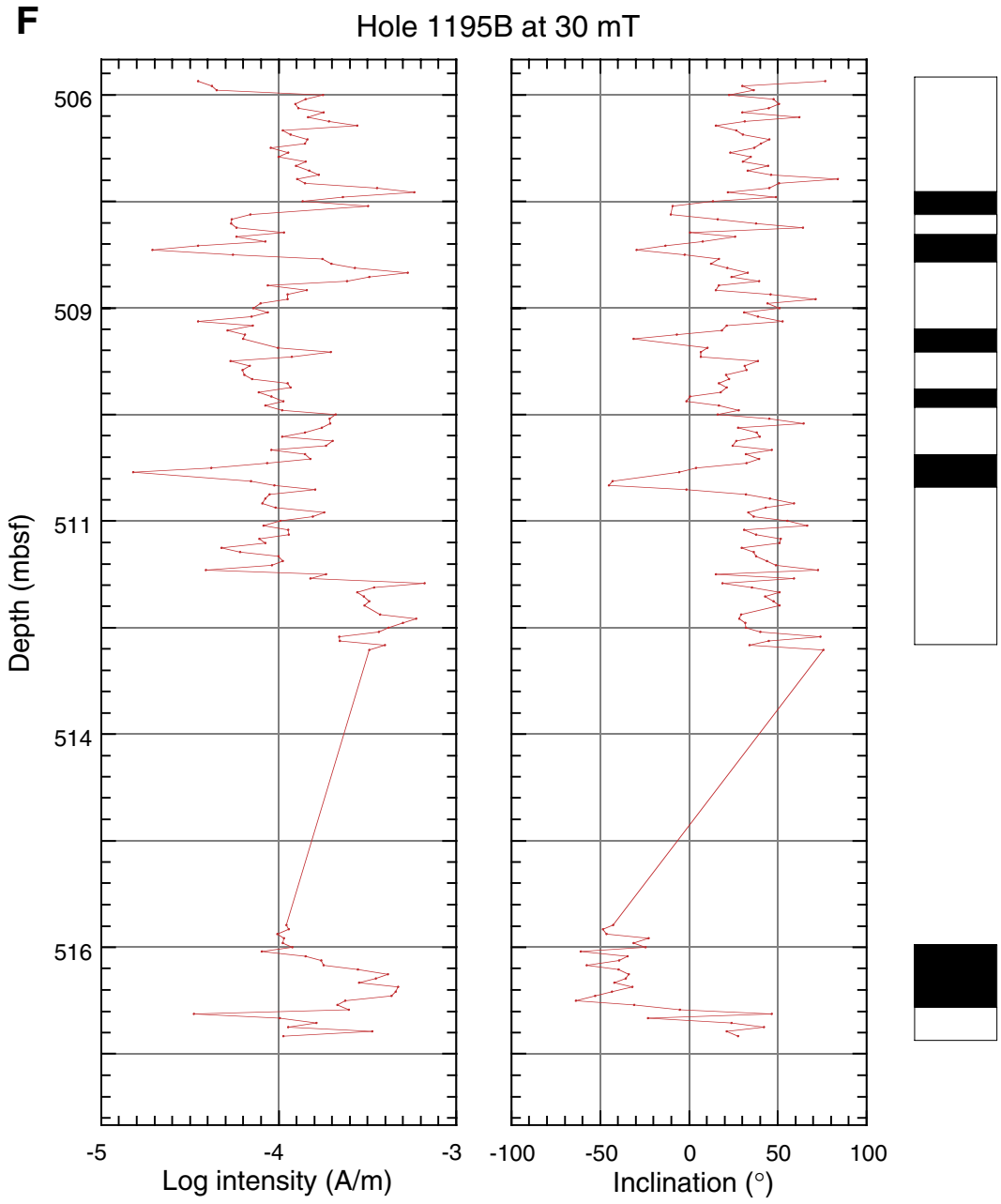

**Figure F13.** Comparison of the observed magnetic stratigraphy with the geomagnetic polarity timescale (Berggren et al., 1995).

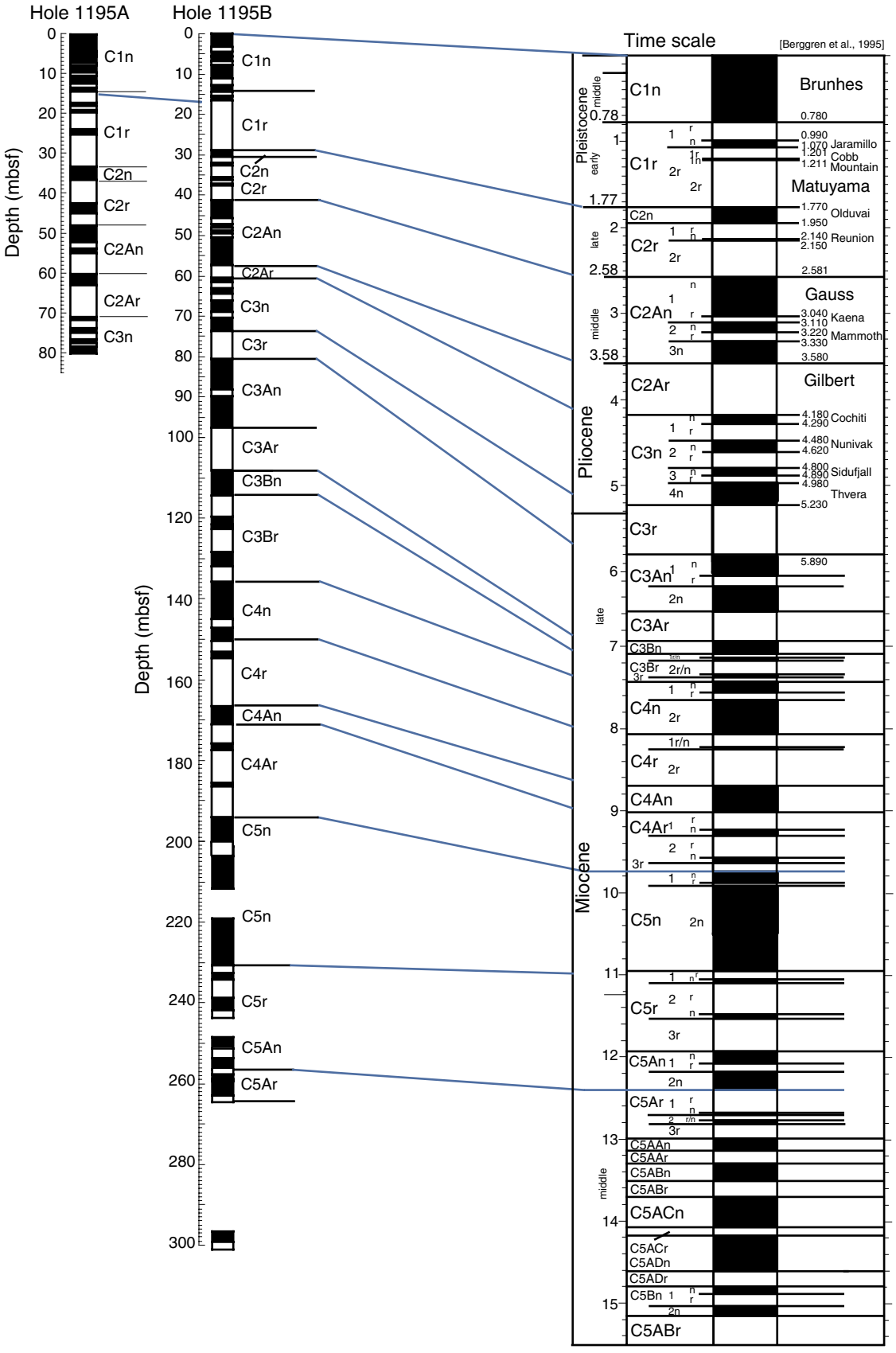

**Figure F14.** Age-depth model and sedimentation rates at Site 1195. Horizontal lines spanning from the left figure margin to the age-depth curve are lithologic unit (solid) and subunit (dashed) boundaries. Horizontal lines spanning from the right margin of the figure to the age-depth curve are seismic megasequence boundaries (solid) and major reflectors within megasequences (dashed). Vertical lines are epoch boundaries as labeled at the top of the diagram. MS = Megasequence.

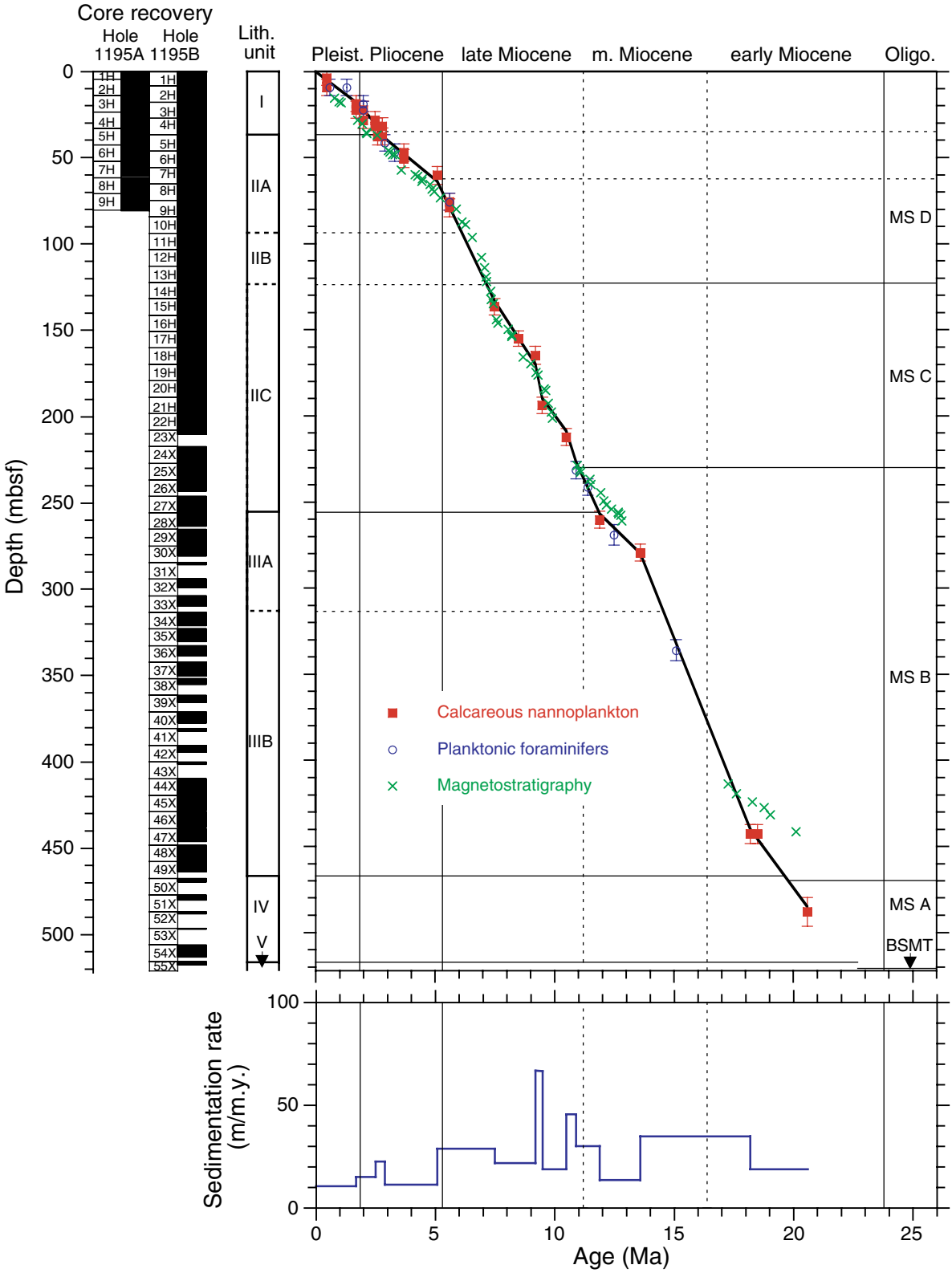

**Figure F15.** Concentrations of dissolved constituents vs. depth, Site 1195. **A.** Chloride. **B.** Alkalinity. **C.** Sulfate. **D.** Ammonium. **E.** Magnesium. **F.** Calcium. **G.** Strontium. **H.** Potassium. Solid circles = Hole 1195A, open circles = Hole 1195B.

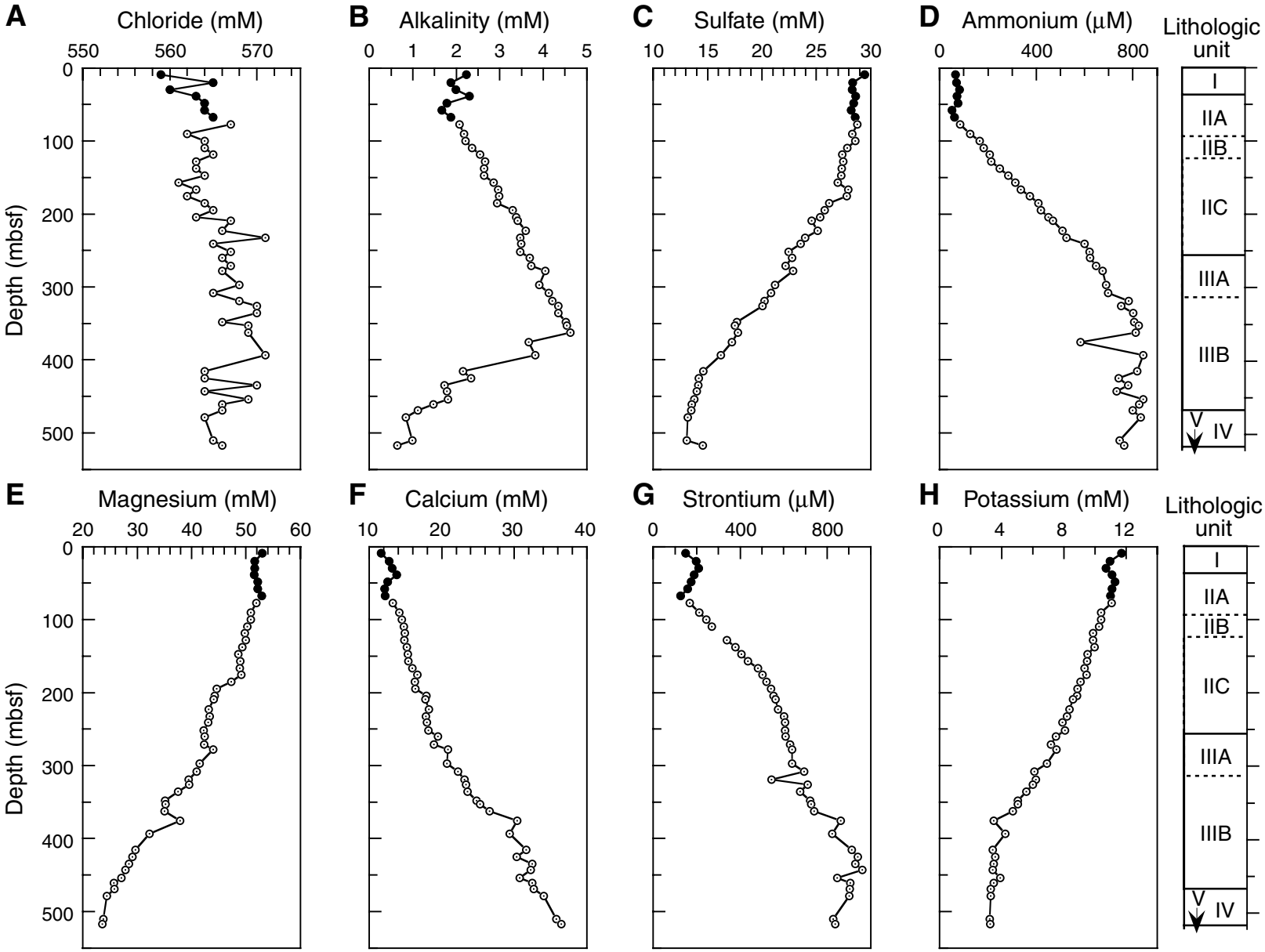

**Figure F16.** Dissolved magnesium vs. calcium, Site 1195. Solid blue circles = Hole 1195A, open blue circles = Hole 1195B. Also shown is the linear trend line with equation and correlation coefficient.

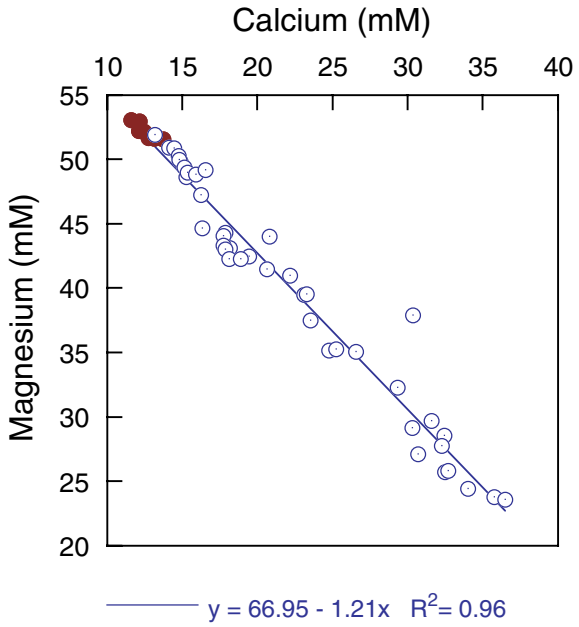

**Figure F17.** Percentages of carbonate minerals and noncarbonate fraction, Site 1195.

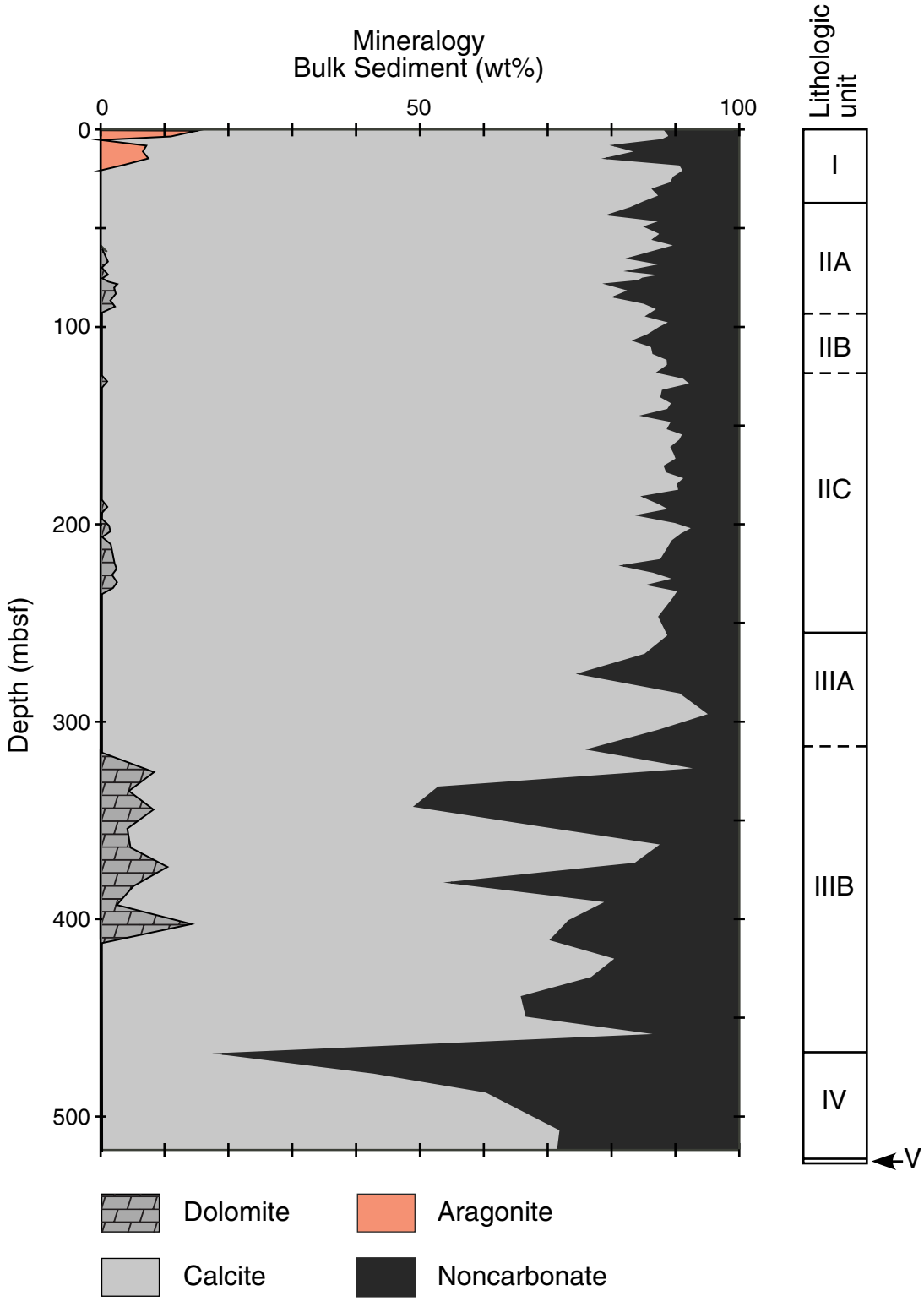

**Figure F18.** Plots of carbonate and total organic carbon content, hydrogen index values, total sulfur content, and C/N and C/S ratios, Site 1195. Solid vertical lines at HI = 150 and C/S = 2 mark the approximate boundary between terrigenous (<150) and marine organic matter and the transition between marine and brackish environments of formation, respectively.

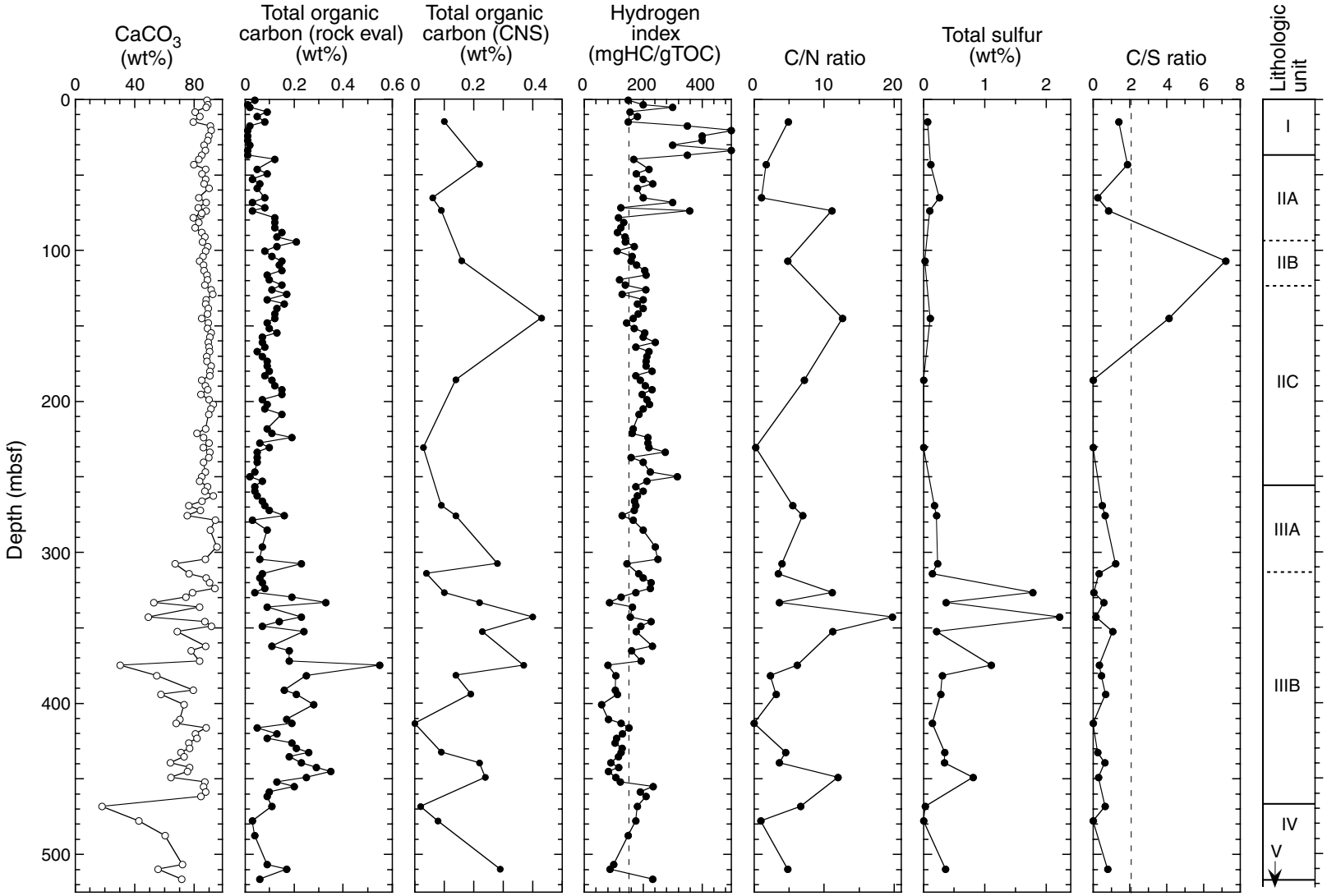

**Figure F19.** GRA bulk density (black dots) and MAD bulk density (red circles) plotted as a function of depth for Site 1195.

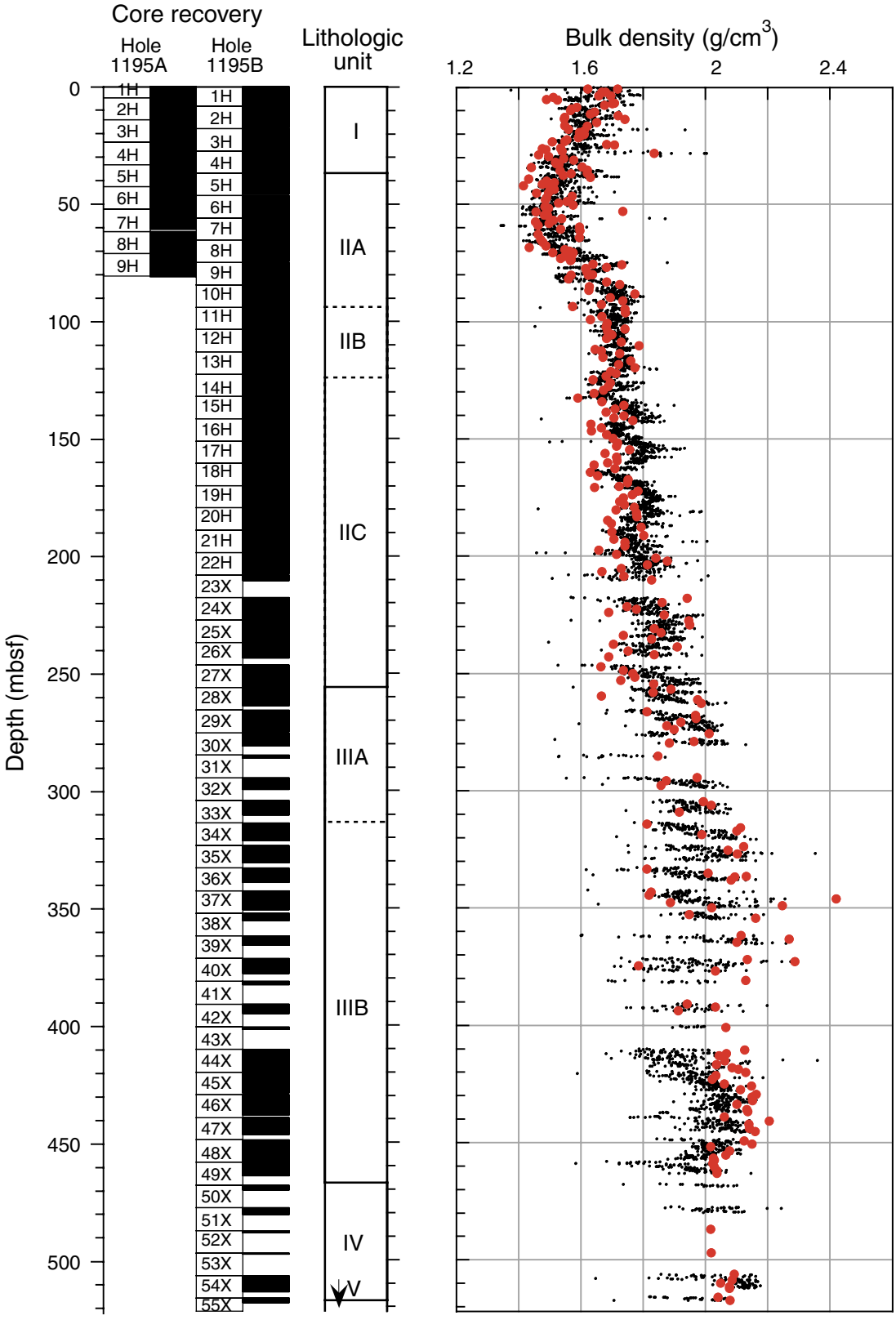

**Figure F20. A.** Bulk density, grain density, and porosity as a function of depth at Site 1195. Exponential least-squares regression of porosity using the combined Holes 1195A and 1195B data set (line) is superimposed on the porosity values (solid circles). (Continued on next two pages.)

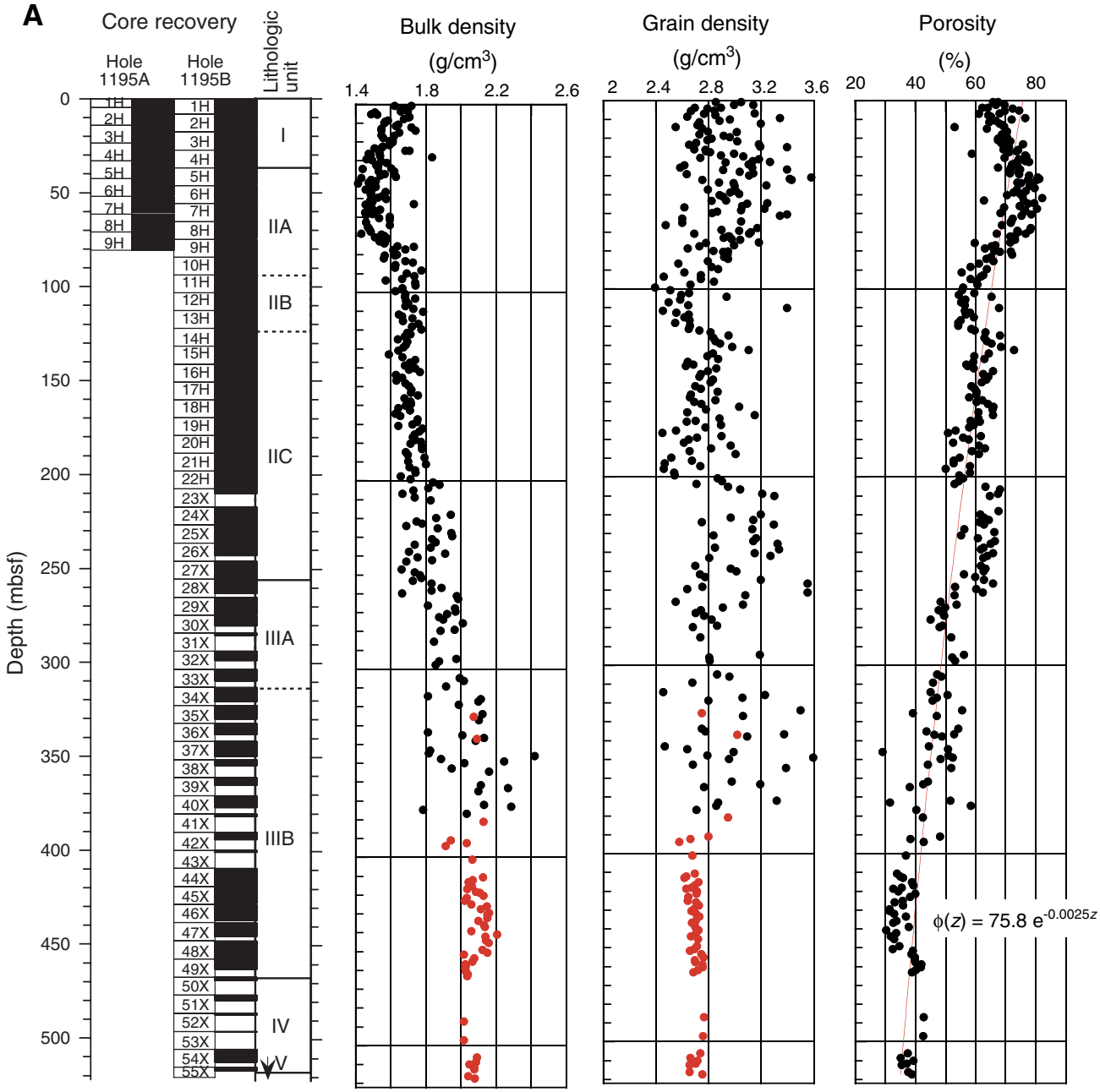

**Figure F20 (continued). B.** Comparison of original and remeasured grain density. Open circles = original beaker sample estimates, solid circles = original cube sample estimates, triangles = remeasured beaker sample estimates.

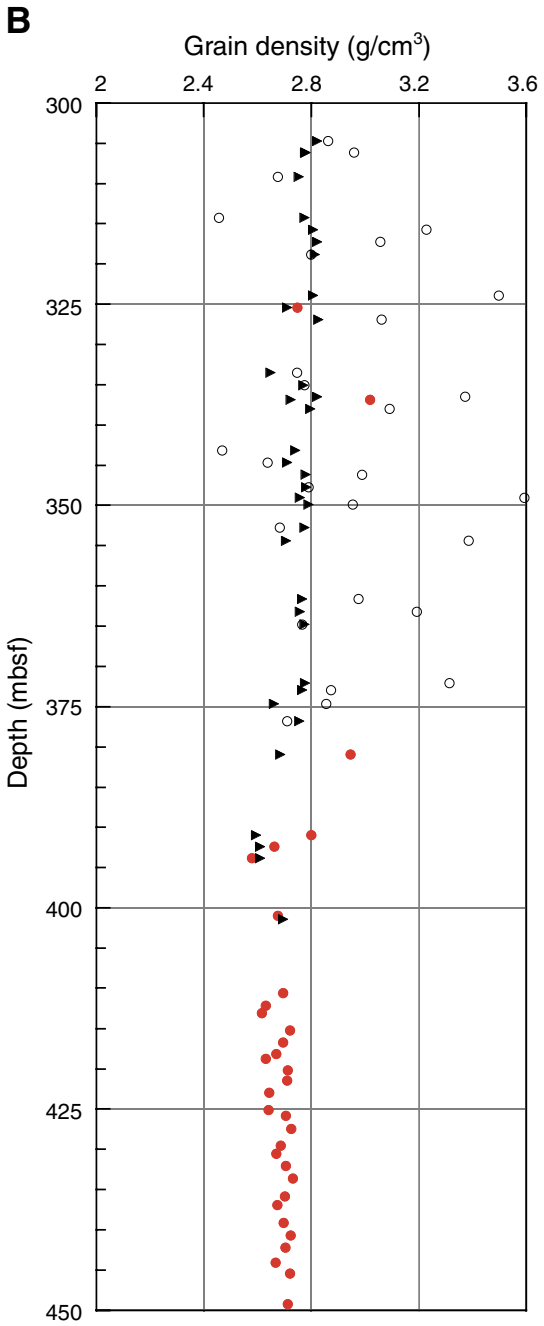

**Figure F20 (continued).** C. Residual porosity, being the difference between the observed porosity and the exponential least-squares regression shown in Figure F20A, p. 53, compared with carbonate grain size and lithologic units. Prominent offsets in the residual porosity are highlighted.

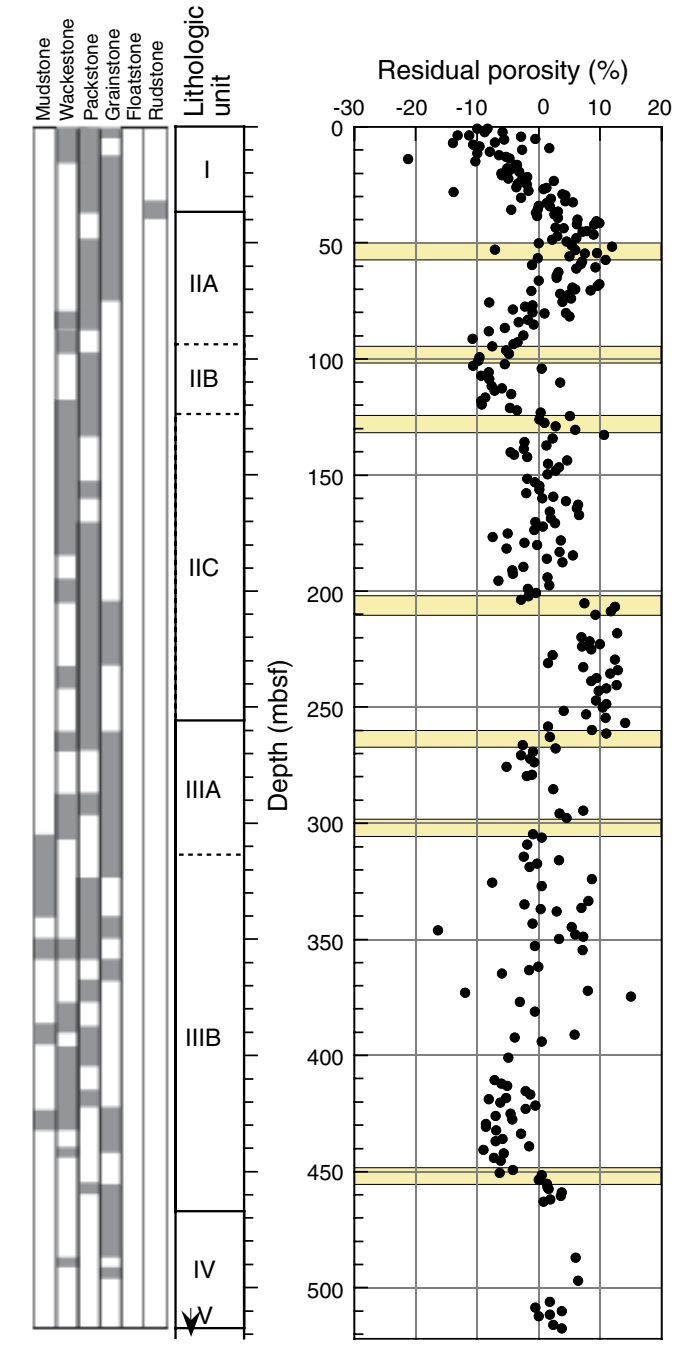

**Figure F21.** *P*-wave velocity as a function of depth at Site 1195 using the PWS1 (z-direction) and PWS2 (y-direction) insertion probe system and the PWS3 contact probe system. **A.** Original (solid and open circles) and adjusted (solid circles) velocities. Circles represent data affected by measurement errors. For data offsets below 120 mbsf, a correction of 100 m/s was applied. For data between 200 and 250 mbsf, velocity values were reduced by 310 m/s. **B.** Seismic anisotropy between the average transverse and longitudinal velocities as a function of depth. Location of dolomitized zones are shown by the yellow intervals.

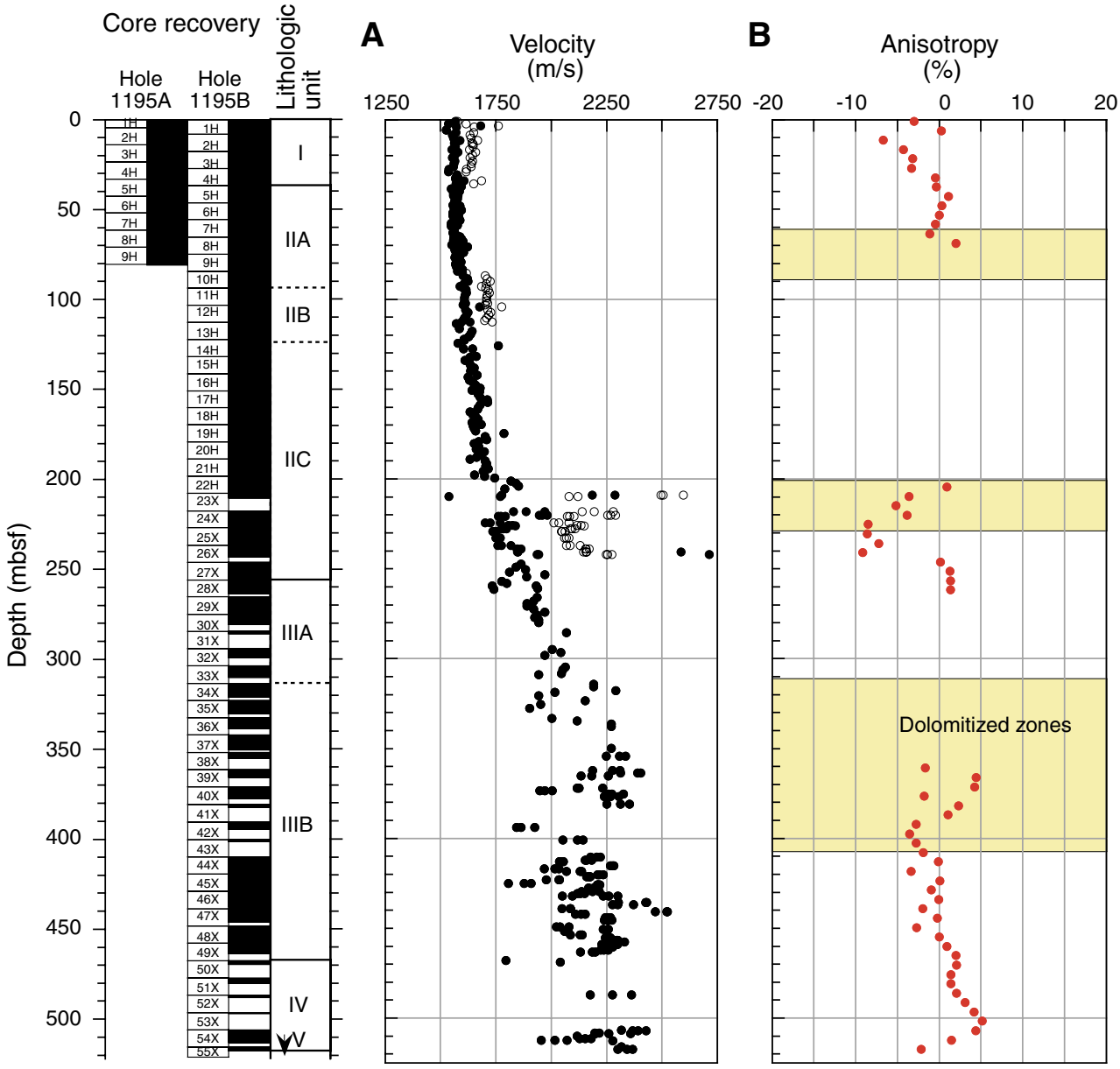

**Figure F22.** Crossplot of velocity vs. porosity for Site 1195. Bold and thin solid lines represent the time-average equations for calcite (Wyllie et al., 1956) and a power law least-squares fit to the velocity data, respectively.

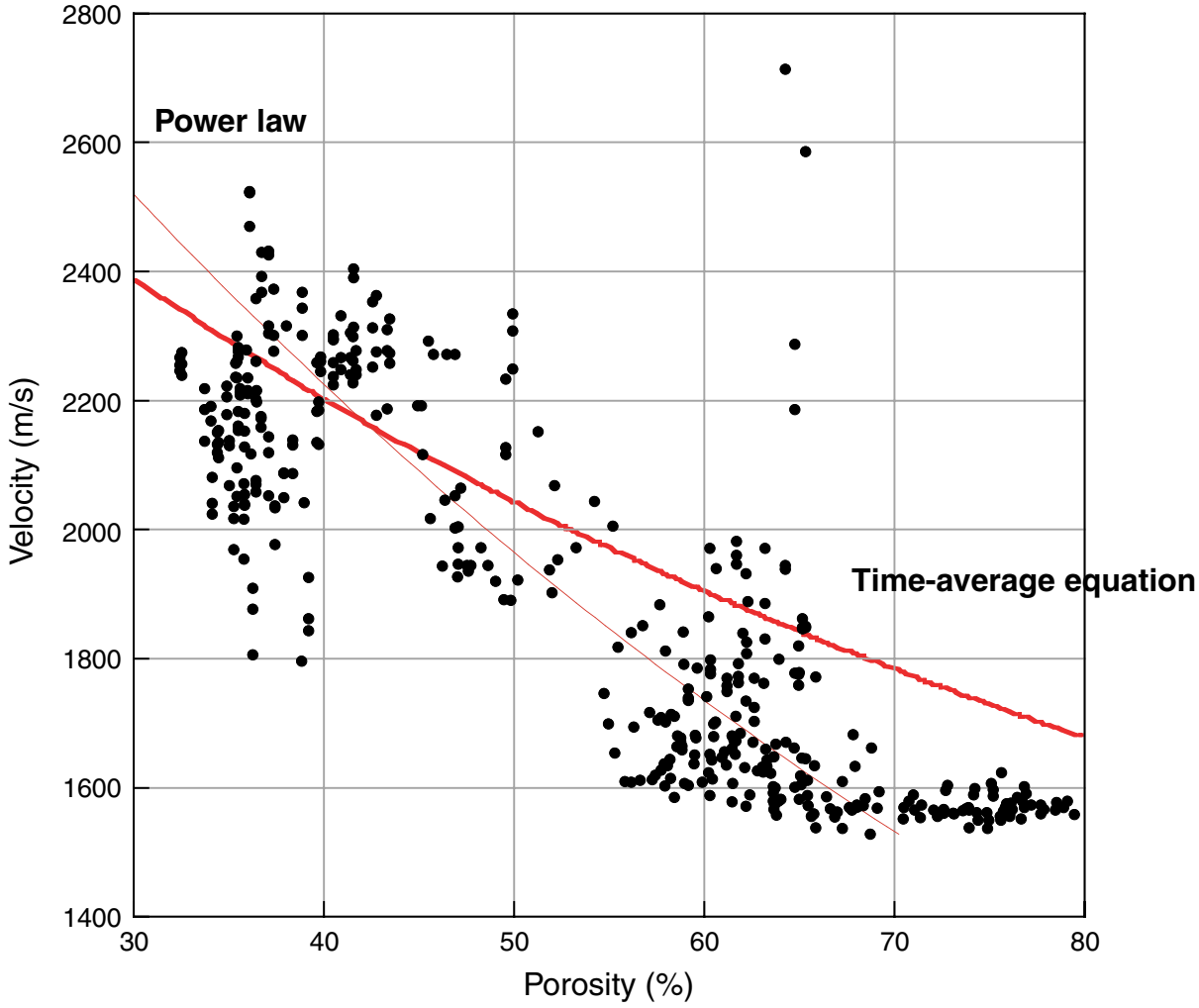

**Figure F23.** Average thermal conductivity as a function of depth for Site 1195.

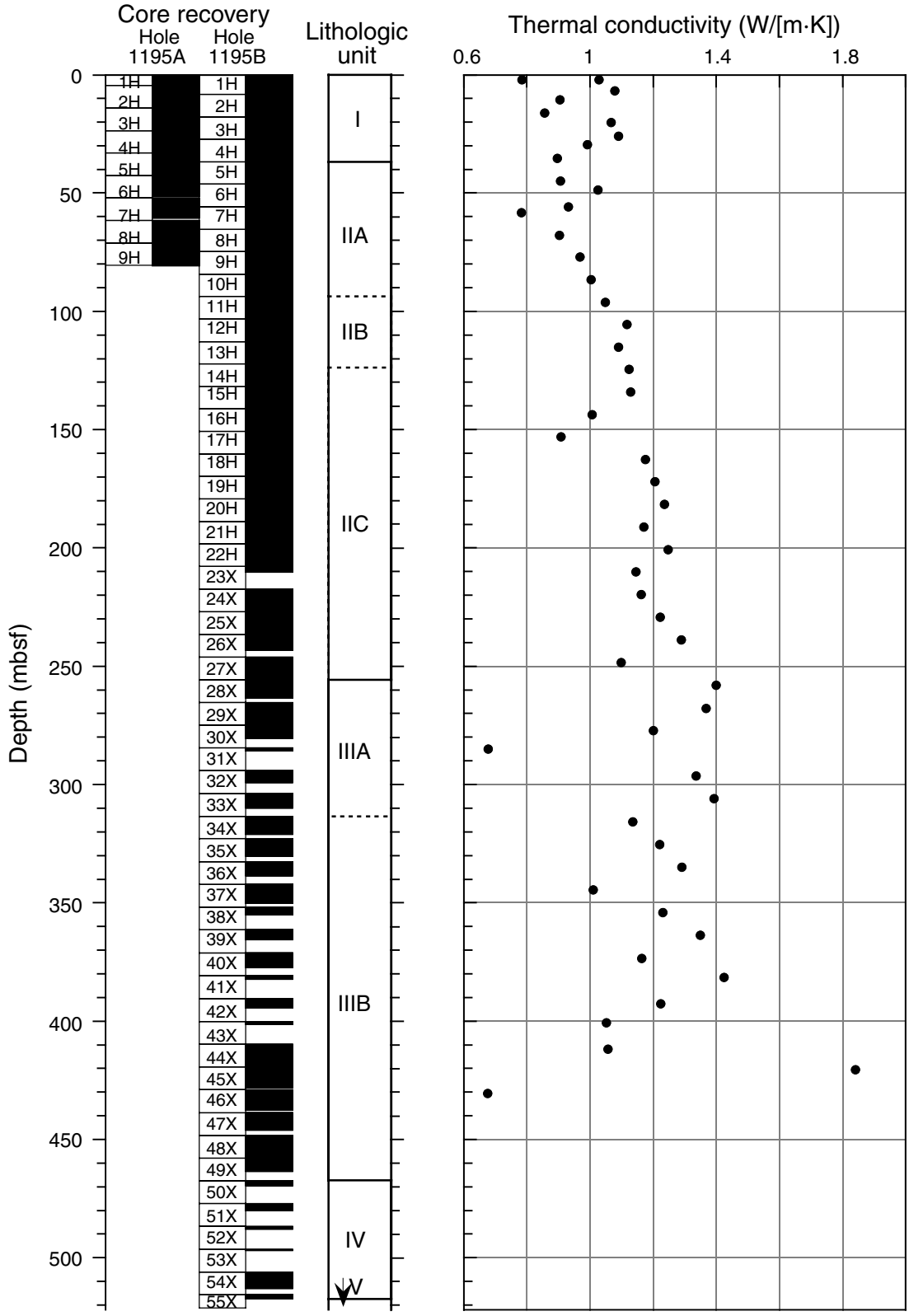

**Figure F24.** Crossplot of Site 1195 porosity and thermal conductivity. Superimposed are the power law curves, constructed from the observed range in porosity, for ideal end-member sedimentary facies: sandstones (red/upper curve), limestones (blue/center curve) and shales (black/lower curve). The observed thermal conductivity values lay between the shale and sandstone curves, and given the large carbonate content of the sedimentary section, suggests that much of the sediment at Site 1195 represents a mixing of clay and sandstone with carbonates.

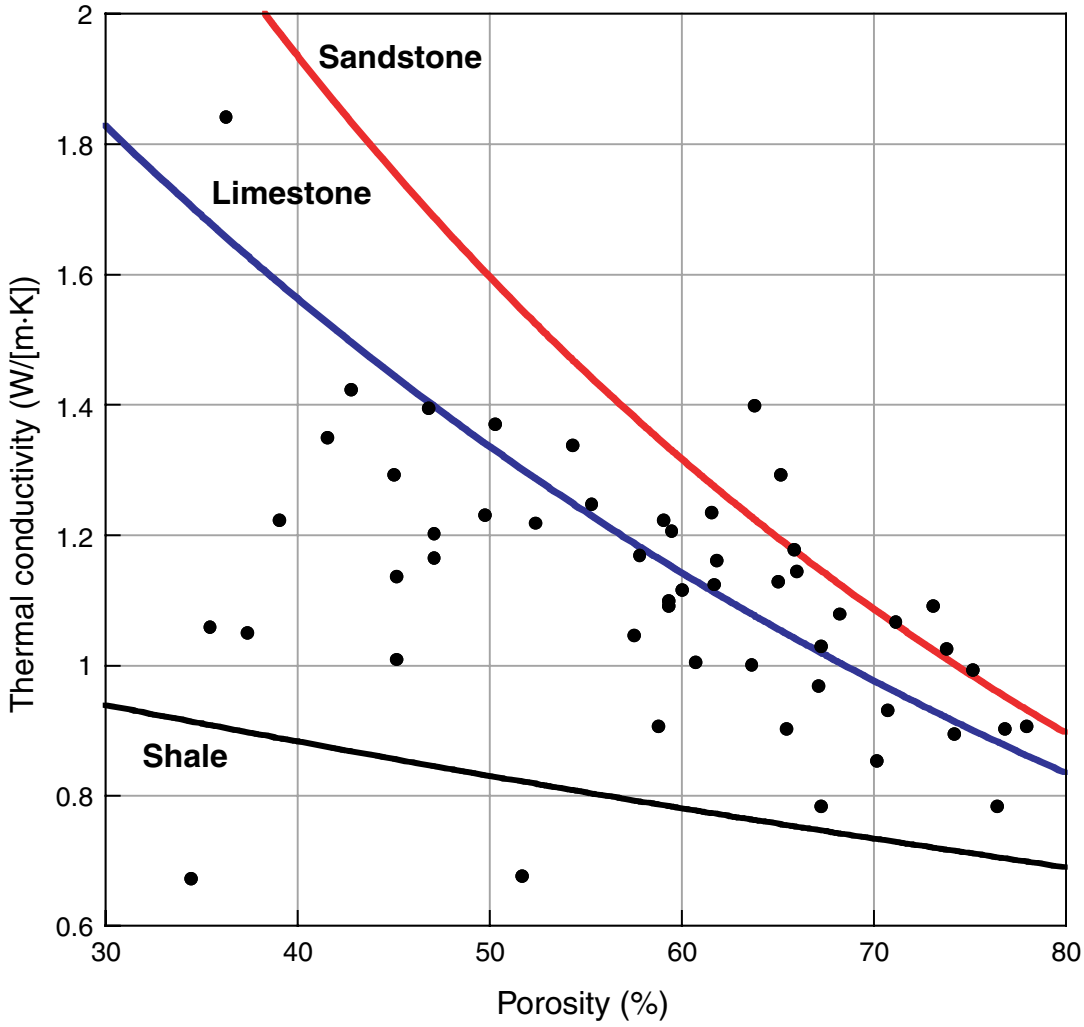

**Figure F25.** Comparison of magnetic susceptibility (MS) (line = Hole 1195A; circles = Hole 1195B), carbonate content (triangles), natural gamma radiation (NGR) (line = 1195A; dots = 1195B) and color reflectance (thin gray line) for Site 1195.

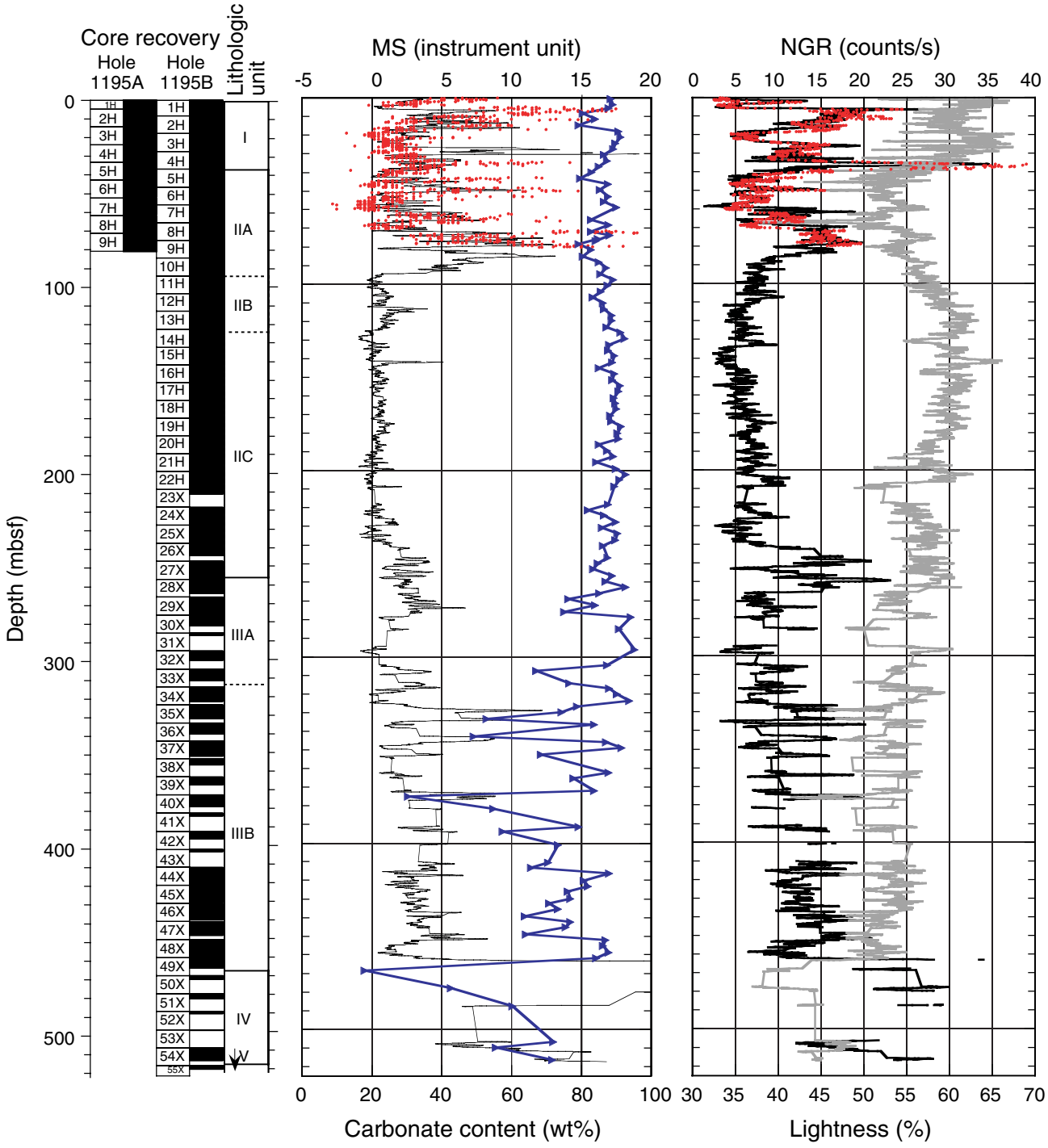

**Figure F26.** Depth offset between Holes 1195A and 1195B estimated from (**A**, **B**) magnetic susceptibility and (**C**, **D**) natural gamma radiation data for the interval 0–150 mbsf. The correspondence of the NGR peak at 36 mbsf suggests minimal offset between the two holes. However, the correspondence is not as good for the magnetic susceptibility data (e.g., the interval at 27–30 mbsf in Hole 1195B that does not seem to exist in Hole 1195A).

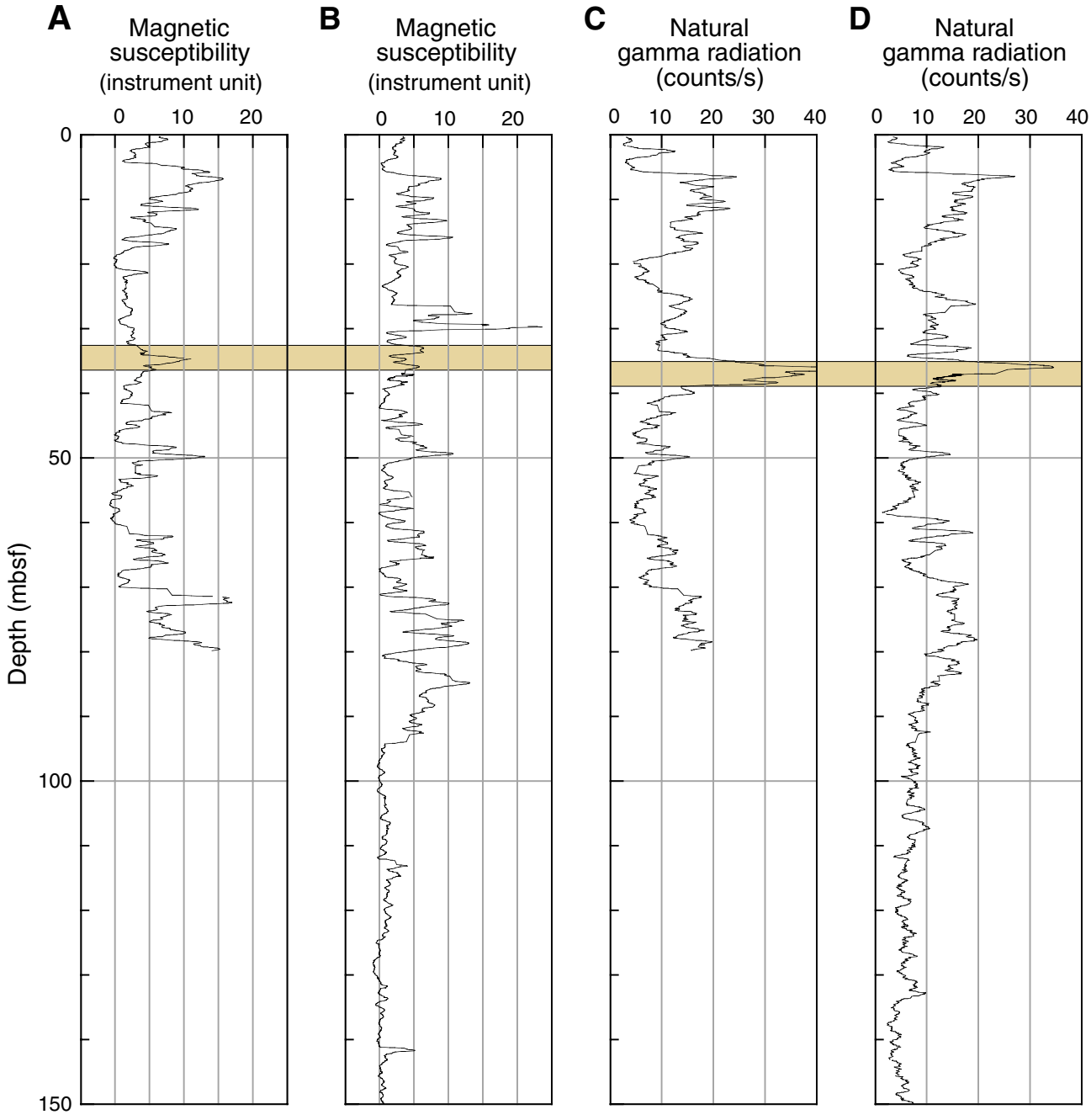

**Figure F27. A.** Comparison between the color reflectance parameter a* (left graph), the MST-NGR (red dots), and the logging HNGS (black line) gamma radiation data and glauconite-rich sediment units (yellow intervals) for Site 1195B. (Continued on next page.)

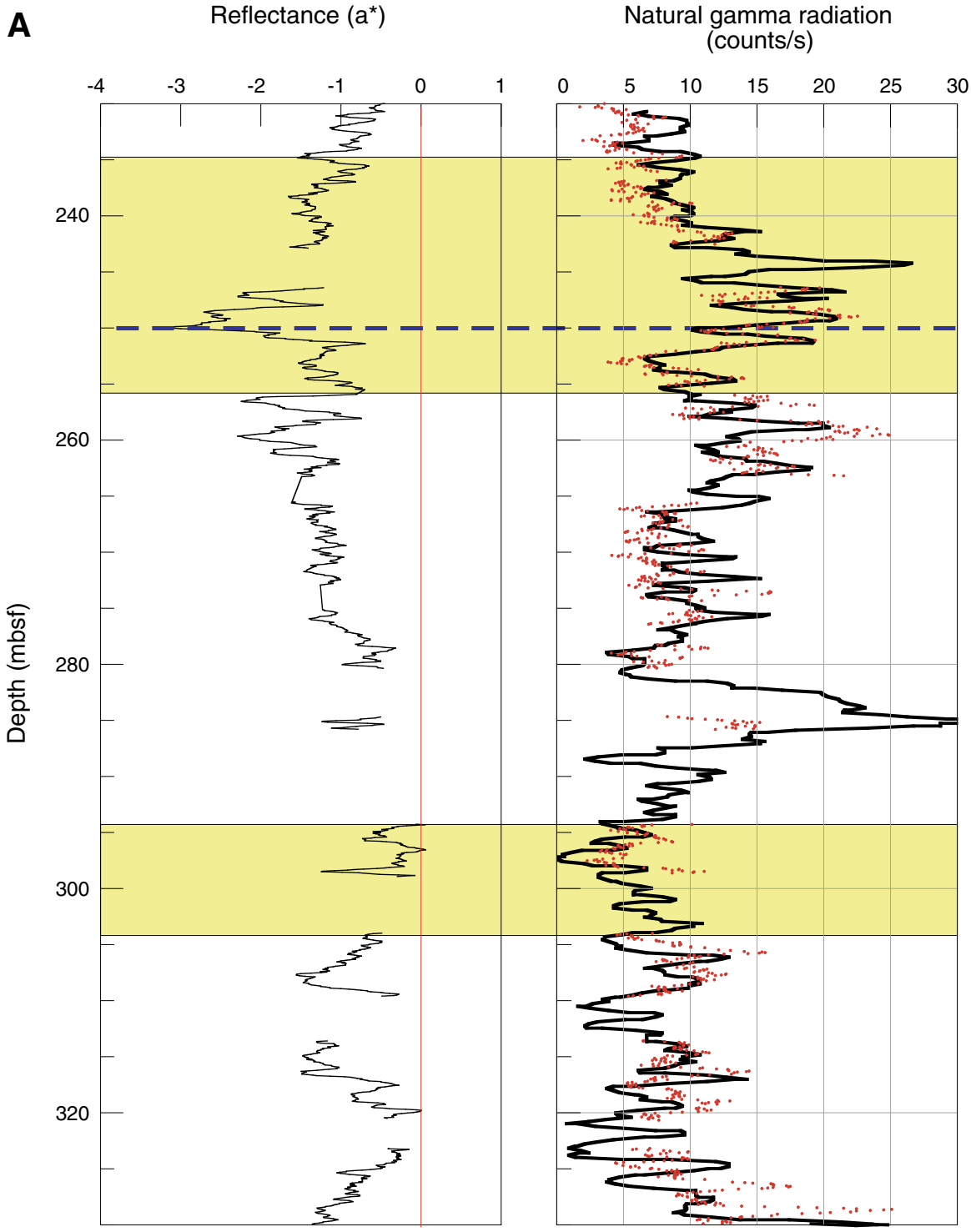

**Figure F27 (continued). B.** Comparison between color reflectance parameter a* (left graph), magnetic susceptibility (red line), and glauconite-rich units (yellow intervals) for Site 1195B. The glauconite-rich intervals do not show any correlation with the magnetic susceptibility.

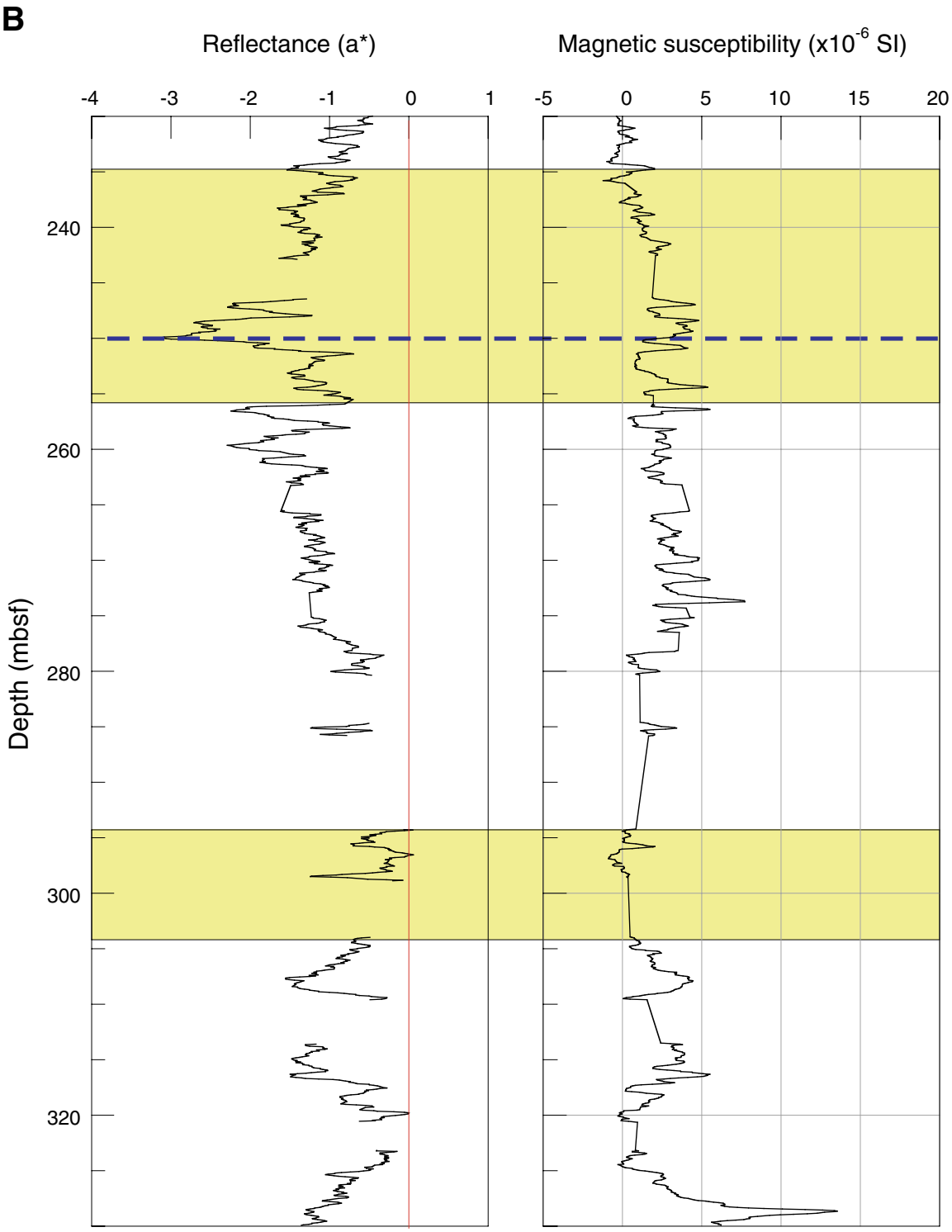

**Figure F28.** Downhole logging data at Site 1195. Logging units, megasequence boundaries, and lithologic units are shown for comparison. Gray rectangles in the natural gamma ray column = intervals identified in the core as glauconite-rich sediments (see Fig. F4, p. 32). The darker the gray rectangle, the more glauconite is present.

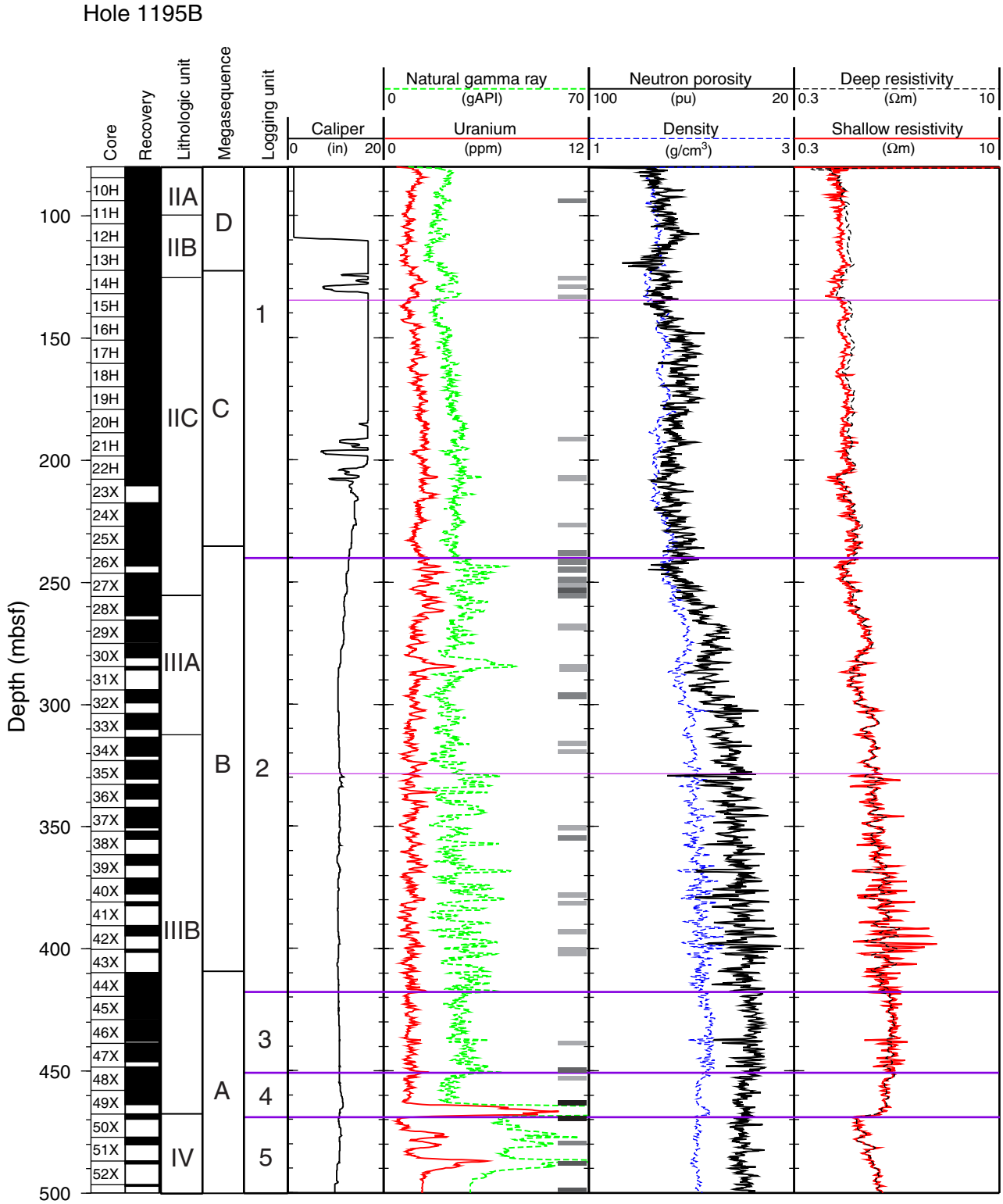

**Figure F29.** Comparison of core measurements and corresponding downhole logs at Site 1195. There is an overall good correlation of the curve shapes, with slight differences in absolute values in density. Note the different units for the core and log natural gamma ray data.

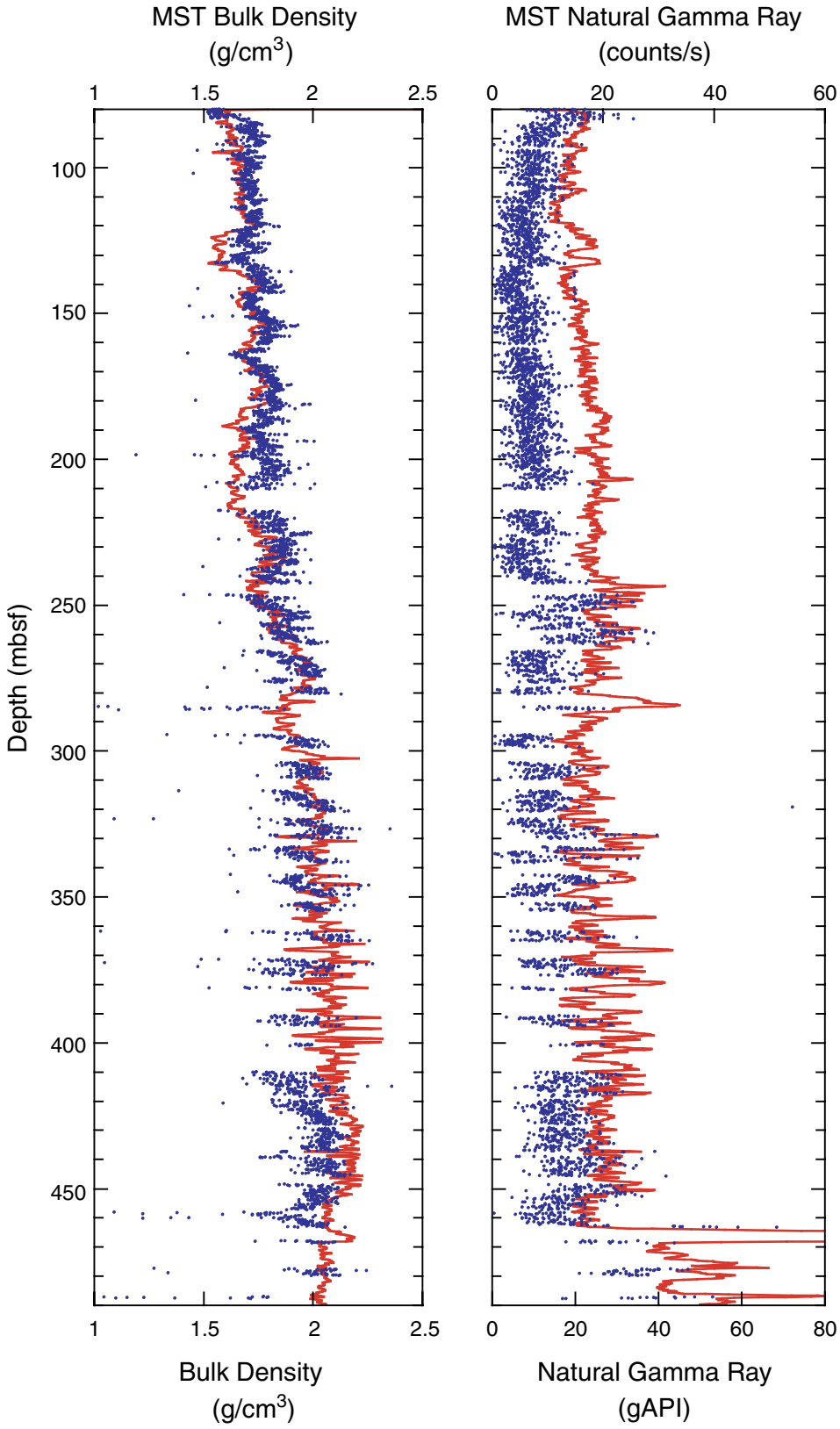

**Figure F30.** Log spectral gamma ray data showing potassium, thorium, and uranium concentrations. Note the high amount and variability of potassium and thorium in the lower half of logging Unit 2.

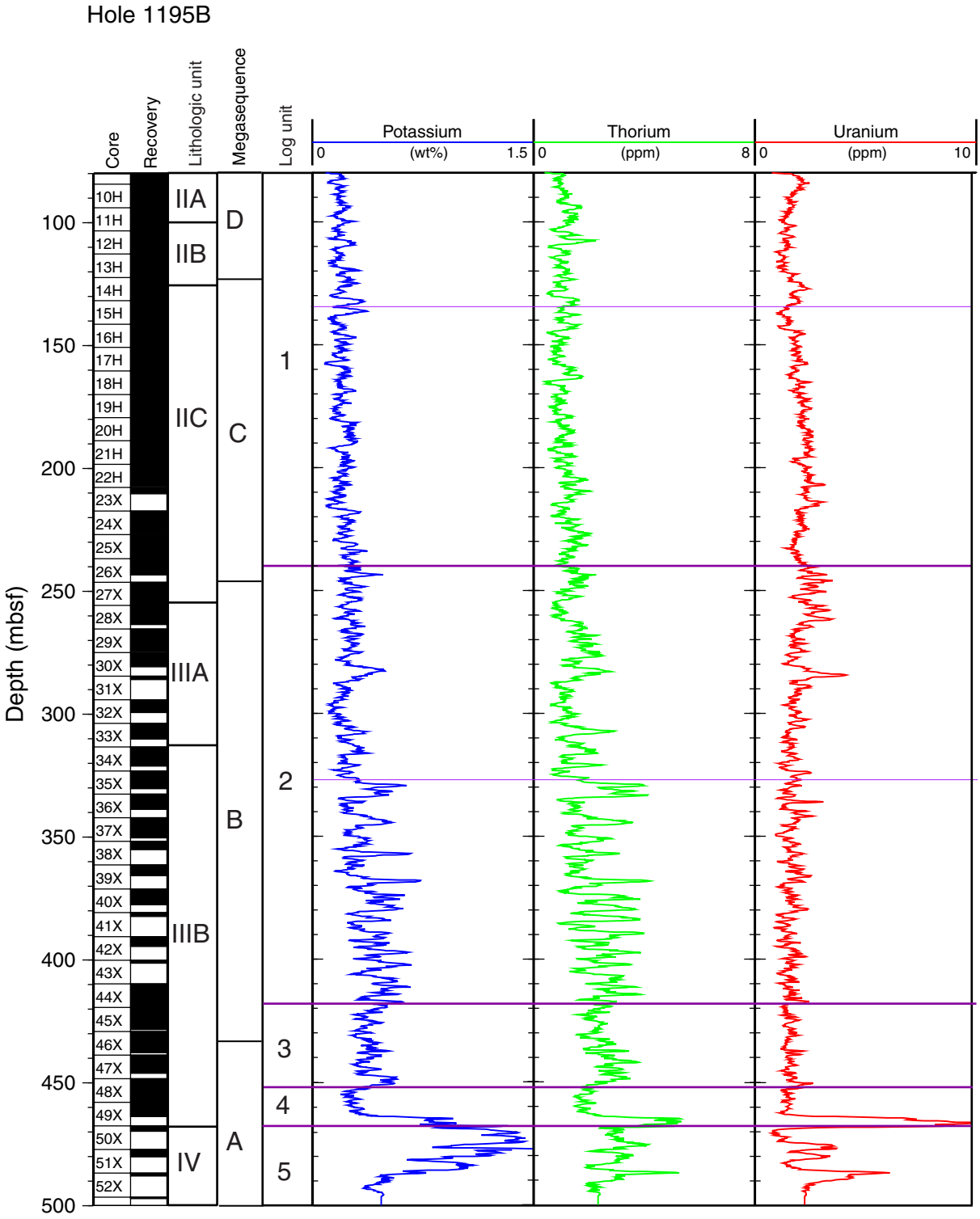

**Figure F31.** Temperature profile in Hole 1195B measured with the LDEO temperature tool.

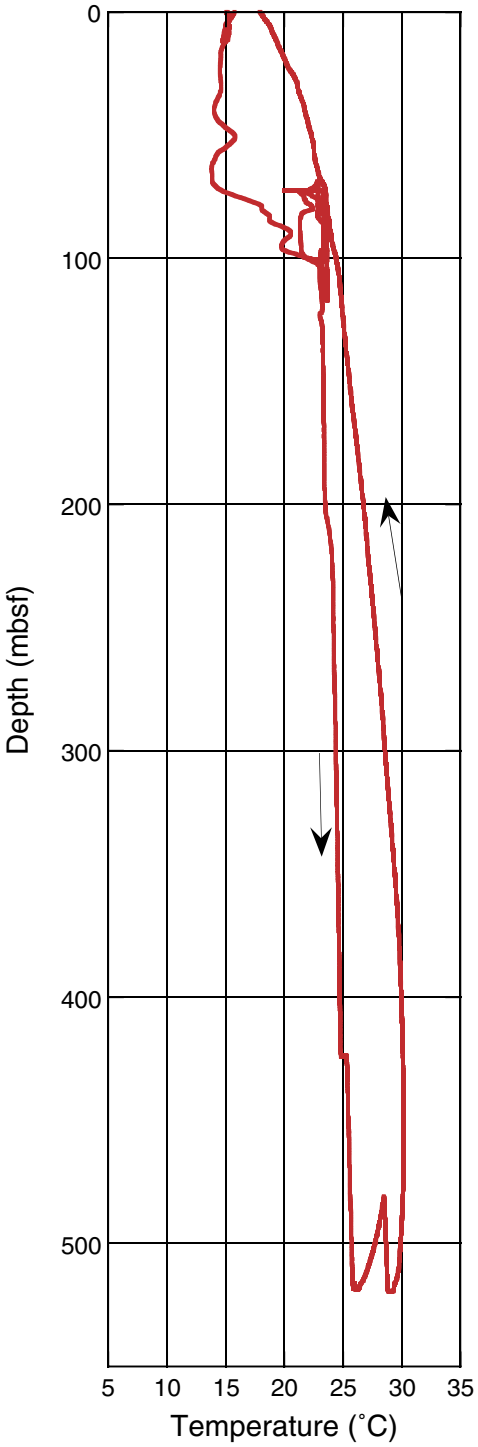

**Figure F32.** Synthetic seismogram plotted on line MAR15 with two-way traveltime-to-depth velocity data (m/s), *P*-wave velocity and GRA bulk density, extracted sonic wavelet, synthetic seismogram, the megasequence boundaries, and lithologic boundaries. The traveltime vs. depth plot was used to correlate seismic reflection events and their location with depth in the sedimentary section.

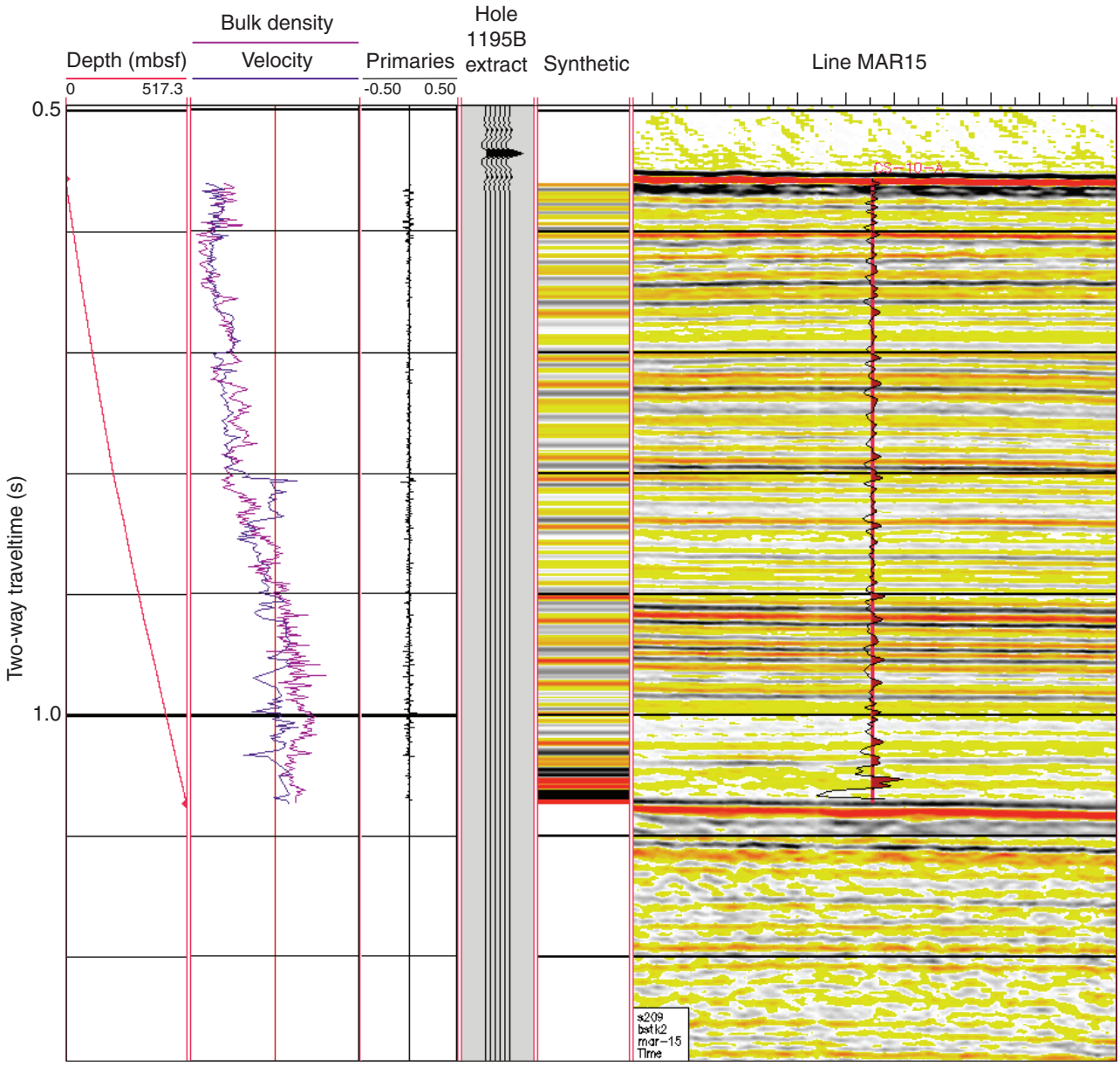

**Table T1.** Coring summary, Site 1195.

| Core | Date (Jan. 2001) | Time (local) | Depth (mbsf) Top | Depth (mbsf) Bottom | Length (m) Cored | Length (m) Recovered | Recovery (%) |
|---|---|---|---|---|---|---|---|
| 194-1195A- | | | | | | | |
| 1H | 26 | 0915 | 0.0 | 4.7 | 4.7 | 4.75 | 101.1 |
| 2H | 26 | 0945 | 4.7 | 14.2 | 9.5 | 9.57 | 100.7 |
| 3H | 26 | 1010 | 14.2 | 23.7 | 9.5 | 9.50 | 100.0 |
| 4H | 26 | 1105 | 23.7 | 33.2 | 9.5 | 9.46 | 99.6 |
| 5H | 26 | 1130 | 33.2 | 42.7 | 9.5 | 9.26 | 97.5 |
| 6H | 26 | 1155 | 42.7 | 52.2 | 9.5 | 8.89 | 93.6 |
| 7H | 26 | 1235 | 52.2 | 61.7 | 9.5 | 8.63 | 90.8 |
| 8H | 26 | 1330 | 61.7 | 71.2 | 9.5 | 9.43 | 99.3 |
| 9H | 26 | 1815 | 71.2 | 80.7 | 9.5 | 9.78 | 102.9 |
| | | | | Cored total: | 80.7 | 79.27 | 98.2 |
| | | | | Drilled total: | 0.0 | | |
| | | | | Total: | 80.7 | | |
| 194-1195B- | | | | | | | |
| 1H | 26 | 2245 | 0.0 | 8.4 | 8.4 | 8.41 | 100.1 |
| 2H | 26 | 2320 | 8.4 | 17.9 | 9.5 | 9.14 | 96.2 |
| 3H | 26 | 2350 | 17.9 | 27.4 | 9.5 | 9.36 | 98.5 |
| 4H | 27 | 0020 | 27.4 | 36.9 | 9.5 | 9.52 | 100.2 |
| 5H | 27 | 0050 | 36.9 | 46.4 | 9.5 | 9.02 | 94.9 |
| 6H | 27 | 0120 | 46.4 | 55.9 | 9.5 | 9.17 | 96.5 |
| 7H | 27 | 0145 | 55.9 | 65.4 | 9.5 | 9.88 | 104.0 |
| 8H | 27 | 0215 | 65.4 | 74.9 | 9.5 | 9.01 | 94.8 |
| 9H | 27 | 0245 | 74.9 | 84.4 | 9.5 | 9.62 | 101.3 |
| 10H | 27 | 0315 | 84.4 | 93.9 | 9.5 | 9.75 | 102.6 |
| 11H | 27 | 0345 | 93.9 | 103.4 | 9.5 | 9.60 | 101.1 |
| 12H | 27 | 0420 | 103.4 | 112.9 | 9.5 | 9.64 | 101.5 |
| 13H | 27 | 0605 | 112.9 | 122.4 | 9.5 | 9.95 | 104.7 |
| 14H | 27 | 0630 | 122.4 | 131.9 | 9.5 | 9.79 | 103.1 |
| 15H | 27 | 0700 | 131.9 | 141.4 | 9.5 | 9.79 | 103.1 |
| 16H | 27 | 0730 | 141.4 | 150.9 | 9.5 | 9.57 | 100.7 |
| 17H | 27 | 0855 | 150.9 | 160.4 | 9.5 | 9.85 | 103.7 |
| 18H | 27 | 0925 | 160.4 | 169.9 | 9.5 | 10.10 | 106.3 |
| 19H | 27 | 0945 | 169.9 | 179.4 | 9.5 | 9.99 | 105.2 |
| 20H | 27 | 1020 | 179.4 | 188.9 | 9.5 | 9.98 | 105.1 |
| 21H | 27 | 1045 | 188.9 | 198.4 | 9.5 | 10.06 | 105.9 |
| 22H | 27 | 1125 | 198.4 | 207.9 | 9.5 | 9.03 | 95.1 |
| 23X | 27 | 1215 | 207.9 | 217.5 | 9.6 | 2.59 | 27.0 |
| 24X | 27 | 1250 | 217.5 | 227.1 | 9.6 | 9.37 | 97.6 |
| 25X | 27 | 1315 | 227.1 | 236.7 | 9.6 | 9.96 | 103.8 |
| 26X | 27 | 1345 | 236.7 | 246.3 | 9.6 | 6.67 | 69.5 |
| 27X | 27 | 1405 | 246.3 | 255.9 | 9.6 | 9.63 | 100.3 |
| 28X | 27 | 1430 | 255.9 | 265.5 | 9.6 | 7.73 | 80.5 |
| 29X | 27 | 1500 | 265.5 | 275.1 | 9.6 | 9.10 | 94.8 |
| 30X | 27 | 1530 | 275.1 | 284.6 | 9.5 | 5.70 | 60.0 |
| 31X | 27 | 1605 | 284.6 | 294.2 | 9.6 | 1.37 | 14.3 |
| 32X | 27 | 1640 | 294.2 | 303.9 | 9.7 | 5.13 | 52.9 |
| 33X | 27 | 1710 | 303.9 | 313.5 | 9.6 | 6.29 | 65.5 |
| 34X | 27 | 1745 | 313.5 | 323.1 | 9.6 | 7.73 | 80.5 |
| 35X | 27 | 1830 | 323.1 | 332.7 | 9.6 | 7.33 | 76.4 |
| 36X | 27 | 1915 | 332.7 | 342.3 | 9.6 | 6.06 | 63.1 |
| 37X | 27 | 2020 | 342.3 | 351.9 | 9.6 | 8.14 | 84.8 |
| 38X | 27 | 2115 | 351.9 | 361.5 | 9.6 | 3.27 | 34.1 |
| 39X | 27 | 2220 | 361.5 | 371.2 | 9.7 | 4.24 | 43.7 |
| 40X | 27 | 2355 | 371.2 | 380.9 | 9.7 | 6.37 | 65.7 |
| 41X | 27 | 0115 | 380.9 | 390.6 | 9.7 | 1.52 | 15.7 |
| 42X | 28 | 0335 | 390.6 | 400.3 | 9.7 | 4.06 | 41.9 |
| 43X | 28 | 0505 | 400.3 | 409.9 | 9.6 | 1.17 | 12.2 |
| 44X | 28 | 0610 | 409.9 | 419.5 | 9.6 | 9.74 | 101.5 |
| 45X | 28 | 0725 | 419.5 | 429.1 | 9.6 | 8.92 | 92.9 |
| 46X | 28 | 0855 | 429.1 | 438.8 | 9.7 | 8.77 | 90.4 |
| 47X | 28 | 1030 | 438.8 | 448.4 | 9.6 | 7.41 | 77.2 |
| 48X | 28 | 1150 | 448.4 | 458.0 | 9.6 | 9.66 | 100.6 |
| 49X | 28 | 1335 | 458.0 | 467.7 | 9.7 | 5.73 | 59.1 |
| 50X | 28 | 1515 | 467.7 | 477.3 | 9.6 | 2.04 | 21.3 |
| 51X | 28 | 1650 | 477.3 | 486.9 | 9.6 | 2.98 | 31.0 |
| 52X | 28 | 1835 | 486.9 | 496.6 | 9.7 | 1.16 | 12.0 |
| 53X | 28 | 1935 | 496.6 | 506.2 | 9.6 | 0.54 | 5.6 |
| 54X | 28 | 2115 | 506.2 | 515.7 | 9.5 | 6.91 | 72.7 |
| 55X | 28 | 2330 | 515.7 | 521.2 | 5.5 | 2.00 | 36.4 |
| | | | | Cored total: | 521.2 | 399.52 | 76.6 |
| | | | | Drilled total: | 0.0 | | |
| | | | | Total: | 521.2 | | |

**Table T2.** Expanded coring summary, Site 1195. (See table notes. Continued on next seven pages.)

| Core | Date (Jan. 2001) | Time (local) | Core depth (mbsf) Top | Core depth (mbsf) Bottom | Length (m) Cored | Length (m) Recovered | Recovery (%) | Section | Length (m) Liner | Length (m) Curated | Section depth (mbsf) Top | Section depth (mbsf) Bottom | Catwalk samples |
|---|---|---|---|---|---|---|---|---|---|---|---|---|---|
| 194-1195A- | | | | | | | | | | | | | |
| 1H | 26 | 0915 | 0.0 | 4.7 | 4.7 | 4.75 | 101.1 | | | | | | |
| | | | | | | | | 1 | 1.50 | 1.50 | 0.00 | 1.50 | |
| | | | | | | | | 2 | 1.50 | 1.50 | 1.50 | 3.00 | |
| | | | | | | | | 3 | 1.00 | 1.00 | 3.00 | 4.00 | |
| | | | | | | | | 4 | 0.59 | 0.59 | 4.00 | 4.59 | |
| | | | | | | | | CC (w/4) | 0.16 | 0.16 | 4.59 | 4.75 | PAL |
| | | | | | | | | Totals: | 4.75 | 4.75 | | | |
| 2H | 26 | 0945 | 4.7 | 14.2 | 9.5 | 9.57 | 100.7 | | | | | | |
| | | | | | | | | 1 | 1.50 | 1.50 | 4.70 | 6.20 | |
| | | | | | | | | 2 | 1.50 | 1.50 | 6.20 | 7.70 | |
| | | | | | | | | 3 | 1.50 | 1.50 | 7.70 | 9.20 | IW |
| | | | | | | | | 4 | 1.50 | 1.50 | 9.20 | 10.70 | HS |
| | | | | | | | | 5 | 1.50 | 1.50 | 10.70 | 12.20 | |
| | | | | | | | | 6 | 1.50 | 1.50 | 12.20 | 13.70 | |
| | | | | | | | | 7 | 0.39 | 0.39 | 13.70 | 14.09 | |
| | | | | | | | | CC (w/7) | 0.18 | 0.18 | 14.09 | 14.27 | PAL |
| | | | | | | | | Totals: | 9.57 | 9.57 | | | |
| 3H | 26 | 1010 | 14.2 | 23.7 | 9.5 | 9.50 | 100.0 | | | | | | |
| | | | | | | | | 1 | 1.50 | 1.50 | 14.20 | 15.70 | |
| | | | | | | | | 2 | 1.50 | 1.50 | 15.70 | 17.20 | |
| | | | | | | | | 3 | 1.50 | 1.50 | 17.20 | 18.70 | |
| | | | | | | | | 4 | 1.50 | 1.50 | 18.70 | 20.20 | IW |
| | | | | | | | | 5 | 1.50 | 1.50 | 20.20 | 21.70 | HS |
| | | | | | | | | 6 | 1.50 | 1.50 | 21.70 | 23.20 | |
| | | | | | | | | 7 | 0.30 | 0.30 | 23.20 | 23.50 | |
| | | | | | | | | CC (w/7) | 0.20 | 0.20 | 23.50 | 23.70 | PAL |
| | | | | | | | | Totals: | 9.50 | 9.50 | | | |
| 4H | 26 | 1105 | 23.7 | 33.2 | 9.5 | 9.46 | 99.6 | | | | | | |
| | | | | | | | | 1 | 1.50 | 1.50 | 23.70 | 25.20 | |
| | | | | | | | | 2 | 1.50 | 1.50 | 25.20 | 26.70 | |
| | | | | | | | | 3 | 1.50 | 1.50 | 26.70 | 28.20 | |
| | | | | | | | | 4 | 1.50 | 1.50 | 28.20 | 29.70 | IW |
| | | | | | | | | 5 | 1.50 | 1.50 | 29.70 | 31.20 | HS |
| | | | | | | | | 6 | 1.50 | 1.50 | 31.20 | 32.70 | |
| | | | | | | | | 7 | 0.29 | 0.29 | 32.70 | 32.99 | |
| | | | | | | | | CC (w/7) | 0.17 | 0.17 | 32.99 | 33.16 | PAL |
| | | | | | | | | Totals: | 9.46 | 9.46 | | | |
| 5H | 26 | 1130 | 33.2 | 42.7 | 9.5 | 9.26 | 97.5 | | | | | | |
| | | | | | | | | 1 | 1.50 | 1.50 | 33.20 | 34.70 | |
| | | | | | | | | 2 | 1.50 | 1.50 | 34.70 | 36.20 | |
| | | | | | | | | 3 | 1.50 | 1.50 | 36.20 | 37.70 | |
| | | | | | | | | 4 | 1.50 | 1.50 | 37.70 | 39.20 | IW |
| | | | | | | | | 5 | 1.50 | 1.50 | 39.20 | 40.70 | HS |
| | | | | | | | | 6 | 1.20 | 1.20 | 40.70 | 41.90 | |
| | | | | | | | | 7 | 0.39 | 0.39 | 41.90 | 42.29 | |
| | | | | | | | | CC (w/7) | 0.17 | 0.17 | 42.29 | 42.46 | PAL |
| | | | | | | | | Totals: | 9.26 | 9.26 | | | |
| 6H | 26 | 1155 | 42.7 | 52.2 | 9.5 | 8.89 | 93.6 | | | | | | |
| | | | | | | | | 1 | 1.50 | 1.50 | 42.70 | 44.20 | |
| | | | | | | | | 2 | 1.50 | 1.50 | 44.20 | 45.70 | |
| | | | | | | | | 3 | 1.50 | 1.50 | 45.70 | 47.20 | |
| | | | | | | | | 4 | 1.50 | 1.50 | 47.20 | 48.70 | IW |
| | | | | | | | | 5 | 1.50 | 1.50 | 48.70 | 50.20 | HS |
| | | | | | | | | 6 | 1.15 | 1.15 | 50.20 | 51.35 | |
| | | | | | | | | CC (w/6) | 0.24 | 0.24 | 51.35 | 51.59 | PAL |
| | | | | | | | | Totals: | 8.89 | 8.89 | | | |
| 7H | 26 | 1235 | 52.2 | 61.7 | 9.5 | 8.63 | 90.8 | | | | | | |
| | | | | | | | | 1 | 1.50 | 1.50 | 52.20 | 53.70 | |
| | | | | | | | | 2 | 1.50 | 1.50 | 53.70 | 55.20 | |
| | | | | | | | | 3 | 1.50 | 1.50 | 55.20 | 56.70 | |
| | | | | | | | | 4 | 1.50 | 1.50 | 56.70 | 58.20 | IW |
| | | | | | | | | 5 | 1.50 | 1.50 | 58.20 | 59.70 | HS |
| | | | | | | | | 6 | 0.90 | 0.90 | 59.70 | 60.60 | |
| | | | | | | | | CC (w/6) | 0.23 | 0.23 | 60.60 | 60.83 | PAL |
| | | | | | | | | Totals: | 8.63 | 8.63 | | | |
| 8H | 26 | 1330 | 61.7 | 71.2 | 9.5 | 9.43 | 99.3 | | | | | | |
| | | | | | | | | 1 | 1.50 | 1.50 | 61.70 | 63.20 | |

**Table T2 (continued).**

| Core | Date (Jan. 2001) | Time (local) | Core depth (mbsf) Top | Core depth (mbsf) Bottom | Length (m) Cored | Length (m) Recovered | Recovery (%) | Section | Length (m) Liner | Length (m) Curated | Section depth (mbsf) Top | Section depth (mbsf) Bottom | Catwalk samples |
|---|---|---|---|---|---|---|---|---|---|---|---|---|---|
| | | | | | | | | 2 | 1.50 | 1.50 | 63.20 | 64.70 | |
| | | | | | | | | 3 | 1.50 | 1.50 | 64.70 | 66.20 | |
| | | | | | | | | 4 | 1.50 | 1.50 | 66.20 | 67.70 | IW |
| | | | | | | | | 5 | 1.50 | 1.50 | 67.70 | 69.20 | HS |
| | | | | | | | | 6 | 1.20 | 1.20 | 69.20 | 70.40 | |
| | | | | | | | | 7 | 0.57 | 0.57 | 70.40 | 70.97 | |
| | | | | | | | | CC (w/7) | 0.16 | 0.16 | 70.97 | 71.13 | PAL |
| | | | | | | | | Totals: | 9.43 | 9.43 | | | |
| 9H | 26 | 1815 | 71.2 | 80.7 | 9.5 | 9.78 | 102.9 | | | | | | |
| | | | | | | | | 1 | 1.00 | 1.00 | 71.20 | 72.20 | |
| | | | | | | | | 2 | 0.90 | 0.90 | 72.20 | 73.12 | |
| | | | | | | | | 3 | 1.50 | 1.50 | 73.12 | 74.62 | |
| | | | | | | | | 4 | 1.50 | 1.50 | 74.62 | 76.12 | |
| | | | | | | | | 5 | 1.50 | 1.50 | 76.12 | 77.62 | IW |
| | | | | | | | | 6 | 1.50 | 1.50 | 77.62 | 79.12 | HS |
| | | | | | | | | 7 | 1.00 | 1.00 | 79.12 | 80.12 | |
| | | | | | | | | 8 | 0.63 | 0.63 | 80.12 | 80.75 | |
| | | | | | | | | CC (w/8) | 0.23 | 0.23 | 80.75 | 80.98 | PAL |
| | | | | | | | | Totals: | 9.78 | 9.78 | | | |
| | | | | Totals: | 80.7 | 79.27 | 98.2 | | | | | | |
| 194-1195B- | | | | | | | | | | | | | |
| 1H | 26 | 2245 | 0.0 | 8.4 | 8.4 | 8.41 | 100.1 | | | | | | |
| | | | | | | | | 1 | 1.50 | 1.50 | 0.00 | 1.50 | |
| | | | | | | | | 2 | 1.50 | 1.50 | 1.50 | 3.00 | |
| | | | | | | | | 3 | 1.50 | 1.50 | 3.00 | 4.50 | |
| | | | | | | | | 4 | 1.50 | 1.50 | 4.50 | 6.00 | |
| | | | | | | | | 5 | 1.50 | 1.50 | 6.00 | 7.50 | |
| | | | | | | | | 6 | 0.76 | 0.76 | 7.50 | 8.26 | |
| | | | | | | | | CC (w/6) | 0.15 | 0.15 | 8.26 | 8.41 | PAL |
| | | | | | | | | Totals: | 8.41 | 8.41 | | | |
| 2H | 26 | 2320 | 8.4 | 17.9 | 9.5 | 9.14 | 96.2 | | | | | | |
| | | | | | | | | 1 | 1.50 | 1.50 | 8.40 | 9.90 | |
| | | | | | | | | 2 | 1.50 | 1.50 | 9.90 | 11.40 | |
| | | | | | | | | 3 | 1.50 | 1.50 | 11.40 | 12.90 | |
| | | | | | | | | 4 | 1.50 | 1.50 | 12.90 | 14.40 | |
| | | | | | | | | 5 | 1.50 | 1.50 | 14.40 | 15.90 | |
| | | | | | | | | 6 | 1.50 | 1.50 | 15.90 | 17.40 | |
| | | | | | | | | CC (w/CC) | 0.14 | 0.14 | 17.40 | 17.54 | PAL |
| | | | | | | | | Totals: | 9.14 | 9.14 | | | |
| 3H | 26 | 2350 | 17.9 | 27.4 | 9.5 | 9.36 | 98.5 | | | | | | |
| | | | | | | | | 1 | 1.50 | 1.50 | 17.90 | 19.40 | |
| | | | | | | | | 2 | 1.50 | 1.50 | 19.40 | 20.90 | |
| | | | | | | | | 3 | 1.50 | 1.50 | 20.90 | 22.40 | |
| | | | | | | | | 4 | 1.50 | 1.50 | 22.40 | 23.90 | |
| | | | | | | | | 5 | 1.50 | 1.50 | 23.90 | 25.40 | |
| | | | | | | | | 6 | 1.20 | 1.20 | 25.40 | 26.60 | |
| | | | | | | | | 7 | 0.51 | 0.51 | 26.60 | 27.11 | |
| | | | | | | | | CC (w/7) | 0.15 | 0.15 | 27.11 | 27.26 | PAL |
| | | | | | | | | Totals: | 9.36 | 9.36 | | | |
| 4H | 27 | 0020 | 27.4 | 36.9 | 9.5 | 9.52 | 100.2 | | | | | | |
| | | | | | | | | 1 | 1.50 | 1.50 | 27.40 | 28.90 | |
| | | | | | | | | 2 | 1.50 | 1.50 | 28.90 | 30.40 | |
| | | | | | | | | 3 | 1.50 | 1.50 | 30.40 | 31.90 | |
| | | | | | | | | 4 | 1.50 | 1.50 | 31.90 | 33.40 | |
| | | | | | | | | 5 | 1.50 | 1.50 | 33.40 | 34.90 | |
| | | | | | | | | 6 | 1.50 | 1.50 | 34.90 | 36.40 | |
| | | | | | | | | 7 | 0.34 | 0.34 | 36.40 | 36.74 | |
| | | | | | | | | CC (w/7) | 0.18 | 0.18 | 36.74 | 36.92 | PAL |
| | | | | | | | | Totals: | 9.52 | 9.52 | | | |
| 5H | 27 | 0050 | 36.9 | 46.4 | 9.5 | 9.02 | 94.9 | | | | | | |
| | | | | | | | | 1 | 1.50 | 1.50 | 36.90 | 38.40 | |
| | | | | | | | | 2 | 1.50 | 1.50 | 38.40 | 39.90 | |
| | | | | | | | | 3 | 1.50 | 1.50 | 39.90 | 41.40 | |
| | | | | | | | | 4 | 1.50 | 1.50 | 41.40 | 42.90 | |
| | | | | | | | | 5 | 1.50 | 1.50 | 42.90 | 44.40 | |
| | | | | | | | | 6 | 1.30 | 1.30 | 44.40 | 45.70 | |
| | | | | | | | | CC (w/CC) | 0.22 | 0.22 | 45.70 | 45.92 | PAL |
| | | | | | | | | Totals: | 9.02 | 9.02 | | | |

Table T2 (continued).

| Core | Date (Jan. 2001) | Time (local) | Core depth (mbsf) Top | Core depth (mbsf) Bottom | Length (m) Cored | Length (m) Recovered | Recovery (%) | Section | Length (m) Liner | Length (m) Curated | Section depth (mbsf) Top | Section depth (mbsf) Bottom | Catwalk samples |
|---|---|---|---|---|---|---|---|---|---|---|---|---|---|
| 6H | 27 | 0120 | 46.4 | 55.9 | 9.5 | 9.17 | 96.5 | | | | | | |
| | | | | | | | | 1 | 1.50 | 1.50 | 46.40 | 47.90 | |
| | | | | | | | | 2 | 1.50 | 1.50 | 47.90 | 49.40 | |
| | | | | | | | | 3 | 1.50 | 1.50 | 49.40 | 50.90 | |
| | | | | | | | | 4 | 1.50 | 1.50 | 50.90 | 52.40 | |
| | | | | | | | | 5 | 1.50 | 1.50 | 52.40 | 53.90 | |
| | | | | | | | | 6 | 1.49 | 1.49 | 53.90 | 55.39 | |
| | | | | | | | | CC (w/CC) | 0.18 | 0.18 | 55.39 | 55.57 | PAL |
| | | | | | | | | Totals: | 9.17 | 9.17 | | | |
| 7H | 27 | 0145 | 55.9 | 65.4 | 9.5 | 9.88 | 104.0 | | | | | | |
| | | | | | | | | 1 | 1.50 | 1.50 | 55.90 | 57.40 | |
| | | | | | | | | 2 | 1.50 | 1.50 | 57.40 | 58.90 | |
| | | | | | | | | 3 | 1.50 | 1.50 | 58.90 | 60.40 | |
| | | | | | | | | 4 | 1.50 | 1.50 | 60.40 | 61.90 | |
| | | | | | | | | 5 | 1.50 | 1.50 | 61.90 | 63.40 | |
| | | | | | | | | 6 | 1.50 | 1.50 | 63.40 | 64.90 | |
| | | | | | | | | 7 | 0.70 | 0.70 | 64.90 | 65.60 | |
| | | | | | | | | CC (w/7) | 0.18 | 0.18 | 65.60 | 65.78 | PAL |
| | | | | | | | | Totals: | 9.88 | 9.88 | | | |
| 8H | 27 | 0215 | 65.4 | 74.9 | 9.5 | 9.01 | 94.8 | | | | | | |
| | | | | | | | | 1 | 1.50 | 1.50 | 65.40 | 66.90 | |
| | | | | | | | | 2 | 1.50 | 1.50 | 66.90 | 68.40 | |
| | | | | | | | | 3 | 1.50 | 1.50 | 68.40 | 69.90 | |
| | | | | | | | | 4 | 1.50 | 1.50 | 69.90 | 71.40 | |
| | | | | | | | | 5 | 1.50 | 1.50 | 71.40 | 72.90 | |
| | | | | | | | | 6 | 1.34 | 1.34 | 72.90 | 74.24 | |
| | | | | | | | | CC (w/CC) | 0.17 | 0.17 | 74.24 | 74.41 | PAL |
| | | | | | | | | Totals: | 9.01 | 9.01 | | | |
| 9H | 27 | 0245 | 74.9 | 84.4 | 9.5 | 9.62 | 101.3 | | | | | | |
| | | | | | | | | 1 | 1.50 | 1.50 | 74.90 | 76.40 | |
| | | | | | | | | 2 | 1.50 | 1.50 | 76.40 | 77.90 | |
| | | | | | | | | 3 | 1.50 | 1.50 | 77.90 | 79.40 | |
| | | | | | | | | 4 | 1.50 | 1.50 | 79.40 | 80.90 | |
| | | | | | | | | 5 | 1.50 | 1.50 | 80.90 | 82.40 | |
| | | | | | | | | 6 | 1.50 | 1.50 | 82.40 | 83.90 | |
| | | | | | | | | 7 | 0.51 | 0.51 | 83.90 | 84.41 | |
| | | | | | | | | CC (w/7) | 0.11 | 0.11 | 84.41 | 84.52 | PAL |
| | | | | | | | | Totals: | 9.62 | 9.62 | | | |
| 10H | 27 | 0315 | 84.4 | 93.9 | 9.5 | 9.75 | 102.6 | | | | | | |
| | | | | | | | | 1 | 1.50 | 1.50 | 84.40 | 85.90 | |
| | | | | | | | | 2 | 1.50 | 1.50 | 85.90 | 87.40 | |
| | | | | | | | | 3 | 1.50 | 1.50 | 87.40 | 88.90 | |
| | | | | | | | | 4 | 1.50 | 1.50 | 88.90 | 90.40 | IW |
| | | | | | | | | 5 | 1.50 | 1.50 | 90.40 | 91.90 | HS |
| | | | | | | | | 6 | 1.50 | 1.50 | 91.90 | 93.40 | |
| | | | | | | | | 7 | 0.57 | 0.57 | 93.40 | 93.97 | |
| | | | | | | | | CC (w/7) | 0.18 | 0.18 | 93.97 | 94.15 | PAL |
| | | | | | | | | Totals: | 9.75 | 9.75 | | | |
| 11H | 27 | 0345 | 93.9 | 103.4 | 9.5 | 9.60 | 101.1 | | | | | | |
| | | | | | | | | 1 | 1.50 | 1.50 | 93.90 | 95.40 | |
| | | | | | | | | 2 | 1.50 | 1.50 | 95.40 | 96.90 | |
| | | | | | | | | 3 | 1.50 | 1.50 | 96.90 | 98.40 | |
| | | | | | | | | 4 | 1.50 | 1.50 | 98.40 | 99.90 | IW |
| | | | | | | | | 5 | 1.50 | 1.50 | 99.90 | 101.40 | HS |
| | | | | | | | | 6 | 1.50 | 1.50 | 101.40 | 102.90 | |
| | | | | | | | | 7 | 0.42 | 0.42 | 102.90 | 103.32 | |
| | | | | | | | | CC (w/7) | 0.18 | 0.18 | 103.32 | 103.50 | PAL |
| | | | | | | | | Totals: | 9.60 | 9.60 | | | |
| 12H | 27 | 0420 | 103.4 | 112.9 | 9.5 | 9.64 | 101.5 | | | | | | |
| | | | | | | | | 1 | 1.50 | 1.50 | 103.40 | 104.90 | |
| | | | | | | | | 2 | 1.50 | 1.50 | 104.90 | 106.40 | |
| | | | | | | | | 3 | 1.50 | 1.50 | 106.40 | 107.90 | |
| | | | | | | | | 4 | 1.50 | 1.50 | 107.90 | 109.40 | IW |
| | | | | | | | | 5 | 1.50 | 1.50 | 109.40 | 110.90 | HS |
| | | | | | | | | 6 | 1.50 | 1.50 | 110.90 | 112.40 | |
| | | | | | | | | 7 | 0.49 | 0.49 | 112.40 | 112.89 | |
| | | | | | | | | CC (w/7) | 0.15 | 0.15 | 112.89 | 113.04 | PAL |
| | | | | | | | | Totals: | 9.64 | 9.64 | | | |

Table T2 (continued).

| Core | Date (Jan. 2001) | Time (local) | Core depth (mbsf) Top | Core depth (mbsf) Bottom | Length (m) Cored | Length (m) Recovered | Recovery (%) | Section | Length (m) Liner | Length (m) Curated | Section depth (mbsf) Top | Section depth (mbsf) Bottom | Catwalk samples |
|---|---|---|---|---|---|---|---|---|---|---|---|---|---|
| 13H | 27 | 0605 | 112.9 | 122.4 | 9.5 | 9.95 | 104.7 | | | | | | |
| | | | | | | | | 1 | 1.50 | 1.50 | 112.90 | 114.40 | |
| | | | | | | | | 2 | 1.50 | 1.50 | 114.40 | 115.90 | |
| | | | | | | | | 3 | 1.50 | 1.50 | 115.90 | 117.40 | |
| | | | | | | | | 4 | 1.50 | 1.50 | 117.40 | 118.90 | IW |
| | | | | | | | | 5 | 1.50 | 1.50 | 118.90 | 120.40 | HS |
| | | | | | | | | 6 | 1.50 | 1.50 | 120.40 | 121.90 | |
| | | | | | | | | 7 | 0.80 | 0.80 | 121.90 | 122.70 | |
| | | | | | | | | CC (w/7) | 0.15 | 0.15 | 122.70 | 122.85 | PAL |
| | | | | | | | | Totals: | 9.95 | 9.95 | | | |
| 14H | 27 | 0630 | 122.4 | 131.9 | 9.5 | 9.79 | 103.1 | | | | | | |
| | | | | | | | | 1 | 1.50 | 1.50 | 122.40 | 123.90 | |
| | | | | | | | | 2 | 1.50 | 1.50 | 123.90 | 125.40 | |
| | | | | | | | | 3 | 1.50 | 1.50 | 125.40 | 126.90 | |
| | | | | | | | | 4 | 1.50 | 1.50 | 126.90 | 128.40 | IW |
| | | | | | | | | 5 | 1.50 | 1.50 | 128.40 | 129.90 | HS |
| | | | | | | | | 6 | 1.50 | 1.50 | 129.90 | 131.40 | |
| | | | | | | | | 7 | 0.65 | 0.65 | 131.40 | 132.05 | |
| | | | | | | | | CC (w/7) | 0.14 | 0.14 | 132.05 | 132.19 | PAL |
| | | | | | | | | Totals: | 9.79 | 9.79 | | | |
| 15H | 27 | 0700 | 131.9 | 141.4 | 9.5 | 9.79 | 103.1 | | | | | | |
| | | | | | | | | 1 | 1.50 | 1.50 | 131.90 | 133.40 | |
| | | | | | | | | 2 | 1.50 | 1.50 | 133.40 | 134.90 | |
| | | | | | | | | 3 | 1.50 | 1.50 | 134.90 | 136.40 | |
| | | | | | | | | 4 | 1.50 | 1.50 | 136.40 | 137.90 | IW |
| | | | | | | | | 5 | 1.50 | 1.50 | 137.90 | 139.40 | HS |
| | | | | | | | | 6 | 1.50 | 1.50 | 139.40 | 140.90 | |
| | | | | | | | | 7 | 0.58 | 0.58 | 140.90 | 141.48 | |
| | | | | | | | | CC (w/7) | 0.21 | 0.21 | 141.48 | 141.69 | PAL |
| | | | | | | | | Totals: | 9.79 | 9.79 | | | |
| 16H | 27 | 0730 | 141.4 | 150.9 | 9.5 | 9.57 | 100.7 | | | | | | |
| | | | | | | | | 1 | 1.50 | 1.50 | 141.40 | 142.90 | |
| | | | | | | | | 2 | 1.50 | 1.50 | 142.90 | 144.40 | |
| | | | | | | | | 3 | 1.50 | 1.50 | 144.40 | 145.90 | |
| | | | | | | | | 4 | 1.50 | 1.50 | 145.90 | 147.40 | IW |
| | | | | | | | | 5 | 1.50 | 1.50 | 147.40 | 148.90 | HS |
| | | | | | | | | 6 | 1.50 | 1.50 | 148.90 | 150.40 | |
| | | | | | | | | 7 | 0.40 | 0.40 | 150.40 | 150.80 | |
| | | | | | | | | CC (w/7) | 0.17 | 0.17 | 150.80 | 150.97 | PAL |
| | | | | | | | | Totals: | 9.57 | 9.57 | | | |
| 17H | 27 | 0855 | 150.9 | 160.4 | 9.5 | 9.85 | 103.7 | | | | | | |
| | | | | | | | | 1 | 1.50 | 1.50 | 150.90 | 152.40 | |
| | | | | | | | | 2 | 1.50 | 1.50 | 152.40 | 153.90 | |
| | | | | | | | | 3 | 1.50 | 1.50 | 153.90 | 155.40 | |
| | | | | | | | | 4 | 1.50 | 1.50 | 155.40 | 156.90 | IW |
| | | | | | | | | 5 | 1.50 | 1.50 | 156.90 | 158.40 | HS |
| | | | | | | | | 6 | 1.50 | 1.50 | 158.40 | 159.90 | |
| | | | | | | | | 7 | 0.64 | 0.64 | 159.90 | 160.54 | |
| | | | | | | | | CC (w/7) | 0.21 | 0.21 | 160.54 | 160.75 | PAL |
| | | | | | | | | Totals: | 9.85 | 9.85 | | | |
| 18H | 27 | 0925 | 160.4 | 169.9 | 9.5 | 10.10 | 106.3 | | | | | | |
| | | | | | | | | 1 | 1.50 | 1.50 | 160.40 | 161.90 | |
| | | | | | | | | 2 | 1.50 | 1.50 | 161.90 | 163.40 | |
| | | | | | | | | 3 | 1.50 | 1.50 | 163.40 | 164.90 | |
| | | | | | | | | 4 | 1.50 | 1.50 | 164.90 | 166.40 | IW |
| | | | | | | | | 5 | 1.50 | 1.50 | 166.40 | 167.90 | HS |
| | | | | | | | | 6 | 1.50 | 1.50 | 167.90 | 169.40 | |
| | | | | | | | | 7 | 0.84 | 0.84 | 169.40 | 170.24 | |
| | | | | | | | | CC (w/7) | 0.26 | 0.26 | 170.24 | 170.50 | PAL |
| | | | | | | | | Totals: | 10.10 | 10.10 | | | |
| 19H | 27 | 0945 | 169.9 | 179.4 | 9.5 | 9.99 | 105.2 | | | | | | |
| | | | | | | | | 1 | 1.50 | 1.50 | 169.90 | 171.40 | |
| | | | | | | | | 2 | 1.50 | 1.50 | 171.40 | 172.90 | |
| | | | | | | | | 3 | 1.50 | 1.50 | 172.90 | 174.40 | |
| | | | | | | | | 4 | 1.50 | 1.50 | 174.40 | 175.90 | IW |
| | | | | | | | | 5 | 1.50 | 1.50 | 175.90 | 177.40 | HS |
| | | | | | | | | 6 | 1.50 | 1.50 | 177.40 | 178.90 | |
| | | | | | | | | 7 | 0.78 | 0.78 | 178.90 | 179.68 | |

Table T2 (continued).

| Core | Date (Jan. 2001) | Time (local) | Core depth (mbsf) Top | Core depth (mbsf) Bottom | Length (m) Cored | Length (m) Recovered | Recovery (%) | Section | Length (m) Liner | Length (m) Curated | Section depth (mbsf) Top | Section depth (mbsf) Bottom | Catwalk samples |
|---|---|---|---|---|---|---|---|---|---|---|---|---|---|
| | | | | | | | | CC (w/7) | 0.21 | 0.21 | 179.68 | 179.89 | PAL |
| | | | | | | | | Totals: | 9.99 | 9.99 | | | |
| 20H | 27 | 1020 | 179.4 | 188.9 | 9.5 | 9.98 | 105.1 | | | | | | |
| | | | | | | | | 1 | 1.50 | 1.50 | 179.40 | 180.90 | |
| | | | | | | | | 2 | 1.50 | 1.50 | 180.90 | 182.40 | |
| | | | | | | | | 3 | 1.50 | 1.50 | 182.40 | 183.90 | |
| | | | | | | | | 4 | 1.50 | 1.50 | 183.90 | 185.40 | IW |
| | | | | | | | | 5 | 1.50 | 1.50 | 185.40 | 186.90 | HS |
| | | | | | | | | 6 | 1.50 | 1.50 | 186.90 | 188.40 | |
| | | | | | | | | 7 | 0.80 | 0.80 | 188.40 | 189.20 | |
| | | | | | | | | CC (w/7) | 0.18 | 0.18 | 189.20 | 189.38 | PAL |
| | | | | | | | | Totals: | 9.98 | 9.98 | | | |
| 21H | 27 | 1045 | 188.9 | 198.4 | 9.5 | 10.06 | 105.9 | | | | | | |
| | | | | | | | | 1 | 1.50 | 1.50 | 188.90 | 190.40 | |
| | | | | | | | | 2 | 1.50 | 1.50 | 190.40 | 191.90 | |
| | | | | | | | | 3 | 1.50 | 1.50 | 191.90 | 193.40 | |
| | | | | | | | | 4 | 1.50 | 1.50 | 193.40 | 194.90 | IW |
| | | | | | | | | 5 | 1.50 | 1.50 | 194.90 | 196.40 | HS |
| | | | | | | | | 6 | 1.50 | 1.50 | 196.40 | 197.90 | |
| | | | | | | | | 7 | 0.86 | 0.86 | 197.90 | 198.76 | |
| | | | | | | | | CC (w/7) | 0.20 | 0.20 | 198.76 | 198.96 | PAL |
| | | | | | | | | Totals: | 10.06 | 10.06 | | | |
| 22H | 27 | 1125 | 198.4 | 207.9 | 9.5 | 9.03 | 95.1 | | | | | | |
| | | | | | | | | 1 | 1.50 | 1.50 | 198.40 | 199.90 | |
| | | | | | | | | 2 | 1.50 | 1.50 | 199.90 | 201.40 | |
| | | | | | | | | 3 | 1.50 | 1.50 | 201.40 | 202.90 | |
| | | | | | | | | 4 | 1.50 | 1.50 | 202.90 | 204.40 | IW |
| | | | | | | | | 5 | 1.45 | 1.45 | 204.40 | 205.85 | HS |
| | | | | | | | | 6 | 1.51 | 1.51 | 205.85 | 207.36 | |
| | | | | | | | | CC (w/CC) | 0.07 | 0.07 | 207.36 | 207.43 | PAL |
| | | | | | | | | Totals: | 9.03 | 9.03 | | | |
| 23X | 27 | 1215 | 207.9 | 217.5 | 9.6 | 2.59 | 27.0 | | | | | | |
| | | | | | | | | 1 | 1.50 | 1.50 | 207.90 | 209.40 | IW |
| | | | | | | | | 2 | 0.87 | 0.87 | 209.40 | 210.27 | HS |
| | | | | | | | | CC (w/2) | 0.22 | 0.22 | 210.27 | 210.49 | PAL |
| | | | | | | | | Totals: | 2.59 | 2.59 | | | |
| 24X | 27 | 1250 | 217.5 | 227.1 | 9.6 | 9.37 | 97.6 | | | | | | |
| | | | | | | | | 1 | 1.50 | 1.50 | 217.50 | 219.00 | |
| | | | | | | | | 2 | 1.50 | 1.50 | 219.00 | 220.50 | |
| | | | | | | | | 3 | 1.50 | 1.50 | 220.50 | 222.00 | |
| | | | | | | | | 4 | 1.50 | 1.50 | 222.00 | 223.50 | IW |
| | | | | | | | | 5 | 1.50 | 1.50 | 223.50 | 225.00 | HS |
| | | | | | | | | 6 | 1.20 | 1.20 | 225.00 | 226.20 | |
| | | | | | | | | 7 | 0.36 | 0.36 | 226.20 | 226.56 | |
| | | | | | | | | CC (w/7) | 0.31 | 0.31 | 226.56 | 226.87 | PAL |
| | | | | | | | | Totals: | 9.37 | 9.37 | | | |
| 25X | 27 | 1315 | 227.1 | 236.7 | 9.6 | 9.96 | 103.8 | | | | | | |
| | | | | | | | | 1 | 1.50 | 1.50 | 227.10 | 228.60 | |
| | | | | | | | | 2 | 1.50 | 1.50 | 228.60 | 230.10 | |
| | | | | | | | | 3 | 1.50 | 1.50 | 230.10 | 231.60 | |
| | | | | | | | | 4 | 1.50 | 1.50 | 231.60 | 233.10 | IW |
| | | | | | | | | 5 | 1.50 | 1.50 | 233.10 | 234.60 | HS |
| | | | | | | | | 6 | 1.50 | 1.50 | 234.60 | 236.10 | |
| | | | | | | | | 7 | 0.55 | 0.55 | 236.10 | 236.65 | |
| | | | | | | | | CC (w/7) | 0.41 | 0.41 | 236.65 | 237.06 | PAL |
| | | | | | | | | Totals: | 9.96 | 9.96 | | | |
| 26X | 27 | 1345 | 236.7 | 246.3 | 9.6 | 6.67 | 69.5 | | | | | | |
| | | | | | | | | 1 | 1.47 | 1.47 | 236.70 | 238.17 | |
| | | | | | | | | 2 | 1.50 | 1.50 | 238.17 | 239.67 | |
| | | | | | | | | 3 | 1.50 | 1.50 | 239.67 | 241.17 | IW |
| | | | | | | | | 4 | 1.50 | 1.50 | 241.17 | 242.67 | HS |
| | | | | | | | | 5 | 0.39 | 0.39 | 242.67 | 243.06 | |
| | | | | | | | | CC (w/CC) | 0.31 | 0.31 | 243.06 | 243.37 | PAL |
| | | | | | | | | Totals: | 6.67 | 6.67 | | | |
| 27X | 27 | 1405 | 246.3 | 255.9 | 9.6 | 9.63 | 100.3 | | | | | | |
| | | | | | | | | 1 | 1.50 | 1.50 | 246.30 | 247.80 | |
| | | | | | | | | 2 | 1.50 | 1.50 | 247.80 | 249.30 | |
| | | | | | | | | 3 | 1.50 | 1.50 | 249.30 | 250.80 | |

**Table T2 (continued).**

| Core | Date (Jan. 2001) | Time (local) | Core depth (mbsf) Top | Core depth (mbsf) Bottom | Length (m) Cored | Length (m) Recovered | Recovery (%) | Section | Length (m) Liner | Length (m) Curated | Section depth (mbsf) Top | Section depth (mbsf) Bottom | Catwalk samples |
|---|---|---|---|---|---|---|---|---|---|---|---|---|---|
| | | | | | | | | 4 | 1.50 | 1.50 | 250.80 | 252.30 | IW |
| | | | | | | | | 5 | 1.50 | 1.50 | 252.30 | 253.80 | HS |
| | | | | | | | | 6 | 1.50 | 1.50 | 253.80 | 255.30 | |
| | | | | | | | | 7 | 0.29 | 0.29 | 255.30 | 255.59 | |
| | | | | | | | | CC (w/7) | 0.34 | 0.34 | 255.59 | 255.93 | PAL |
| | | | | | | | | Totals: | 9.63 | 9.63 | | | |
| 28X | 27 | 1430 | 255.9 | 265.5 | 9.6 | 7.73 | 80.5 | | | | | | |
| | | | | | | | | 1 | 1.50 | 1.50 | 255.90 | 257.40 | |
| | | | | | | | | 2 | 1.50 | 1.50 | 257.40 | 258.90 | |
| | | | | | | | | 3 | 1.50 | 1.50 | 258.90 | 260.40 | IW |
| | | | | | | | | 4 | 1.50 | 1.50 | 260.40 | 261.90 | HS |
| | | | | | | | | 5 | 1.43 | 1.43 | 261.90 | 263.33 | |
| | | | | | | | | CC (w/CC) | 0.30 | 0.30 | 263.33 | 263.63 | PAL |
| | | | | | | | | Totals: | 7.73 | 7.73 | | | |
| 29X | 27 | 1500 | 265.5 | 275.1 | 9.6 | 9.10 | 94.8 | | | | | | |
| | | | | | | | | 1 | 1.50 | 1.50 | 265.50 | 267.00 | |
| | | | | | | | | 2 | 1.50 | 1.50 | 267.00 | 268.50 | |
| | | | | | | | | 3 | 1.50 | 1.50 | 268.50 | 270.00 | |
| | | | | | | | | 4 | 1.50 | 1.50 | 270.00 | 271.50 | IW |
| | | | | | | | | 5 | 1.50 | 1.50 | 271.50 | 273.00 | HS |
| | | | | | | | | 6 | 1.43 | 1.43 | 273.00 | 274.43 | |
| | | | | | | | | CC (w/CC) | 0.17 | 0.17 | 274.43 | 274.60 | PAL |
| | | | | | | | | Totals: | 9.10 | 9.10 | | | |
| 30X | 27 | 1530 | 275.1 | 284.6 | 9.5 | 5.70 | 60.0 | | | | | | |
| | | | | | | | | 1 | 1.50 | 1.50 | 275.10 | 276.60 | |
| | | | | | | | | 2 | 1.50 | 1.50 | 276.60 | 278.10 | IW |
| | | | | | | | | 3 | 1.50 | 1.50 | 278.10 | 279.60 | HS |
| | | | | | | | | 4 | 0.89 | 0.89 | 279.60 | 280.49 | |
| | | | | | | | | CC (w/4) | 0.31 | 0.31 | 280.49 | 280.80 | PAL |
| | | | | | | | | Totals: | 5.70 | 5.70 | | | |
| 31X | 27 | 1605 | 284.6 | 294.2 | 9.6 | 1.37 | 14.3 | | | | | | |
| | | | | | | | | 1 | 1.37 | 1.37 | 284.60 | 285.97 | PAL, HS |
| | | | | | | | | Totals: | 1.37 | 1.37 | | | |
| 32X | 27 | 1640 | 294.2 | 303.9 | 9.7 | 5.13 | 52.9 | | | | | | |
| | | | | | | | | 1 | 1.50 | 1.50 | 294.20 | 295.70 | |
| | | | | | | | | 2 | 1.50 | 1.50 | 295.70 | 297.20 | IW |
| | | | | | | | | 3 | 1.50 | 1.50 | 297.20 | 298.70 | HS |
| | | | | | | | | 4 | 0.29 | 0.29 | 298.70 | 298.99 | |
| | | | | | | | | CC (w/CC) | 0.34 | 0.34 | 298.99 | 299.33 | PAL |
| | | | | | | | | Totals: | 5.13 | 5.13 | | | |
| 33X | 27 | 1710 | 303.9 | 313.5 | 9.6 | 6.29 | 65.5 | | | | | | |
| | | | | | | | | 1 | 1.50 | 1.50 | 303.90 | 305.40 | |
| | | | | | | | | 2 | 1.50 | 1.50 | 305.40 | 306.90 | |
| | | | | | | | | 3 | 1.50 | 1.50 | 306.90 | 308.40 | IW |
| | | | | | | | | 4 | 1.35 | 1.35 | 308.40 | 309.75 | HS |
| | | | | | | | | CC (w/CC) | 0.44 | 0.44 | 309.75 | 310.19 | PAL |
| | | | | | | | | Totals: | 6.29 | 6.29 | | | |
| 34X | 27 | 1745 | 313.5 | 323.1 | 9.6 | 7.73 | 80.5 | | | | | | |
| | | | | | | | | 1 | 1.50 | 1.50 | 313.50 | 315.00 | |
| | | | | | | | | 2 | 1.50 | 1.50 | 315.00 | 316.50 | |
| | | | | | | | | 3 | 1.50 | 1.50 | 316.50 | 318.00 | |
| | | | | | | | | 4 | 1.50 | 1.50 | 318.00 | 319.50 | IW |
| | | | | | | | | 5 | 1.22 | 1.22 | 319.50 | 320.72 | HS |
| | | | | | | | | CC (w/CC) | 0.51 | 0.51 | 320.72 | 321.23 | PAL |
| | | | | | | | | Totals: | 7.73 | 7.73 | | | |
| 35X | 27 | 1830 | 323.1 | 332.7 | 9.6 | 7.33 | 76.4 | | | | | | |
| | | | | | | | | 1 | 1.50 | 1.50 | 323.10 | 324.60 | |
| | | | | | | | | 2 | 1.50 | 1.50 | 324.60 | 326.10 | IW |
| | | | | | | | | 3 | 1.50 | 1.50 | 326.10 | 327.60 | HS |
| | | | | | | | | 4 | 1.50 | 1.50 | 327.60 | 329.10 | |
| | | | | | | | | 5 | 0.91 | 0.91 | 329.10 | 330.01 | |
| | | | | | | | | CC (w/5) | 0.42 | 0.42 | 330.01 | 330.43 | PAL |
| | | | | | | | | Totals: | 7.33 | 7.33 | | | |
| 36X | 27 | 1915 | 332.7 | 342.3 | 9.6 | 6.06 | 63.1 | | | | | | |
| | | | | | | | | 1 | 1.50 | 1.50 | 332.70 | 334.20 | |
| | | | | | | | | 2 | 1.50 | 1.50 | 334.20 | 335.70 | IW |
| | | | | | | | | 3 | 1.50 | 1.50 | 335.70 | 337.20 | HS |
| | | | | | | | | 4 | 1.11 | 1.11 | 337.20 | 338.31 | |

**Table T2 (continued).**

| Core | Date (Jan. 2001) | Time (local) | Core depth (mbsf) Top | Core depth (mbsf) Bottom | Length (m) Cored | Length (m) Recovered | Recovery (%) | Section | Length (m) Liner | Length (m) Curated | Section depth (mbsf) Top | Section depth (mbsf) Bottom | Catwalk samples |
|---|---|---|---|---|---|---|---|---|---|---|---|---|---|
| | | | | | | | | CC (w/CC) | 0.45 | 0.45 | 338.31 | 338.76 | PAL |
| | | | | | | | | Totals: | 6.06 | 6.06 | | | |
| 37X | 27 | 2020 | 342.3 | 351.9 | 9.6 | 8.14 | 84.8 | | | | | | |
| | | | | | | | | 1 | 1.50 | 1.50 | 342.30 | 343.80 | |
| | | | | | | | | 2 | 1.50 | 1.50 | 343.80 | 345.30 | |
| | | | | | | | | 3 | 1.50 | 1.50 | 345.30 | 346.80 | |
| | | | | | | | | 4 | 1.50 | 1.50 | 346.80 | 348.30 | IW |
| | | | | | | | | 5 | 1.40 | 1.40 | 348.30 | 349.70 | HS |
| | | | | | | | | 6 | 0.33 | 0.33 | 349.70 | 350.03 | |
| | | | | | | | | CC (w/6) | 0.41 | 0.41 | 350.03 | 350.44 | PAL |
| | | | | | | | | Totals: | 8.14 | 8.14 | | | |
| 38X | 27 | 2115 | 351.9 | 361.5 | 9.6 | 3.27 | 34.1 | | | | | | |
| | | | | | | | | 1 | 1.50 | 1.50 | 351.90 | 353.40 | IW |
| | | | | | | | | 2 | 1.36 | 1.36 | 353.40 | 354.76 | HS |
| | | | | | | | | CC (w/CC) | 0.41 | 0.41 | 354.76 | 355.17 | PAL |
| | | | | | | | | Totals: | 3.27 | 3.27 | | | |
| 39X | 27 | 2220 | 361.5 | 371.2 | 9.7 | 4.24 | 43.7 | | | | | | |
| | | | | | | | | 1 | 1.50 | 1.50 | 361.50 | 363.00 | IW |
| | | | | | | | | 2 | 1.50 | 1.50 | 363.00 | 364.50 | HS |
| | | | | | | | | 3 | 0.83 | 0.83 | 364.50 | 365.33 | |
| | | | | | | | | CC (w/3) | 0.41 | 0.41 | 365.33 | 365.74 | PAL |
| | | | | | | | | Totals: | 4.24 | 4.24 | | | |
| 40X | 27 | 2355 | 371.2 | 380.9 | 9.7 | 6.37 | 65.7 | | | | | | |
| | | | | | | | | 1 | 1.50 | 1.50 | 371.20 | 372.70 | |
| | | | | | | | | 2 | 1.50 | 1.50 | 372.70 | 374.20 | |
| | | | | | | | | 3 | 1.50 | 1.50 | 374.20 | 375.70 | IW |
| | | | | | | | | 4 | 1.46 | 1.46 | 375.70 | 377.16 | HS |
| | | | | | | | | CC (w/CC) | 0.41 | 0.41 | 377.16 | 377.57 | PAL |
| | | | | | | | | Totals: | 6.37 | 6.37 | | | |
| 41X | 28 | 0115 | 380.9 | 390.6 | 9.7 | 1.52 | 15.7 | | | | | | |
| | | | | | | | | 1 | 1.09 | 1.09 | 380.90 | 381.99 | |
| | | | | | | | | CC (w/CC) | 0.43 | 0.43 | 381.99 | 382.42 | PAL |
| | | | | | | | | Totals: | 1.52 | 1.52 | | | |
| 42X | 28 | 0335 | 390.6 | 400.3 | 9.7 | 4.06 | 41.9 | | | | | | |
| | | | | | | | | 1 | 1.50 | 1.50 | 390.60 | 392.10 | |
| | | | | | | | | 2 | 1.22 | 1.22 | 392.10 | 393.32 | HS, IW |
| | | | | | | | | 3 | 0.98 | 0.98 | 393.32 | 394.30 | |
| | | | | | | | | CC (w/3) | 0.36 | 0.36 | 394.30 | 394.66 | PAL |
| | | | | | | | | Totals: | 4.06 | 4.06 | | | |
| 43X | 28 | 0505 | 400.3 | 409.9 | 9.6 | 1.17 | 12.2 | | | | | | |
| | | | | | | | | 1 | 0.76 | 0.76 | 400.30 | 401.06 | |
| | | | | | | | | CC (w/1) | 0.41 | 0.41 | 401.06 | 401.47 | PAL |
| | | | | | | | | Totals: | 1.17 | 1.17 | | | |
| 44X | 28 | 0610 | 409.9 | 419.5 | 9.6 | 9.74 | 101.5 | | | | | | |
| | | | | | | | | 1 | 1.50 | 1.50 | 409.90 | 411.40 | |
| | | | | | | | | 2 | 1.50 | 1.50 | 411.40 | 412.90 | |
| | | | | | | | | 3 | 1.50 | 1.50 | 412.90 | 414.40 | |
| | | | | | | | | 4 | 1.50 | 1.50 | 414.40 | 415.90 | HS, IW |
| | | | | | | | | 5 | 1.50 | 1.50 | 415.90 | 417.40 | |
| | | | | | | | | 6 | 1.35 | 1.35 | 417.40 | 418.75 | |
| | | | | | | | | 7 | 0.37 | 0.37 | 418.75 | 419.12 | |
| | | | | | | | | CC (w/7) | 0.52 | 0.52 | 419.12 | 419.64 | PAL |
| | | | | | | | | Totals: | 9.74 | 9.74 | | | |
| 45X | 28 | 0725 | 419.5 | 429.1 | 9.6 | 8.92 | 92.9 | | | | | | |
| | | | | | | | | 1 | 1.50 | 1.50 | 419.50 | 421.00 | |
| | | | | | | | | 2 | 1.50 | 1.50 | 421.00 | 422.50 | |
| | | | | | | | | 3 | 1.50 | 1.50 | 422.50 | 424.00 | |
| | | | | | | | | 4 | 1.50 | 1.50 | 424.00 | 425.50 | HS, IW |
| | | | | | | | | 5 | 1.50 | 1.50 | 425.50 | 427.00 | |
| | | | | | | | | 6 | 1.05 | 1.05 | 427.00 | 428.05 | |
| | | | | | | | | CC (w/6) | 0.37 | 0.37 | 428.05 | 428.42 | PAL |
| | | | | | | | | Totals: | 8.92 | 8.92 | | | |
| 46X | 28 | 0855 | 429.1 | 438.8 | 9.7 | 8.77 | 90.4 | | | | | | |
| | | | | | | | | 1 | 1.20 | 1.20 | 429.10 | 430.30 | |
| | | | | | | | | 2 | 1.50 | 1.50 | 430.30 | 431.80 | |
| | | | | | | | | 3 | 1.50 | 1.50 | 431.80 | 433.30 | |
| | | | | | | | | 4 | 1.50 | 1.50 | 433.30 | 434.80 | HS, IW |
| | | | | | | | | 5 | 1.50 | 1.50 | 434.80 | 436.30 | |

**Table T2 (continued).**

| Core | Date (Jan. 2001) | Time (local) | Core depth (mbsf) Top | Core depth (mbsf) Bottom | Length (m) Cored | Length (m) Recovered | Recovery (%) | Section | Length (m) Liner | Length (m) Curated | Section depth (mbsf) Top | Section depth (mbsf) Bottom | Catwalk samples |
|---|---|---|---|---|---|---|---|---|---|---|---|---|---|
| | | | | | | | | 6 | 1.18 | 1.18 | 436.30 | 437.48 | |
| | | | | | | | | CC (w/CC) | 0.39 | 0.39 | 437.48 | 437.87 | PAL |
| | | | | | | | | Totals: | 8.77 | 8.77 | | | |
| 47X | 28 | 1030 | 438.8 | 448.4 | 9.6 | 7.41 | 77.2 | | | | | | |
| | | | | | | | | 1 | 1.50 | 1.50 | 438.80 | 440.30 | |
| | | | | | | | | 2 | 1.45 | 1.45 | 440.30 | 441.75 | |
| | | | | | | | | 3 | 1.32 | 1.32 | 441.75 | 443.07 | HS, IW |
| | | | | | | | | 4 | 1.50 | 1.50 | 443.07 | 444.57 | |
| | | | | | | | | 5 | 1.17 | 1.17 | 444.57 | 445.74 | |
| | | | | | | | | CC (w/CC) | 0.47 | 0.47 | 445.74 | 446.21 | PAL |
| | | | | | | | | Totals: | 7.41 | 7.41 | | | |
| 48X | 28 | 1150 | 448.4 | 458.0 | 9.6 | 9.66 | 100.6 | | | | | | |
| | | | | | | | | 1 | 1.50 | 1.50 | 448.40 | 449.90 | |
| | | | | | | | | 2 | 1.50 | 1.50 | 449.90 | 451.40 | |
| | | | | | | | | 3 | 1.50 | 1.50 | 451.40 | 452.90 | |
| | | | | | | | | 4 | 1.50 | 1.50 | 452.90 | 454.40 | IW |
| | | | | | | | | 5 | 1.50 | 1.50 | 454.40 | 455.90 | HS |
| | | | | | | | | 6 | 1.50 | 1.50 | 455.90 | 457.40 | |
| | | | | | | | | 7 | 0.29 | 0.29 | 457.40 | 457.69 | |
| | | | | | | | | CC (w/7) | 0.37 | 0.37 | 457.69 | 458.06 | PAL |
| | | | | | | | | Totals: | 9.66 | 9.66 | | | |
| 49X | 28 | 1335 | 458.0 | 467.7 | 9.7 | 5.73 | 59.1 | | | | | | |
| | | | | | | | | 1 | 1.50 | 1.50 | 458.00 | 459.50 | |
| | | | | | | | | 2 | 1.50 | 1.50 | 459.50 | 461.00 | IW |
| | | | | | | | | 3 | 1.50 | 1.50 | 461.00 | 462.50 | HS |
| | | | | | | | | 4 | 0.83 | 0.83 | 462.50 | 463.33 | |
| | | | | | | | | CC (w/4) | 0.40 | 0.40 | 463.33 | 463.73 | PAL |
| | | | | | | | | Totals: | 5.73 | 5.73 | | | |
| 50X | 28 | 1515 | 467.7 | 477.3 | 9.6 | 2.04 | 21.3 | | | | | | |
| | | | | | | | | 1 | 1.20 | 1.20 | 467.70 | 468.90 | IW |
| | | | | | | | | 2 | 0.52 | 0.52 | 468.90 | 469.42 | HS |
| | | | | | | | | CC (w/2) | 0.32 | 0.32 | 469.42 | 469.74 | PAL |
| | | | | | | | | Totals: | 2.04 | 2.04 | | | |
| 51X | 28 | 1650 | 477.3 | 486.9 | 9.6 | 2.98 | 31.0 | | | | | | |
| | | | | | | | | 1 | 1.50 | 1.50 | 477.30 | 478.80 | IW |
| | | | | | | | | 2 | 1.07 | 1.07 | 478.80 | 479.87 | HS |
| | | | | | | | | CC (w/2) | 0.41 | 0.41 | 479.87 | 480.28 | PAL |
| | | | | | | | | Totals: | 2.98 | 2.98 | | | |
| 52X | 28 | 1835 | 486.9 | 496.6 | 9.7 | 1.16 | 12.0 | | | | | | |
| | | | | | | | | 1 | 0.87 | 0.87 | 486.90 | 487.77 | HS |
| | | | | | | | | CC (w/1) | 0.29 | 0.29 | 487.77 | 488.06 | PAL |
| | | | | | | | | Totals: | 1.16 | 1.16 | | | |
| 53X | 28 | 1935 | 496.6 | 506.2 | 9.6 | 0.54 | 5.6 | | | | | | |
| | | | | | | | | CC (w/CC) | 0.54 | 0.54 | 496.60 | 497.14 | PAL, HS |
| | | | | | | | | Totals: | 0.54 | 0.54 | | | |
| 54X | 28 | 2115 | 506.2 | 515.7 | 9.5 | 6.91 | 72.7 | | | | | | |
| | | | | | | | | 1 | 1.50 | 1.50 | 506.20 | 507.70 | |
| | | | | | | | | 2 | 1.50 | 1.50 | 507.70 | 509.20 | |
| | | | | | | | | 3 | 1.50 | 1.50 | 509.20 | 510.70 | IW |
| | | | | | | | | 4 | 1.50 | 1.50 | 510.70 | 512.20 | HS |
| | | | | | | | | 5 | 0.50 | 0.50 | 512.20 | 512.70 | |
| | | | | | | | | CC (w/5) | 0.41 | 0.41 | 512.70 | 513.11 | |
| | | | | | | | | Totals: | 6.91 | 6.91 | | | |
| 55X | 28 | 2330 | 515.7 | 521.2 | 5.5 | 2.00 | 36.4 | | | | | | |
| | | | | | | | | 1 | 1.43 | 1.43 | 515.70 | 517.13 | IW |
| | | | | | | | | 2 | 0.37 | 0.37 | 517.13 | 517.50 | HS |
| | | | | | | | | CC (w/2) | 0.20 | 0.20 | 517.50 | 517.70 | PAL |
| | | | | | | | | Totals: | 2.00 | 2.00 | | | |
| | | | | Totals: | 521.2 | 399.52 | 76.7 | | | | | | |

Notes: CC = core catcher (number in parentheses indicates which section the core catcher is stored with). Catwalk samples: PAL = paleontology sample, IW = interstitial water, HS = headspace.

**Table T3.** Lithologic units and subunits, Site 1195.

| | | Hole 1195A | | | | Hole 1195B | | | | | |
|---|---|---|---|---|---|---|---|---|---|---|---|
| | | Core, section, interval (cm) | | Depth (mbsf) | | Core, section, interval (cm) | | Depth (mbsf) | | | |
| Unit | Subunit | Top | Base | Top | Base | Top | Base | Top | Base | Description | Interpretation |
| I | | 1H | 5H-1, 133 | 0 | 34.5 | 1H-1, 0 | 5H-1, 133 | 0.0 | 34.5 | Skeletal packstone/grainstone with planktonic foraminifers, light gray to pale yellow, phophatized lithoclasts, mollusks and bryozoans. | Hemipelagic (open plateau), high energy |
| II | IIA | | | | | 5H-1, 133 | 10H-8, 10 | 34.5 | 93.9 | Skeletal packstone/grainstone, planktonic foraminifers, light greenish gray to olive-gray. First occurrence of glauconite-rich layers. | Hemipelagic (open plateau), mixed energy |
| II | IIB | | | | | 11H-1, 0 | 14H-1, 150 | 93.9 | 123.9 | Skeletal packstone, with clay, planktonic foraminifers, light greenish gray. First appearance of pyrite-stained burrows. | Hemipelagic (open plateau), low energy |
| II | IIC | | | | | 14H-2, 0 | 27X-8, 30 | 123.9 | 255.9 | Skeletal wackestone to packstone/grainstone, with clay, planktonic foraminifers, light greenish gray to light olive-gray, pyrite-stained burrows, recurrent alternations between wackestone and packstone and packstone and grainstone. | Hemipelagic (open plateau) to distal periplatform, mixed energy |
| III | IIIA | | | | | 28X-1, 0 | 33X-5, 45 | 255.9 | 313.5 | Skeletal wackestone to packstone/grainstone, with clay, rare reworked planktonic foraminifers, light olive-gray to light greenish gray. | Distal periplatform, mixed energy |
| III | IIIB | | | | | 34X-1, 0 | 49X-4, 80 | 313.5 | 463.3 | Skeletal mudstone/wackestone to packstone/grainstone with clay. Dark greenish gray common. First occurrence of quartz. | Distal periplatform, mixed energy |
| IV | | | | | | 49X-CC, 0 | 55X-2, 40 | 463.3 | 517.5 | Sandstone to grainstone with quartz and glauconite, greenish gray. Quartz angular, glauconite rounded, carbonate lithoclasts. | Proximal periplatform, high energy |
| V | | | | | | 55X-CC, 0 | 55X-CC, 20 | 517.5 | 517.7 | Skeletal grainstone, nummulitids, mollusks, and coralline algae, light yellowish brown. | Shelf to outer slope, high energy |

**Table T4.** Biostratigraphic datums, Site 1195.

| Datum | Core, section, interval (cm) | Depth (mbsf) First absence or presence | Depth (mbsf) Last presence or absence | Mean depth (mbsf) | Age (Ma) |
|---|---|---|---|---|---|
| | 194-1195A- | | | | |
| LO *Pseudoemiliania lacunosa* | 1H-CC to 2H-CC | 4.59 | 14.09 | 9.34 | 0.46 |
| LO *Globorotalia tosaensis* | 1H-CC to 2H-CC | 4.59 | 14.09 | 9.34 | 0.60 |
| FO *Pulleniatina finalis* | 1H-CC to 2H-CC | 4.59 | 14.09 | 9.34 | 1.30 |
| LO *Calcidiscus macintyrei* | 2H-CC to 3H-CC | 14.09 | 23.50 | 18.80 | 1.70 |
| LO *Globigerinoides fistulosus* | 2H-CC to 3H-CC | 14.09 | 23.50 | 18.80 | 2.00 |
| LO *Discoaster brouweri* | 3H-CC to 4H-CC | 23.50 | 32.99 | 28.25 | 2.00 |
| LO *Discoaster pentaradiatus* | 3H-CC to 4H-CC | 23.50 | 32.99 | 28.25 | 2.50 |
| LO *Discoaster surculus* | 4H-CC to 5H-CC | 32.99 | 42.29 | 37.64 | 2.60 |
| LO *Discoaster tamalis* | 4H-CC to 5H-CC | 32.99 | 42.29 | 37.64 | 2.80 |
| LO *Globorotalia margaritae* | 5H-CC to 6H-CC | 42.29 | 51.35 | 46.82 | 3.30 |
| LO *Reticulofenestra pseudoumbilica* | 5H-CC to 6H-CC | 42.29 | 51.35 | 46.82 | 3.70 |
| FO *Globorotalia cibaoensis* | 8H-CC to 9H-CC | 70.97 | 80.75 | 75.86 | 5.60 |
| LO *Discoaster quinqueramus* | 8H-CC to 9H-CC | 70.97 | 80.75 | 75.86 | 5.60 |
| | 194-1195B- | | | | |
| LO *Pseudoemiliania lacunosa* | 1H-1, 0 to 1H-CC | 0.00 | 8.26 | 4.13 | 0.46 |
| LO *Calcidiscus macintyrei* | 2H-CC to 3H-CC | 17.40 | 27.11 | 22.26 | 1.70 |
| LO *Globigerinoides fistulosus* | 2H-CC to 3H-CC | 17.40 | 27.11 | 22.26 | 2.00 |
| LO *Discoaster brouweri* | 2H-CC to 3H-CC | 17.40 | 27.11 | 22.26 | 2.00 |
| LO *Discoaster pentaradiatus* | 3H-CC to 4H-CC | 27.11 | 36.74 | 31.93 | 2.50 |
| LO *Discoaster surculus* | 3H-CC to 4H-CC | 27.11 | 36.74 | 31.93 | 2.60 |
| LO *Discoaster tamalis* | 3H-CC to 4H-CC | 27.11 | 36.74 | 31.93 | 2.80 |
| FO *Globigerinoides fistulosus* | 4H-CC to 5H-CC | 36.74 | 45.70 | 41.22 | 2.90 |
| LO *Reticulofenestra pseudoumbilica* | 5H-CC to 6H-CC | 45.70 | 55.39 | 50.55 | 3.70 |
| FO *Sphaeroidinella dehiscens* | 6H-CC to 7H-CC | 55.39 | 65.60 | 60.50 | 5.10 |
| LO *Discoaster quinqueramus* | 8H-CC to 9H-CC | 74.24 | 84.41 | 79.33 | 5.60 |
| FO *Discoaster surculus* | 14H-CC to 15H-2, 80 | 132.05 | 141.48 | 136.77 | 7.50 |
| FO *Discoaster quinqueramus* | 16X-CC to 17X-CC | 150.80 | 159.90 | 155.35 | 8.50 |
| FO *Discoaster pentaradiatus* | 17X-CC to 18X-CC | 159.90 | 170.24 | 165.07 | 9.20 |
| LO *Discoaster hamatus* | 20X-CC to 21X-CC | 189.20 | 198.76 | 193.98 | 9.50 |
| FO *Discoaster hamatus* | 22X-CC to 23X-CC | 207.36 | 210.27 | 208.82 | 10.50 |
| FO *Globorotalia plesiotumida* | 24X-CC to 25X-CC | 226.56 | 236.65 | 231.61 | 10.90 |
| LO *Globorotalia mayeri-siakensis* | 25X-CC to 26X-CC | 236.65 | 243.06 | 239.86 | 11.40 |
| LO *Cyclicargolithus floridanus* | 27X-CC to 28X-CC | 255.59 | 263.33 | 259.46 | 11.90 |
| LO *Globorotalia peripheroacuta* | 28X-CC to 29X-CC | 263.33 | 274.43 | 268.88 | 12.50 |
| LO *Sphenolithus heteromorphus* | 29X-CC to 30X-CC | 274.43 | 280.49 | 277.46 | 13.60 |
| FO *Orbulina* sp. | 35X-CC to 36X-CC | 330.01 | 338.31 | 334.16 | 15.10 |
| FO *Sphenolithus heteromorphus* | 46X-CC to 47X-CC | 437.48 | 445.74 | 441.61 | 18.20 |
| LO *Sphenolithus belemnos* | 46X-CC to 47X-CC | 437.48 | 445.74 | 441.61 | 18.50 |
| FO *Sphenolithus belemnos* | 51X-CC to 52X-CC | 479.87 | 487.77 | 483.82 | 20.60 |

Note: FO = first occurrence, LO = last occurrence.

**Table T5.** Summary of biostratigraphic and paleoenvironmental interpretations, Site 1195. (See table notes. Continued on next page.)

| Hole, core, section (cm) | Depth (mbsf) | Foraminiferal assemblages | | | | | Comments on sand-sized fraction | Paleowater depth (m) | | | Depositional setting | Lithologic unit |
|---|---|---|---|---|---|---|---|---|---|---|---|---|
| | | PF | ONBF | ESBF | LBF | Pres | | <100 | >100 | >200 | | |
| 194- | | | | | | | | | | | | |
| 1195A-1H | 4.7 | Dom | Div | R | | G | Overwhelmingly PF, including debris | | | X | Hemipelagic | I |
| 1195B-1H | 8.36 | Dom | Div | | | G | Overwhelmingly PF, including debris | | | X | Hemipelagic | |
| 1195A-2H | 14.25 | Dom | R | | | G | Overwhelmingly PF, including debris | | | X | Hemipelagic | II |
| 1195B-2H | 17.49 | Dom | C | | | G | Overwhelmingly PF, including debris | | | X | Hemipelagic | |
| 1195A-3H | 23.67 | Dom | R | | | G | Overwhelmingly PF, including debris | | | X | Hemipelagic | |
| 1195B-3H | 27.23 | Dom | R | | | G | Overwhelmingly PF, including debris | | | X | Hemipelagic | |
| 1195A-4H | 33.14 | Dom | R | | | G | Overwhelmingly PF, including debris | | | X | Hemipelagic | |
| 1195B-4H | 36.9 | Dom | R | | | G | PF, much reworked | | | X | Hemipelagic | |
| 1195A-5H | 42.44 | Dom | R | R | | G | Overwhelmingly PF, including debris | | | X | Hemipelagic | IIA |
| 1195B-5H | 45.9 | Dom | R | | | G | Overwhelmingly PF, including debris | | | X | Hemipelagic | |
| 1195A-6H | 51.55 | Dom | R | | | G | Overwhelmingly PF, including debris | | | X | Hemipelagic | |
| 1195B-6H | 55.55 | Dom | R | | | G | Overwhelmingly PF, including debris | | | X | Hemipelagic | |
| 1195A-7H | 60.79 | Dom | R | | | G | Overwhelmingly PF, including debris | | | X | Hemipelagic | |
| 1195B-7H | 65.76 | Dom | R | | | G | Overwhelmingly PF, including debris | | | X | Hemipelagic | |
| 1195A-8H | 71.1 | Dom | R | | | G | Overwhelmingly PF, including debris | | | X | Hemipelagic | |
| 1195B-8H | 74.39 | Dom | R | | | G | Overwhelmingly PF, including debris | | | X | Hemipelagic | |
| 1195A-9H | 80.93 | Dom | R | | | G | Overwhelmingly PF, including debris | | | X | Hemipelagic | |
| 1195B-9H | 84.5 | Dom | R | | | G | Overwhelmingly PF, including debris | | | X | Hemipelagic | |
| 1195B-10H | 94.13 | Dom | R | | | G | Overwhelmingly PF, including debris | | | X | Hemipelagic | |
| 1195B-11H | 103.48 | Dom | R | | | G | Overwhelmingly PF, including debris | | | X | Hemipelagic | IIB |
| 1195B-12H | 113.02 | Dom | R | | | G | Overwhelmingly PF, including debris | | | X | Hemipelagic | |
| 1195B-13H | 122.83 | Dom | R | | | G | Overwhelmingly PF, including debris | | | X | Hemipelagic | |
| 1195B-14H | 132.16 | Dom | R | | | G | Overwhelmingly PF, including debris | | | X | Hemipelagic | IIC |
| 1195B-16H | 150.95 | Dom | R | | | G | Overwhelmingly PF, including debris | | | X | Hemipelagic | |
| 1195B-17H | 160.72 | Dom | C | | | G | Overwhelmingly PF, including debris | | | X | Hemipelagic | |
| 1195B-18H | 170.46 | Dom | C | | | G | Overwhelmingly PF, including debris | | | X | Hemipelagic | |
| 1195B-19H | 179.84 | Dom | R | | | G | Overwhelmingly PF, including debris | | | X | Hemipelagic | |
| 1195B-20H | 189.36 | Dom | R | | | G | Overwhelmingly PF, including debris | | | X | Hemipelagic | |
| 1195B-21H | 198.93 | Dom | R | | | G | Overwhelmingly PF, including debris | | | X | Hemipelagic | |
| 1195B-22H | 207.36 | Dom | R | | R | G | PF, minor reworked neritic | | | X | Distal periplatform | |
| 1195B-23X | 210.47 | Dom | R | | R | M | PF, minor reworked neritic | | | X | Distal periplatform | |
| 1195B-24X | 226.84 | Dom | C | | | M | Overwhelmingly PF, including debris | | | X | Distal periplatform | |
| 1195B-25X | 237.03 | Dom | R | | | G | Overwhelmingly PF, including debris | | | X | Distal periplatform | |
| 1195B-26X | 243.34 | Dom | R | | R | G | PF with mixed source debris | | | X | Distal periplatform | |
| 1195B-27X | 255.9 | A | R | | | P-G | PF with mixed source debris | | | X | Distal periplatform | IIIA |
| 1195B-28X | 263.6 | A | R | | R | M | PF with mixed source debris | | | X | Distal periplatform | |
| 1195B-29X | 274.58 | Dom | C | | | M | PF with mixed source debris | | | X | Distal periplatform | |
| 1195B-30X | 280.78 | A | R | R | A | M | PF with mixed source debris | | | X | Distal periplatform | |
| 1195B-31X | 285.95 | Dom | Div | | A | M | PF with mixed source debris | | | X | Distal periplatform | |
| 1195B-32X | 299.31 | Dom | A | | | M | PF with mixed source debris | | | X | Distal periplatform | |
| 1195B-33X | 310.16 | C | C | | | P | Neritic dominates, PF, ONBF | | | X | Distal periplatform | IIIB |
| 1195B-34X | 321.21 | A | C | | | G | PF with mixed source debris | | | X | Distal periplatform | |
| 1195B-35X | 330.38 | Dom | R | | | M | PF with mixed source debris | | | X | Distal periplatform | |
| 1195B-36X | 338.71 | A | C | R | R | M | PF with mixed source debris | | | X | Distal periplatform | |
| 1195B-37X | 350.41 | A | C | | R | M | PF with mixed source debris | | | X | Distal periplatform | |

**Table T5 (continued).**

| Hole, core, section (cm) | Depth (mbsf) | Foraminiferal assemblages | | | | | Comments on sand-sized fraction | Paleowater depth (m) | | | Depositional setting | Lithologic unit |
|---|---|---|---|---|---|---|---|---|---|---|---|---|
| | | PF | ONBF | ESBF | LBF | Pres | | <100 | >100 | >200 | | |
| 1195B-38X | 355.14 | A | R | | | P | Recrystallized | | | X | Distal periplatform | |
| 1195B-39X | 365.71 | A | R | | R | M | PF with mixed source debris | | | X | Distal periplatform | |
| 1195B-40X | 377.55 | C | C | | R | M-G | PF with mixed source debris | | | X | Distal periplatform | |
| 1195B-41X | 382.39 | R | R | | | P | Recrystallized | | | X | Distal periplatform | |
| 1195B-42X | 394.61 | A | R | | | P | Recrystallized | | | X | Distal periplatform | |
| 1195B-43X | 401.32 | Dom | R | | | G | PF, limited neritic | | | X | Distal periplatform | |
| 1195B-44X | 419.62 | Dom | R | | | P | PF, limited neritic | | | X | Distal periplatform | |
| 1195B-45X | 428.4 | C | C | R | R | M | PF, some neritic | | | X | Distal periplatform | |
| 1195B-46X | 437.85 | R | R | | | M | PF, limited neritic | | | X | Distal periplatform | |
| 1195B-47X | 446.19 | C | C | R | R | M | PF with mixed source debris | | | X | Distal periplatform | |
| 1195B-48X | 458.04 | C | C | | R | P-M | Bioclasts predominantly neritic | | X | | Distal periplatform | |
| 1195B-49X | 463.46 | C | C | C | A | P-G | Glauconite, bone, black grains | | X | | Distal periplatform | IV |
| 1195B-50X | 469.42 | R | C | | | G | Quartz, glauconite, bioclastic, PF | | X | | Distal periplatform | |
| 1195B-51X | 479.97 | A | C | | | P-G | Quartz, glauconite, bioclastic, PF | | X | | Proximal periplatform | |
| 1195B-52X | 488.04 | C | C | | | M | Quartz, glauconite, bioclastic, PF | | X | | Proximal periplatform | |
| 1195B-53X | 497.11 | C | R | | | P | Quartz, glauconite, bioclastic, PF | | X | | Proximal periplatform | |
| 1195B-54X | 513.11 | C | R | | | P | Quartz, glauconite, bioclastic, PF | | X | | Proximal periplatform | |
| 1195B-55X | 517.67 | C | R | | A | P | Miocene–Eocene LBF, mud matrix | X | X | | Mixed | V |

Notes: Based on microscopic analysis of biogenic sediment constituents >63 µm, particularly benthic foraminifers, from core catcher samples. Foraminiferal assemblages: PF = planktonic foraminifers, ONBF = outer neritic to upper bathyal benthic foraminifers, ESBF = middle to inner neritic smaller benthic foraminifers, LBF = larger benthic foraminifers, Pres = preservation; Dom = dominant, Div = common and diverse, A = abundant, C = common, G = good, M = moderate, P = poor, R = rare.

**Table T6.** Magnetic polarity transitions, Site 1195. (See table note. Continued on next page.)

| Chron | Top observation | | Bottom observation | | Average | | |
|---|---|---|---|---|---|---|---|
| | Core, section, interval (cm) | Depth (mbsf) | Core, section, interval (cm) | Depth (mbsf) | Depth (mbsf) | Error | Age (Ma) |
| | 194-1195A- | | 194-1195A- | | | | |
| C1n (O) | 2H-6, 130 | 13.50 | 3H-2, 80 | 14.50 | 14.00 | 0.50 | 0.78 |
| C1r1r1n (T) | 3H-2, 130 | 17.00 | 3H-4, 30 | 19.00 | 18.00 | 1.00 | 0.99 |
| C1r1r1n (O) | 3H-4, 80 | 19.50 | 3H-4, 80 | 19.50 | 19.50 | 0.00 | 1.07 |
| C1r2r1n (T) | 3H-5, 130 | 21.50 | 4H-1, 30 | 24.00 | 22.75 | 1.25 | 1.20 |
| C1r2r1n (T) | 4H-2, 10 | 25.30 | 4H-2, 10 | 25.30 | 25.30 | 0.00 | 1.21 |
| C2n (T) | 5H-1, 10 | 33.30 | 5H-1, 80 | 34.00 | 33.65 | 0.35 | 1.77 |
| C2n (O) | 5H-3, 30 | 36.50 | 5H-4, 30 | 38.00 | 37.25 | 0.75 | 1.95 |
| C2r1n (T) | 6H-1, 5 | 42.75 | 6H-2, 30 | 44.50 | 43.63 | 0.88 | 2.14 |
| C2r1n (O) | 6H-1, 30 | 43.00 | 6H-1, 80 | 43.50 | 43.25 | 0.25 | 2.15 |
| C2An.1n (T) | 6H-3, 130 | 47.00 | 6H-4, 80 | 48.00 | 47.50 | 0.50 | 2.58 |
| C2An.1n (O) | 6H-5, 130 | 50.00 | 7H-1, 80 | 53.00 | 51.50 | 1.50 | 3.04 |
| C2An.2n (T) | 7H-1, 100 | 53.20 | 7H-1, 130 | 53.50 | 53.35 | 0.15 | 3.11 |
| C2An.2n (O) | 7H-2, 130 | 55.00 | 7H-3, 40 | 55.60 | 55.30 | 0.30 | 3.22 |
| C2An.3n (T) | 7H-6, 30 | 60.00 | 7H-6, 80 | 60.50 | 60.25 | 0.25 | 3.33 |
| C2An.3n (O) | 8H-1, 130 | 63.00 | 8H-2, 80 | 64.00 | 63.50 | 0.50 | 3.58 |
| C3n.1n (T) | 8H-6, 80 | 70.00 | 8H-1, 45 | 70.85 | 70.43 | 0.43 | 4.18 |
| C3n.1n (O) | 9H-1, 60 | 71.80 | 9H-2, 30 | 72.50 | 72.15 | 0.35 | 4.29 |
| C3n.2n (T) | 9H-2, 80 | 73.00 | 9H-3, 38 | 73.50 | 73.25 | 0.25 | 4.48 |
| C3n.2n (O) | 9H-4, 38 | 75.00 | 9H-4, 38 | 75.00 | 75.00 | 0.00 | 4.46 |
| C3n.3n (T) | 9H-5, 38 | 76.50 | 9H-5, 38 | 76.50 | 76.50 | 0.00 | 4.80 |
| C3n.3n (O) | 9H-5, 138 | 77.50 | 9H-6, 38 | 78.00 | 77.75 | 0.25 | 4.89 |
| C3n.4n (T) | 9H-6, 63 | 78.25 | 9H-6, 138 | 79.00 | 78.63 | 0.38 | 4.98 |
| C3n.4n (O) | | 96.32 | | 98.70 | 97.51 | 1.19 | 5.23 |
| | 194-1195B- | | 194-1195B- | | | | |
| C1n (O) | 2H-5, 10 | 14.50 | 2H-6, 60 | 16.50 | 15.50 | 1.00 | 0.78 |
| C1r1r1n (T) | 2H-5, 110 | 15.50 | 3H-2, 60 | 20.00 | 17.75 | 2.25 | 0.99 |
| C1r1r1n (O) | 2H-6, 110 | 17.00 | 3H-2, 60 | 20.00 | 18.50 | 1.50 | 1.07 |
| C2n (T) | 4H-1, 60 | 28.00 | 4H-2, 10 | 29.00 | 28.50 | 0.50 | 1.77 |
| C2n (O) | 4H-3, 10 | 30.50 | 4H-3, 10 | 30.50 | 30.50 | 0.00 | 1.95 |
| C2r1n (T) | 4H-6, 15 | 35.05 | 4H-6, 135 | 36.25 | 35.65 | 0.60 | 2.14 |
| C2r1n (O) | 4H-6, 135 | 36.25 | 4H-6, 135 | 36.25 | 36.25 | 0.00 | 2.15 |
| C2An.1n (T) | 5H-1, 25 | 37.15 | 5H-1, 25 | 37.15 | 37.15 | 0.00 | 2.58 |
| C2An.1n (O) | 5H-6, 125 | 45.65 | 6H-1, 10 | 46.50 | 46.08 | 0.43 | 3.04 |
| C2An.2n (T) | 6H-1, 10 | 46.50 | 6H-1, 60 | 47.00 | 46.75 | 0.25 | 3.11 |
| C2An.2n (O) | 6H-1, 110 | 47.50 | 6H-2, 60 | 48.50 | 48.00 | 0.50 | 3.22 |
| C2An.3n (T) | 6H-2, 60 | 48.50 | 6H-3, 60 | 50.00 | 49.25 | 0.75 | 3.33 |
| C2An.3n (O) | 7H-1, 110 | 57.00 | 7H-2, 60 | 58.00 | 57.50 | 0.50 | 3.58 |
| C3n.1n (T) | 7H-3, 110 | 60.00 | 7H-3, 110 | 60.00 | 60.00 | 0.00 | 4.18 |
| C3n.1n (O) | 7H-4, 60 | 61.00 | 7H-4, 110 | 61.00 | 61.00 | 0.00 | 4.29 |
| C3n.2n (T) | 7H-5, 60 | 62.50 | 7H-5, 60 | 62.50 | 62.50 | 0.00 | 4.48 |
| C3n.2n (O) | 7H-6, 60 | 64.00 | 7H-6, 60 | 64.00 | 64.00 | 0.00 | 4.46 |
| C3n.3n (T) | 7H-7, 60 | 65.50 | 8H-1, 35 | 65.75 | 65.63 | 0.13 | 4.80 |
| C3n.3n (O) | 8H-3, 10 | 68.50 | 8H-3, 10 | 68.50 | 68.50 | 0.00 | 4.89 |
| C3n.4n (T) | 8H-4, 10 | 70.00 | 8H-4, 10 | 70.00 | 70.00 | 0.00 | 4.98 |
| C3n.4n (O) | 8H-6, 35 | 73.25 | 8H-6, 110 | 74.00 | 73.63 | 0.38 | 5.23 |
| C3An.1n (T) | 9H-4, 60 | 80.00 | 9H-4, 60 | 80.00 | 80.00 | 0.00 | 5.89 |
| C3An.1n (O) | 10H-3, 10 | 87.50 | 10H-3, 10 | 87.50 | 87.50 | 0.00 | 6.13 |
| C3An.2n (T) | 10H-4, 15 | 89.15 | 10H-4, 15 | 89.15 | 89.15 | 0.00 | 6.27 |
| C3An.2n (O) | 11H-2, 40 | 95.80 | 11H-3, 10 | 97.00 | 96.40 | 0.60 | 6.57 |
| C3Bn (T) | 12H-4, 10 | 108.00 | 12H-4, 10 | 108.00 | 108.00 | 0.00 | 6.94 |
| C3Bn (O) | 13H-1, 110 | 114.00 | 13H-1, 110 | 114.00 | 114.00 | 0.00 | 7.09 |
| C3Br1n (T) | 13H-5, 60 | 119.50 | 13H-5, 60 | 119.50 | 119.50 | 0.00 | 7.14 |
| C3Br1n (O) | 13H-7, 40 | 122.25 | 13H-7, 40 | 122.25 | 122.25 | 0.00 | 7.17 |
| C3Br2n (T) | 14H-4, 110 | 128.00 | 14H-4, 110 | 128.00 | 128.00 | 0.00 | 7.34 |
| C3Br2n (O) | 15H-1, 60 | 132.50 | 15H-1, 60 | 132.50 | 132.50 | 0.00 | 7.37 |
| C4n.1n (T) | 15H-3, 10 | 135.00 | 15H-3, 10 | 135.00 | 135.00 | 0.00 | 7.43 |
| C4n.1n (O) | 16H-2, 140 | 144.25 | 16H-2, 140 | 144.25 | 144.25 | 0.00 | 7.56 |
| C4n.2n (T) | 16H-4, 60 | 146.50 | 16H-4, 60 | 146.50 | 146.50 | 0.00 | 7.65 |
| C4n.2n (O) | 16H-6, 110 | 150.00 | 16H-6, 110 | 150.00 | 150.00 | 0.00 | 8.07 |
| C4r.1n (T) | 17H-2, 10 | 152.50 | 17H-3, 10 | 154.00 | 153.25 | 0.75 | 8.23 |
| C4r.1n (O) | 17H-3, 10 | 154.00 | 17H-3, 10 | 154.00 | 154.00 | 0.00 | 8.23 |
| C4An (T) | 18H-4, 110 | 166.00 | 18H-4, 110 | 166.00 | 166.00 | 0.00 | 8.70 |
| C4An (O) | 18H-7, 40 | 169.80 | 18H-7, 50 | 170.00 | 169.90 | 0.10 | 9.03 |
| C4Ar.1n (T) | 19H-4, 60 | 175.00 | 19H-4, 60 | 175.00 | 175.00 | 0.00 | 9.23 |
| C4Ar.1n (O) | 19H-5, 60 | 176.50 | 19H-5, 60 | 176.50 | 176.50 | 0.00 | 9.31 |

**Table T6 (continued).**

| Chron | Top observation | | Bottom observation | | Average | | |
|---|---|---|---|---|---|---|---|
| | Core, section, interval (cm) | Depth (mbsf) | Core, section, interval (cm) | Depth (mbsf) | Depth (mbsf) | Error | Age (Ma) |
| C4Ar.2n (T) | 20H-4, 60 | 184.50 | 20H-4, 60 | 184.50 | 184.50 | 0.00 | 9.58 |
| C4Ar.2n (O) | 20H-5, 10 | 185.50 | 20H-5, 10 | 185.50 | 185.50 | 0.00 | 9.64 |
| C5n.1n (T) | 21H-3, 60 | 192.50 | 21H-3, 110 | 193.00 | 192.75 | 0.25 | 9.74 |
| C5n.1n (O) | 21H-6, 60 | 197.00 | 22H-1, 60 | 199.00 | 198.00 | 1.00 | 9.88 |
| C5n.2n (T) | 22H-2, 10 | 200.00 | 22H-4, 10 | 203.00 | 201.50 | 1.50 | 9.92 |
| C5n.2n (O) | 25X-1, 90 | 228.00 | 25X-2, 140 | 230.00 | 229.00 | 1.00 | 10.95 |
| C5r.1r (T) | 25X-3, 90 | 231.00 | 25X-4, 40 | 232.00 | 231.50 | 0.50 | 11.05 |
| C5r.1r (O) | 25X-4, 90 | 232.50 | 25X-4, 140 | 233.00 | 232.75 | 0.25 | 11.10 |
| C5r.2n (T) | 26X-1, 30 | 237.00 | 26X-1, 30 | 237.00 | 237.00 | 0.00 | 11.48 |
| C5r.2n (O) | 26X-3, 33 | 240.00 | 26X-3, 33 | 240.00 | 240.00 | 0.00 | 11.53 |
| C5An.1n (T) | 26X-4, 143 | 242.60 | 27X-1, 70 | 247.00 | 244.80 | 2.20 | 11.94 |
| C5An.1n (O) | 27X-3, 20 | 249.50 | 27X-3, 20 | 249.50 | 249.50 | 0.00 | 12.08 |
| C5An.2n (T) | 27X-4, 120 | 252.00 | 27X-4, 120 | 252.00 | 252.00 | 0.00 | 12.18 |
| C5An.2n (O) | 27X-6, 70 | 254.50 | 27X-6, 70 | 254.50 | 254.50 | 0.00 | 12.40 |
| C5Ar.1r (T) | 28X-1, 10 | 256.00 | 28X-1, 10 | 256.00 | 256.00 | 0.00 | 12.68 |
| C5Ar.1n (O) | 28X-1, 110 | 257.00 | 28X-1, 110 | 257.00 | 257.00 | 0.00 | 12.71 |
| C5Ar.2n (T) | 28X-2, 60 | 258.00 | 28X-2, 60 | 258.00 | 258.00 | 0.00 | 12.78 |
| C5Ar.2n (O) | 28X-4, 60 | 261.00 | 28X-4, 60 | 261.00 | 261.00 | 0.00 | 12.82 |
| C5Dn (T) | 44X-3, 128 | 414.00 | 44X-3, 128 | 414.00 | 414.00 | 0.00 | 17.28 |
| C5Dn (O) | 44X-CC, 11 | 419.50 | 44X-CC, 11 | 419.50 | 419.50 | 0.00 | 17.62 |
| C5En (T) | 45X-4, 50 | 424.50 | 45X-4, 50 | 424.50 | 424.50 | 0.00 | 18.28 |
| C5En (O) | 45X-6, 50 | 427.50 | 45X-6, 50 | 427.50 | 427.50 | 0.00 | 18.78 |
| C6n (T) | 46X-2, 150 | 431.75 | 46X-2, 150 | 431.75 | 431.75 | 0.00 | 19.05 |
| C6n (O) | 47X-2, 120 | 441.50 | 47X-2, 120 | 441.50 | 441.50 | 0.00 | 20.13 |

Note: (T) = termination, (O) = onset.

**Table T7.** Age-depth control points, Site 1195.

| Source | Datum | Age (Ma) | Top: FO presence or LO absence | | Bottom: LO presence or FO absence | | Average depth (mbsf) | Uncertainty (m) | |
|---|---|---|---|---|---|---|---|---|---|
| | | | Core, section, interval (cm) | Depth (mbsf) | Core, section, interval (cm) | Depth (mbsf) | | Up-section | Down-section |
| | | | 194-1195A- | | 194-1195A- | | | | |
| CN | LO *Pseudoemiliania lacunosa* | 0.46 | 1H-CC | 4.59 | 2H-CC | 14.09 | 9.34 | 4.75 | 4.75 |
| PF | LO *Globorotalia tosaensis* | 0.6 | 1H-CC | 4.59 | 2H-CC | 14.09 | 9.34 | 4.75 | 4.75 |
| PF | FO *Pulleniatina finalis* | 1.3 | 1H-CC | 4.59 | 2H-CC | 14.09 | 9.34 | 4.75 | 4.75 |
| CN | LO *Calcidiscus macintyrei* | 1.7 | 2H-CC | 14.09 | 3H-CC | 23.50 | 18.80 | 4.71 | 4.71 |
| PF | LO *Globigerinoides fistulosus* | 2.0 | 2H-CC | 14.09 | 3H-CC | 23.50 | 18.80 | 4.71 | 4.71 |
| CN | LO *Discoaster brouweri* | 2.0 | 3H-CC | 23.50 | 4H-BCI | 33.20 | 28.35 | 4.85 | 4.85 |
| CN | LO *Discoaster pentaradiatus* | 2.5 | 3H-CC | 23.50 | 4H-BCI | 33.20 | 28.35 | 4.85 | 4.85 |
| CN | LO *Discoaster surculus* | 2.6 | 4H-CC | 32.99 | 5H-BCI | 42.70 | 37.85 | 4.86 | 4.86 |
| CN | LO *Discoaster tamalis* | 2.8 | 4H-CC | 32.99 | 5H-BCI | 42.70 | 37.85 | 4.86 | 4.86 |
| PF | LO *Globorotalia margaritae* | 3.3 | 5H-CC | 42.29 | 6H-BCI | 52.20 | 47.25 | 4.96 | 4.96 |
| CN | LO *Reticulofenestra pseudoumbilica* | 3.7 | 5H-CC | 42.29 | 6H-BCI | 52.20 | 47.25 | 4.96 | 4.96 |
| PF | FO *Globorotalia cibaoensis* | 5.6 | 8H-CC | 70.97 | 9H-CC | 80.75 | 75.86 | 4.89 | 4.89 |
| CN | LO *Discoaster quinqueramus* | 5.6 | 8H-CC | 70.97 | 9H-CC | 80.75 | 75.86 | 4.89 | 4.89 |
| | | | 194-1195B- | | 194-1195B- | | | | |
| CN | LO *Pseudoemiliania lacunosa* | 0.4 | 1H-1, 0 | 0.00 | 1H-CC | 8.26 | 4.13 | 4.13 | 4.13 |
| CN | LO *Calcidiscus macintyrei* | 1.7 | 2H-CC | 17.40 | 3H-BCI | 27.40 | 22.40 | 5.00 | 5.00 |
| PF | LO *Globigerinoides fistulosus* | 2.0 | 2H-CC | 17.40 | 3H-BCI | 27.40 | 22.40 | 5.00 | 5.00 |
| CN | LO *Discoaster brouweri* | 2.0 | 2H-CC | 17.40 | 3H-BCI | 27.40 | 22.40 | 5.00 | 5.00 |
| CN | LO *Discoaster pentaradiatus* | 2.5 | 3H-CC | 27.11 | 4H-CC | 36.74 | 31.93 | 4.82 | 4.82 |
| CN | LO *Discoaster surculus* | 2.6 | 3H-CC | 27.11 | 4H-CC | 36.74 | 31.93 | 4.82 | 4.82 |
| CN | LO *Discoaster tamalis* | 2.8 | 3H-CC | 27.11 | 4H-CC | 36.74 | 31.93 | 4.82 | 4.82 |
| PF | FO *Globigerinoides fistulosus* | 2.9 | 4H-CC | 36.74 | 5H-BCI | 46.40 | 41.57 | 4.83 | 4.83 |
| CN | LO *Reticulofenestra pseudoumbilica* | 3.7 | 5H-CC | 45.70 | 6H-BCI | 55.90 | 50.80 | 5.10 | 5.10 |
| CN | FO *Sphaeroidinella dehiscens* | 5.1 | 6H-CC | 55.39 | 7H-CC | 65.60 | 60.50 | 5.11 | 5.11 |
| CN | LO *Discoaster quinqueramus* | 5.6 | 8H-CC | 74.24 | 9H-CC | 84.41 | 79.33 | 5.08 | 5.09 |
| CN | FO *Discoaster surculus* | 7.5 | 14H-CC | 132.05 | 15H-2, 80 | 141.48 | 136.77 | 4.71 | 4.72 |
| CN | FO *Discoaster quinqueramus* | 8.5 | 16X-CC | 150.80 | 17X-CC | 159.90 | 155.35 | 4.55 | 4.55 |
| CN | FO *Discoaster pentaradiatus* | 9.2 | 17X-CC | 159.90 | 18X-CC | 170.24 | 165.07 | 5.17 | 5.17 |
| CN | LO *Discoaster hamatus* | 9.5 | 20X-CC | 189.20 | 21X-CC | 198.76 | 193.98 | 4.78 | 4.78 |
| CN | FO *Discoaster hamatus* | 10.5 | 22X-CC | 207.36 | 23X-BCI | 217.50 | 212.43 | 5.07 | 5.07 |
| PF | FO *Globorotalia plesiotumida* | 10.9 | 24X-CC | 226.56 | 25X-CC | 236.65 | 231.61 | 5.05 | 5.04 |
| PF | LO *Globorotalia mayeri-siakensis* | 11.4 | 25X-CC | 236.65 | 26X-BCI | 246.30 | 241.48 | 4.83 | 4.82 |
| CN | LO *Cyclicargolithus floridanus* | 11.9 | 27X-CC | 255.59 | 28X-BCI | 265.50 | 260.55 | 4.96 | 4.95 |
| PF | LO *Globorotalia peripheroacuta* | 12.5 | 28X-CC | 263.33 | 29X-BCI | 275.10 | 269.22 | 5.89 | 5.88 |
| CN | LO *Sphenolithus heteromorphus* | 13.6 | 29X-CC | 274.43 | 30X-BCI | 284.60 | 279.52 | 5.08 | 5.09 |
| PF | FO *Orbulina* sp. | 15.1 | 35X-CC | 330.01 | 36X-BCI | 342.30 | 336.16 | 6.14 | 6.15 |
| CN | FO *Sphenolithus heteromorphus* | 18.2 | 46X-CC | 437.48 | 47X-BCI | 448.40 | 442.94 | 5.46 | 5.46 |
| CN | LO *Sphenolithus belemnos* | 18.5 | 46X-CC | 437.48 | 47X-BCI | 448.40 | 442.94 | 5.46 | 5.46 |
| CN | FO *Sphenolithus belemnos* | 20.6 | 51X-CC | 479.87 | 52X-BCI | 496.60 | 488.24 | 8.37 | 8.37 |

Notes: Source: CN = calcareous nannoplankton, PF = planktonic foraminifers. Datum: LO = last occurrence, FO = first occurrence. Core, section, interval: BCI = bottom of cored interval.

**Table T8.** Interpolated ages of lithologic unit boundaries and seismic reflectors, Site 1195.

| | Top of unit | | |
|---|---|---|---|
| | Depth (mbsf) | Age (Ma) | Comments |
| Lithologic units: | | | |
| I | 0 | 0.0 | |
| IIA | 36.9 | 2.8 | |
| IIB | 93.9 | 6.1 | |
| IIC | 123.9 | 7.2 | |
| IIIA | 255.9 | 11.9 | |
| IIIB | 313.5 | 14.6 | |
| IV | 467.3 | 19.6 | |
| V | 517.5 | (~22.7) | Extrapolated |
| Seismic sequences and reflectors: | | | |
| Megasequence D | 0 | 0.0 | |
| D-black | 35 | 2.7 | |
| D-turquoise | 62 | 5.0 | |
| Megasequence C | 123 | 7.2 | |
| Megasequence B | 230 | 11.0 | |
| Megasequence A | 470 | 19.8 | |
| Basement | 521 | (~22.7) | Extrapolated |

**Table T9.** Headspace gas composition, Site 1195.

| Core, section | Depth (mbsf) | $C_1$ (ppmv) |
|---|---|---|
| 194-1195A- | | |
| 3H-5 | 20.20 | 1.8 |
| 4H-5 | 29.70 | 2.0 |
| 5H-5 | 39.20 | 1.9 |
| 6H-5 | 48.70 | 2.0 |
| 7H-5 | 58.20 | 1.9 |
| 8H-5 | 67.70 | 1.9 |
| 9H-6 | 77.62 | 2.0 |
| 194-1195B- | | |
| 10H-5 | 90.40 | 1.9 |
| 11H-5 | 99.90 | 1.9 |
| 12H-5 | 109.40 | 1.9 |
| 13H-5 | 118.90 | 1.9 |
| 14H-5 | 128.40 | 2.0 |
| 15H-5 | 137.90 | 1.9 |
| 16H-5 | 147.40 | 2.1 |
| 17H-5 | 156.90 | 1.8 |
| 18H-5 | 166.40 | 1.8 |
| 19H-5 | 175.90 | 1.9 |
| 20H-5 | 185.40 | 1.9 |
| 21H-5 | 194.90 | 1.8 |
| 22H-5 | 204.40 | 2.2 |
| 23X-2 | 209.40 | 2.0 |
| 24X-5 | 223.50 | 2.5 |
| 25X-5 | 233.10 | 2.1 |
| 26X-4 | 241.17 | 2.3 |
| 27X-5 | 252.30 | 2.3 |
| 28X-4 | 260.40 | 1.9 |
| 29X-5 | 271.50 | 2.1 |
| 30X-3 | 278.10 | 2.4 |
| 31X-1 | 284.60 | 1.9 |
| 32X-3 | 297.20 | 2.2 |
| 33X-4 | 308.40 | 2.2 |
| 34X-5 | 319.50 | 2.2 |
| 35X-3 | 326.10 | 2.7 |
| 36X-3 | 335.70 | 2.2 |
| 37X-5 | 348.30 | 2.5 |
| 38X-2 | 353.40 | 3.9 |
| 39X-2 | 363.00 | 3.5 |
| 40X-4 | 375.70 | 3.4 |
| 42X-2 | 393.21 | 2.9 |
| 44X-4 | 414.22 | 2.8 |
| 45X-4 | 424.00 | 2.2 |
| 46X-4 | 433.30 | 2.7 |
| 47X-3 | 442.97 | 2.2 |
| 48X-5 | 454.40 | 2.8 |
| 49X-3 | 461.00 | 4.3 |
| 50X-2 | 468.90 | 3.6 |
| 51X-2 | 478.80 | 10.0 |
| 52X-1 | 487.72 | 2.0 |
| 53X-CC | 497.09 | 2.6 |
| 54X-4 | 510.70 | 3.2 |

Note: $C_1$ = methane.

**Table T10.** Interstitial water chemistry, Site 1195.

| Core, section, interval (cm) | Depth (mbsf) | pH | Alk (mM) | Salinity | $Cl^-$ (mM) | $SO_4^{2-}$ (mM) | $Na^+$ (mM) | $Mg^{2+}$ (mM) | $Ca^{2+}$ (mM) | $K^+$ (mM) | $NH_4^+$ (μM) | $Sr^{2+}$ (μM) | $Li^+$ (μM) | $Mn^{2+}$ (μM) | $Fe^{2+}$ (μM) |
|---|---|---|---|---|---|---|---|---|---|---|---|---|---|---|---|
| 194-1195A- | | | | | | | | | | | | | | | |
| 2H-3, 140–150 | 9.10 | 7.74 | 2.23 | 36.0 | 559 | 29.48 | 477 | 53.04 | 11.63 | 11.71 | 65 | 149 | 34.43 | 0.18 | 9.74 |
| 3H-4, 140–150 | 20.10 | 7.64 | 1.88 | 36.0 | 565 | 28.37 | 482 | 51.66 | 12.78 | 10.96 | 70 | 197 | 41.45 | 0.25 | 2.26 |
| 4H-4, 140–150 | 29.60 | 7.72 | 1.99 | 36.0 | 560 | 28.30 | 476 | 51.62 | 13.18 | 10.72 | 83 | 209 | 40.30 | 0.33 | 1.49 |
| 5H-4, 140–150 | 39.10 | 7.62 | 2.30 | 36.0 | 563 | 28.62 | 478 | 51.57 | 13.77 | 11.11 | 72 | 189 | 37.53 | 0.32 | 2.56 |
| 6H-4, 140–150 | 48.60 | 7.76 | 1.79 | 36.0 | 564 | 28.47 | 480 | 52.16 | 12.51 | 11.30 | 77 | 175 | 34.80 | 0.38 | 18.87 |
| 7H-4, 140–150 | 58.10 | 7.59 | 1.67 | 36.0 | 564 | 28.22 | 481 | 52.20 | 12.15 | 11.10 | 51 | 159 | 34.18 | 0.33 | 0.99 |
| 8H-4, 140–150 | 67.60 | 7.68 | 1.88 | 36.0 | 565 | 28.61 | 481 | 52.93 | 12.21 | 11.00 | 62 | 127 | 27.67 | 0.31 | 0.90 |
| 9H-5, 140–150 | 77.52 | 7.65 | 2.07 | 36.0 | 567 | 28.79 | 483 | 51.92 | 13.21 | 11.08 | 84 | 169 | 36.61 | 0.63 | 19.71 |
| 194-1195B- | | | | | | | | | | | | | | | |
| 10H-4, 140–150 | 90.30 | 7.57 | 2.18 | 35.5 | 562 | 28.32 | 478 | 50.89 | 14.15 | 10.41 | 126 | 211 | 41.34 | 0.21 | 6.77 |
| 11H-4, 140–150 | 99.80 | 7.50 | 2.22 | 35.5 | 564 | 28.61 | 480 | 50.86 | 14.50 | 10.40 | 165 | 243 | 44.51 | 0.11 | 2.06 |
| 12H-4, 140–150 | 109.30 | 7.76 | 2.37 | 35.5 | 564 | 27.84 | 479 | 50.29 | 14.78 | 10.28 | 182 | 270 | 48.60 | 0.16 | 3.15 |
| 13H-4, 140–150 | 118.80 | 7.43 | 2.55 | 35.5 | 565 | 27.41 | 480 | 49.83 | 14.92 | 9.89 | 206 | | | | |
| 14H-4, 140–150 | 128.30 | 7.67 | 2.66 | 35.5 | 563 | 27.47 | 478 | 49.94 | 14.85 | 9.88 | 213 | 339 | 57.47 | 0.12 | 5.41 |
| 15H-4, 140–150 | 137.80 | 7.24 | 2.64 | 35.5 | 563 | 27.36 | 479 | 49.37 | 15.17 | 9.97 | 248 | 377 | 62.38 | 0.15 | 7.26 |
| 16H-4, 140–150 | 147.30 | 7.61 | 2.64 | 35.5 | 564 | 27.31 | 481 | 48.60 | 15.31 | 9.51 | 283 | 405 | 68.94 | 0.11 | 4.04 |
| 17H-4, 140–150 | 156.80 | 7.60 | 2.86 | 35.5 | 561 | 26.97 | 477 | 48.94 | 15.38 | 9.50 | 313 | 436 | 72.80 | 0.11 | 4.25 |
| 18H-4, 140–150 | 166.30 | 7.08 | 2.96 | 35.5 | 563 | 27.94 | 480 | 48.84 | 15.94 | 9.34 | 337 | 482 | 80.46 | 0.11 | 8.00 |
| 19H-4, 140–150 | 175.80 | 7.64 | 2.99 | 35.5 | 562 | 27.82 | 477 | 49.15 | 16.60 | 9.46 | 374 | 502 | 86.06 | 0.28 | 67.35 |
| 20H-4, 140–150 | 185.30 | 7.58 | 2.93 | 35.5 | 564 | 26.21 | 480 | 47.25 | 16.28 | 9.07 | 409 | 522 | 90.89 | 0.10 | 2.46 |
| 21H-4, 140–150 | 194.80 | 7.58 | 3.30 | 35.5 | 565 | 25.75 | 486 | 44.66 | 16.38 | 8.87 | 418 | 541 | 96.52 | 0.10 | 10.06 |
| 22H-4, 140–150 | 204.30 | 7.41 | 3.38 | 35.5 | 563 | 25.36 | 481 | 44.28 | 17.88 | 8.84 | 451 | 553 | 105.81 | 0.09 | 1.81 |
| 23X-1, 140–150 | 209.30 | 7.63 | 3.42 | 35.5 | 567 | 24.58 | 484 | 44.05 | 17.77 | 8.58 | 468 | 562 | 109.14 | 0.14 | 3.09 |
| 24X-4, 140–150 | 223.40 | 7.29 | 3.59 | 35.5 | 566 | 25.13 | 485 | 43.10 | 18.22 | 8.37 | 508 | 574 | 120.88 | 0.16 | 7.66 |
| 25X-4, 140–150 | 233.00 | 7.63 | 3.47 | 35.5 | 571 | 23.99 | 489 | 43.32 | 17.78 | 8.19 | 524 | 602 | 129.82 | 0.08 | 1.46 |
| 26X-3, 140–150 | 241.07 | 7.62 | 3.49 | 35.5 | 565 | 23.57 | 482 | 43.02 | 17.91 | 7.92 | 599 | 606 | 138.93 | 0.16 | 7.61 |
| 27X-4, 140–150 | 252.20 | 7.67 | 3.47 | 35.5 | 567 | 22.46 | 483 | 42.26 | 18.15 | 8.07 | 620 | 607 | 141.63 | 0.24 | 3.00 |
| 28X-3, 140–150 | 260.30 | 7.65 | 3.69 | 35.5 | 566 | 22.78 | 480 | 42.46 | 19.46 | 7.49 | 623 | 609 | 151.97 | 0.20 | 10.65 |
| 29X-4, 140–150 | 271.40 | 7.65 | 3.72 | 35.5 | 567 | 22.19 | 482 | 42.27 | 18.91 | 7.16 | 648 | 629 | 161.31 | 0.26 | 21.01 |
| 30X-2, 140–150 | 278.00 | 7.69 | 4.05 | 35.5 | 566 | 22.87 | 475 | 43.97 | 20.86 | 7.51 | 674 | 639 | 174.27 | 0.19 | 2.96 |
| 32X-2, 140–150 | 297.10 | 7.65 | 3.91 | 35.5 | 568 | 21.20 | 479 | 41.48 | 20.68 | 6.90 | 690 | 639 | 190.13 | 0.32 | 6.41 |
| 33X-3, 140–150 | 308.30 | 7.37 | 4.13 | 35.0 | 565 | 20.82 | 474 | 40.94 | 22.23 | 6.11 | 697 | 693 | 203.45 | 0.27 | 17.75 |
| 34X-4, 140–150 | 319.40 | 7.22 | 4.21 | 35.5 | 568 | 20.25 | 477 | 39.49 | 23.13 | 6.18 | 782 | 545 | 171.66 | 0.14 | 1.38 |
| 35X-2, 140–150 | 326.00 | 7.31 | 4.34 | 35.0 | 570 | 20.04 | 478 | 39.53 | 23.32 | 5.99 | 752 | 710 | 204.26 | 0.25 | 11.36 |
| 36X-2, 140–150 | 335.60 | 7.24 | 4.35 | 35.0 | 570 | 28.88 | 500 | 37.48 | 23.56 | 5.57 | 801 | 676 | 218.67 | 0.24 | 4.90 |
| 37X-4, 135–150 | 348.15 | 7.66 | 4.53 | 35.0 | 566 | 17.69 | 476 | 35.15 | 24.82 | 5.02 | 806 | 722 | 237.79 | 0.19 | 0.92 |
| 38X-1, 135–150 | 353.25 | 7.65 | 4.54 | 35.0 | 569 | 17.52 | 478 | 35.24 | 25.27 | 5.03 | 824 | 725 | 250.35 | 0.18 | 1.99 |
| 39X-1, 135–150 | 362.85 | 7.68 | 4.62 | 35.0 | 569 | 17.80 | 477 | 35.07 | 26.59 | 4.70 | 812 | 740 | 253.23 | 0.21 | 1.44 |
| 40X-3, 135–150 | 375.55 | 7.21 | 3.67 | 34.0 | 553 | 17.24 | 447 | 37.88 | 30.38 | 3.48 | 583 | 862 | 250.34 | 0.62 | 19.78 |
| 42X-2, 111–122 | 393.21 | 7.55 | 3.82 | 34.5 | 571 | 16.21 | 476 | 32.25 | 29.37 | 4.21 | 843 | 823 | 250.88 | 0.40 | 3.94 |
| 44X-4, 140–150 | 415.62 | 7.40 | 2.15 | 34.0 | 564 | 14.61 | 467 | 29.67 | 31.63 | 3.41 | 817 | 914 | 261.93 | 0.31 | 7.66 |
| 45X-4, 140–150 | 425.40 | 7.54 | 2.34 | 34.0 | 564 | 14.18 | 470 | 29.13 | 30.34 | 3.58 | 740 | 941 | 246.24 | 0.26 | 2.28 |
| 46X-4, 140–150 | 434.70 | 7.47 | 1.72 | 34.0 | 570 | 14.16 | 473 | 28.51 | 32.46 | 3.48 | 780 | 930 | 245.90 | 0.29 | 1.02 |
| 47X-3, 122–132 | 442.97 | 7.47 | 1.78 | 34.0 | 564 | 14.00 | 468 | 27.77 | 32.29 | 3.40 | 733 | 962 | 239.31 | 0.42 | 6.74 |
| 48X-4, 140–150 | 454.30 | 7.45 | 1.81 | 34.0 | 569 | 13.77 | 477 | 27.09 | 30.75 | 3.90 | 843 | 847 | 213.63 | 0.30 | 0.67 |
| 49X-2, 140–150 | 460.90 | 7.74 | 1.47 | 34.5 | 566 | 13.54 | 473 | 25.74 | 32.50 | 3.47 | 826 | 906 | 214.86 | 0.32 | 1.01 |
| 50X-1, 110–120 | 468.80 | 8.33 | 1.12 | 34.0 | 566 | 13.49 | 473 | 25.78 | 32.72 | 3.30 | 799 | 904 | 204.52 | 0.46 | 1.60 |
| 51X-1, 140–150 | 478.70 | 8.60 | 0.85 | 34.0 | 564 | 13.16 | 470 | 24.39 | 34.06 | 3.29 | 833 | 901 | 207.33 | 0.35 | 22.09 |
| 54X-3, 140–150 | 510.60 | 8.01 | 0.99 | 34.0 | 565 | 13.09 | 469 | 23.80 | 35.80 | 3.22 | 745 | 828 | 192.84 | 0.32 | 0.61 |
| 55X-1, 129–143 | 516.99 | 8.42 | 0.65 | 34.0 | 566 | 14.56 | 472 | 23.56 | 36.50 | 3.25 | 765 | 837 | 184.40 | 0.24 | 1.14 |

Note: Alk = alkalinity.

**Table T11.** Percentages of aragonite, calcite, dolomite, and noncarbonate minerals, Site 1195.

| Core, section, interval (cm) | Depth (mbsf) | Aragonite (wt%) | Calcite (wt%) | Dolomite (wt%) | Non-carbonate (wt%) |
|---|---|---|---|---|---|
| 194-1195A- | | | | | |
| 1H-1, 64–65 | 0.64 | 15 | 73 | 0 | 12 |
| 1H-3, 64–65 | 3.64 | 11 | 78 | 0 | 11 |
| 2H-1, 64–65 | 5.34 | 0 | 88 | 0 | 12 |
| 2H-3, 64–65 | 8.34 | 7 | 73 | 0 | 20 |
| 2H-5, 64–65 | 11.34 | 7 | 77 | 0 | 16 |
| 3H-1, 64–65 | 14.84 | 7 | 72 | 0 | 21 |
| 3H-3, 64–65 | 17.84 | 4 | 87 | 0 | 9 |
| 3H-5, 64–65 | 20.84 | 0 | 91 | 0 | 9 |
| 4H-1, 64–65 | 24.34 | 0 | 90 | 0 | 10 |
| 4H-3, 64–65 | 27.34 | 0 | 89 | 0 | 11 |
| 4H-5, 64–65 | 30.34 | 0 | 87 | 0 | 13 |
| 5H-1, 64–65 | 33.84 | 0 | 87 | 0 | 13 |
| 5H-3, 64–65 | 36.84 | 0 | 85 | 0 | 15 |
| 5H-5, 64–65 | 39.84 | 0 | 83 | 0 | 17 |
| 6H-1, 64–65 | 43.34 | 0 | 80 | 0 | 20 |
| 6H-3, 64–65 | 46.34 | 0 | 88 | 0 | 12 |
| 6H–5, 64-65 | 49.34 | 0 | 85 | 0 | 15 |
| 7H–1, 64-65 | 52.84 | 0 | 88 | 0 | 12 |
| 7H–3, 64-65 | 55.84 | 0 | 87 | 0 | 13 |
| 7H-5, 64–65 | 58.84 | 0 | 90 | 0 | 10 |
| 8H-3, 64–65 | 65.34 | 0 | 82 | 1 | 17 |
| 8H-5, 64–65 | 68.34 | 0 | 88 | 0 | 12 |
| 9H-1, 64–65 | 71.84 | 0 | 82 | 1 | 17 |
| 9H-3, 64–65 | 73.76 | 0 | 88 | 0 | 12 |
| 9H-5, 64–65 | 76.76 | 0 | 82 | 2 | 16 |
| 194-1195B- | | | | | |
| 9H-1, 64–65 | 75.54 | 0 | 84 | 1 | 15 |
| 9H-3, 64–65 | 78.54 | 0 | 77 | 2 | 21 |
| 9H-5, 64–65 | 81.54 | 0 | 81 | 2 | 17 |
| 10H-1, 64–65 | 85.04 | 0 | 79 | 1 | 20 |
| 10H-3, 64–65 | 88.04 | 0 | 83 | 2 | 15 |
| 10H-5, 64–65 | 91.04 | 0 | 87 | 0 | 13 |
| 11H-1, 64–65 | 94.54 | 0 | 86 | 0 | 14 |
| 11H-3, 64–65 | 97.54 | 0 | 89 | 0 | 11 |
| 11H-5, 64–65 | 100.54 | 0 | 88 | 0 | 12 |
| 12H-1, 64–65 | 104.04 | 0 | 86 | 0 | 14 |
| 12H-3, 64–65 | 107.04 | 0 | 84 | 0 | 16 |
| 12H-5, 64–65 | 110.04 | 0 | 86 | 0 | 14 |
| 13H-1, 64–65 | 113.54 | 0 | 87 | 0 | 13 |
| 13H-3, 64–65 | 116.54 | 0 | 89 | 0 | 11 |
| 13H-5, 64–65 | 119.54 | 0 | 89 | 0 | 11 |
| 14H-1, 64–65 | 123.04 | 0 | 87 | 0 | 13 |
| 14H-3, 64–65 | 126.04 | 0 | 90 | 1 | 9 |
| 14H-5, 64–65 | 129.04 | 0 | 92 | 0 | 8 |
| 15H-1, 64–65 | 132.54 | 0 | 88 | 0 | 12 |
| 15H-3, 64–65 | 135.54 | 0 | 88 | 0 | 12 |
| 15H-5, 64–65 | 138.54 | 0 | 90 | 0 | 10 |
| 16H-1, 64–65 | 142.04 | 0 | 89 | 0 | 11 |
| 16H-3, 64–65 | 145.04 | 0 | 85 | 0 | 15 |
| 16H-5, 64–65 | 148.04 | 0 | 89 | 0 | 11 |
| 17H-1, 64–65 | 151.54 | 0 | 89 | 0 | 11 |
| 17H-3, 64–65 | 154.54 | 0 | 91 | 0 | 9 |
| 17H-5, 64–65 | 157.54 | 0 | 91 | 0 | 9 |
| 18H-1, 64–65 | 161.04 | 0 | 89 | 0 | 11 |
| 18H-3, 64–65 | 164.04 | 0 | 90 | 0 | 10 |
| 18H-5, 64–65 | 167.04 | 0 | 90 | 0 | 10 |
| 19H-1, 64–65 | 170.54 | 0 | 88 | 0 | 12 |
| 19H-3, 64–65 | 173.54 | 0 | 89 | 0 | 11 |
| 19H-5, 64–65 | 176.54 | 0 | 91 | 0 | 9 |
| 20H-1, 64–65 | 180.04 | 0 | 90 | 0 | 10 |
| 20H-3, 64–65 | 183.04 | 0 | 91 | 0 | 9 |
| 20H-5, 64–65 | 186.04 | 0 | 85 | 0 | 15 |
| 21H-1, 64–65 | 189.54 | 0 | 87 | 1 | 13 |
| 21H-3, 64–65 | 192.54 | 0 | 89 | 0 | 11 |
| 21H-5, 64–65 | 195.54 | 0 | 84 | 0 | 16 |
| 22H-1, 64–65 | 199.04 | 0 | 89 | 1 | 10 |
| 22H-3, 64–65 | 202.04 | 0 | 91 | 1 | 7 |
| 22H-5, 64–65 | 205.04 | 0 | 91 | 0 | 9 |
| 23X-1, 64–65 | 208.54 | 0 | 88 | 1 | 10 |
| 24X-1, 64–65 | 218.14 | 0 | 86 | 2 | 12 |
| 24X-3, 65–66 | 221.15 | 0 | 80 | 2 | 18 |
| 24X-5, 68–69 | 224.18 | 0 | 85 | 2 | 13 |
| 25X-1, 64–65 | 227.74 | 0 | 88 | 2 | 10 |
| 25X-3, 64–65 | 230.74 | 0 | 84 | 2 | 14 |
| 25X-5, 69–70 | 233.79 | 0 | 90 | 0 | 10 |
| 26X-1, 64–65 | 237.34 | 0 | 90 | 0 | 10 |
| 27X-1, 64–65 | 246.94 | 0 | 88 | 0 | 12 |
| 28X-1, 64–65 | 256.54 | 0 | 89 | 0 | 11 |
| 29X-1, 63–64 | 266.13 | 0 | 85 | 0 | 15 |
| 30X-1, 71–73 | 275.81 | 0 | 75 | 0 | 25 |
| 31X-1, 68–69 | 285.28 | 0 | 91 | 0 | 9 |
| 32X-2, 63–64 | 296.33 | 0 | 95 | 0 | 5 |
| 33X-1, 68–69 | 304.58 | 0 | 87 | 0 | 13 |
| 34X-1, 65–66 | 314.15 | 0 | 77 | 0 | 23 |
| 35X-1, 70–71 | 323.80 | 0 | 86 | 8 | 6 |
| 36X-1, 64–65 | 333.34 | 0 | 49 | 4 | 47 |
| 37X-1, 64–65 | 342.94 | 0 | 41 | 8 | 51 |
| 38X-1, 64–65 | 352.54 | 0 | 65 | 4 | 31 |
| 39X-1, 66–67 | 362.16 | 0 | 83 | 4 | 12 |
| 40X-1, 72–73 | 371.92 | 0 | 74 | 10 | 16 |
| 41X-1, 64–65 | 381.54 | 0 | 50 | 5 | 45 |
| 42X-1, 64–65 | 391.24 | 0 | 77 | 2 | 21 |
| 43X-1, 64–65 | 400.94 | 0 | 59 | 14 | 27 |
| 44X-1, 64–65 | 410.54 | 0 | 71 | 0 | 29 |
| 45X-1, 64–65 | 420.14 | 0 | 81 | 0 | 19 |
| 46X-1, 64–65 | 429.74 | 0 | 77 | 0 | 23 |
| 47X-1, 64–65 | 439.44 | 0 | 66 | 0 | 34 |
| 48X-1, 64–65 | 449.04 | 0 | 67 | 0 | 33 |
| 49X-1, 64–65 | 458.64 | 0 | 88 | 0 | 12 |
| 50X-1, 64–65 | 468.34 | 0 | 19 | 0 | 81 |
| 51X-1, 64–65 | 477.94 | 0 | 43 | 0 | 57 |
| 52X-1, 64–65 | 487.54 | 0 | 60 | 0 | 40 |
| 54X-1, 63–64 | 506.83 | 0 | 72 | 0 | 28 |
| 55X-1, 63–64 | 516.33 | 0 | 72 | 0 | 28 |

**Table T12.** Carbon, nitrogen, sulfur, and hydrogen values and C/N and C/S ratios in sediments, Site 1195. (See table notes. Continued on next page.)

| Core, section | Depth (mbsf) | IC (wt%) | $CaCO_3$ (wt%) | TC (wt%) | TOC (wt%) | Total N (wt%) | Total S (wt%) | Total H (wt%) | C/N ratio | C/S ratio |
|---|---|---|---|---|---|---|---|---|---|---|
| 194-1195A- | | | | | | | | | | |
| 1H-1 | 0.64 | 10.61 | 88.4 | — | — | — | — | — | — | — |
| 1H-3 | 3.64 | 10.70 | 89.1 | — | — | — | — | — | — | — |
| 2H-1 | 5.34 | 10.56 | 87.9 | — | — | — | — | — | — | — |
| 2H-3 | 8.34 | 9.65 | 80.4 | — | — | — | — | — | — | — |
| 2H-5 | 11.34 | 10.08 | 84.0 | — | — | — | — | — | — | — |
| 3H-1 | 14.84 | 9.52 | 79.3 | 9.62 | 0.10 | 0.02 | 0.07 | 0.29 | 4.91 | 1.40 |
| 3H-3 | 17.84 | 10.89 | 90.7 | — | — | — | — | — | — | — |
| 3H-5 | 20.84 | 10.96 | 91.3 | — | — | — | — | — | — | — |
| 4H-1 | 24.34 | 10.77 | 89.7 | — | — | — | — | — | — | — |
| 4H-3 | 27.34 | 10.72 | 89.3 | — | — | — | — | — | — | — |
| 4H-5 | 30.34 | 10.39 | 86.5 | — | — | — | — | — | — | — |
| 5H-1 | 33.84 | 10.50 | 87.5 | — | — | — | — | — | — | — |
| 5H-3 | 36.84 | 10.22 | 85.1 | — | — | — | — | — | — | — |
| 5H-5 | 39.84 | 9.97 | 83.0 | — | — | — | — | — | — | — |
| 6H-1 | 43.34 | 9.56 | 79.7 | 9.79 | 0.23 | 0.13 | 0.12 | 0.28 | 1.76 | 1.89 |
| 6H-3 | 46.34 | 10.54 | 87.8 | — | — | — | — | — | — | — |
| 6H-5 | 49.34 | 10.25 | 85.4 | — | — | — | — | — | — | — |
| 7H-1 | 52.84 | 10.53 | 87.7 | — | — | — | — | — | — | — |
| 7H-3 | 55.84 | 10.39 | 86.6 | — | — | — | — | — | — | — |
| 7H-5 | 58.84 | 10.82 | 90.1 | — | — | — | — | — | — | — |
| 8H-3 | 65.34 | 9.95 | 82.9 | 10.01 | 0.06 | 0.06 | 0.26 | 0.21 | 1.09 | 0.25 |
| 8H-5 | 68.34 | 10.56 | 88.0 | — | — | — | — | — | — | — |
| 9H-1 | 71.84 | 9.94 | 82.8 | — | — | — | — | — | — | — |
| 9H-3 | 73.76 | 10.58 | 88.1 | 10.67 | 0.09 | 0.01 | 0.11 | 0.20 | 11.10 | 0.85 |
| 9H-5 | 76.76 | 10.11 | 84.2 | — | — | — | — | — | — | — |
| 194-1195B- | | | | | | | | | | |
| 9H-1 | 75.54 | 10.19 | 84.9 | — | — | — | — | — | — | — |
| 9H-3 | 78.54 | 9.53 | 79.4 | — | — | — | — | — | — | — |
| 9H-5 | 81.54 | 9.95 | 82.9 | — | — | — | — | — | — | — |
| 10H-1 | 85.04 | 9.66 | 80.5 | — | — | — | — | — | — | — |
| 10H-3 | 88.04 | 10.22 | 85.1 | — | — | — | — | — | — | — |
| 10H-5 | 91.04 | 10.47 | 87.2 | — | — | — | — | — | — | — |
| 11H-1 | 94.54 | 10.27 | 85.6 | — | — | — | — | — | — | — |
| 11H-3 | 97.54 | 10.71 | 89.2 | — | — | — | — | — | — | — |
| 11H-5 | 100.54 | 10.52 | 87.6 | — | — | — | — | — | — | — |
| 12H-1 | 104.04 | 10.29 | 85.7 | — | — | — | — | — | — | — |
| 12H-3 | 107.04 | 10.02 | 83.4 | 10.20 | 0.18 | 0.04 | 0.10 | 0.24 | 4.50 | 1.84 |
| 12H-5 | 110.04 | 10.36 | 86.3 | — | — | — | — | — | — | — |
| 13H-1 | 113.54 | 10.39 | 86.6 | — | — | — | — | — | — | — |
| 13H-3 | 116.54 | 10.65 | 88.7 | — | — | — | — | — | — | — |
| 13H-5 | 119.54 | 10.66 | 88.8 | — | — | — | — | — | — | — |
| 14H-1 | 123.04 | 10.48 | 87.3 | — | — | — | — | — | — | — |
| 14H-3 | 126.04 | 10.96 | 91.3 | — | — | — | — | — | — | — |
| 14H-5 | 129.04 | 11.10 | 92.4 | — | — | — | — | — | — | — |
| 15H-1 | 132.54 | 10.57 | 88.1 | — | — | — | — | — | — | — |
| 15H-3 | 135.54 | 10.55 | 87.8 | — | — | — | — | — | — | — |
| 15H-5 | 138.54 | 10.75 | 89.5 | — | — | — | — | — | — | — |
| 16H-1 | 142.04 | 10.66 | 88.8 | — | — | — | — | — | — | — |
| 16H-3 | 145.04 | 10.20 | 85.0 | 10.64 | 0.44 | 0.05 | 0.12 | 0.21 | 9.69 | 3.63 |
| 16H-5 | 148.04 | 10.74 | 89.5 | — | — | — | — | — | — | — |
| 17H-1 | 151.54 | 10.67 | 88.9 | — | — | — | — | — | — | — |
| 17H-3 | 154.54 | 10.95 | 91.2 | — | — | — | — | — | — | — |
| 17H-5 | 157.54 | 10.89 | 90.7 | — | — | — | — | — | — | — |
| 18H-1 | 161.04 | 10.73 | 89.4 | — | — | — | — | — | — | — |
| 18H-3 | 164.04 | 10.79 | 89.9 | — | — | — | — | — | — | — |
| 18H-5 | 167.04 | 10.83 | 90.2 | — | — | — | — | — | — | — |
| 19H-1 | 170.54 | 10.61 | 88.4 | — | — | — | — | — | — | — |
| 19H-3 | 173.54 | 10.64 | 88.7 | — | — | — | — | — | — | — |
| 19H-5 | 176.54 | 10.98 | 91.5 | — | — | — | — | — | — | — |
| 20H-1 | 180.04 | 10.85 | 90.4 | — | — | — | — | — | — | — |
| 20H-3 | 183.04 | 10.88 | 90.6 | — | — | — | — | — | — | — |
| 20H-5 | 186.04 | 10.21 | 85.0 | 10.35 | 0.14 | 0.02 | 0.00 | 0.24 | 7.20 | — |
| 21H-1 | 189.54 | 10.50 | 87.5 | — | — | — | — | — | — | — |
| 21H-3 | 192.54 | 10.71 | 89.2 | — | — | — | — | — | — | — |
| 21H-5 | 195.54 | 10.13 | 84.4 | — | — | — | — | — | — | — |
| 22H-1 | 199.04 | 10.80 | 89.9 | — | — | — | — | — | — | — |
| 22H-3 | 202.04 | 11.14 | 92.8 | — | — | — | — | — | — | — |

Table T12 (continued).

| Core, section | Depth (mbsf) | IC (wt%) | $CaCO_3$ (wt%) | TC (wt%) | TOC (wt%) | Total N (wt%) | Total S (wt%) | Total H (wt%) | C/N ratio | C/S ratio |
|---|---|---|---|---|---|---|---|---|---|---|
| 22H-5 | 205.04 | 10.92 | 91.0 | — | — | — | — | — | — | — |
| 23X-1 | 208.54 | 10.75 | 89.6 | — | — | — | — | — | — | — |
| 24X-1 | 218.14 | 10.53 | 87.7 | — | — | — | — | — | — | — |
| 24X-3 | 221.15 | 9.83 | 81.9 | — | — | — | — | — | — | — |
| 24X-5 | 224.18 | 10.39 | 86.5 | — | — | — | — | — | — | — |
| 25X-1 | 227.74 | 10.79 | 89.9 | — | — | — | — | — | — | — |
| 25X-3 | 230.74 | 10.80 | 86.0 | 10.83 | 0.03 | 0.09 | 0.00 | 0.17 | 0.29 | — |
| 25X-5 | 233.79 | 10.86 | 90.5 | — | — | — | — | — | — | — |
| 26X-1 | 237.34 | 10.77 | 89.7 | — | — | — | — | — | — | — |
| 26X-3 | 240.33 | 10.36 | 86.3 | — | — | — | — | — | — | — |
| 27X-1 | 246.94 | 10.51 | 87.5 | — | — | — | — | — | — | — |
| 27X-3 | 249.94 | 10.18 | 84.8 | — | — | — | — | — | — | — |
| 27X-5 | 252.94 | 10.02 | 83.5 | — | — | — | — | — | — | — |
| 28X-1 | 256.54 | 10.67 | 88.9 | — | — | — | — | — | — | — |
| 28X-3 | 259.54 | 10.45 | 87.0 | — | — | — | — | — | — | — |
| 28X-5 | 262.57 | 11.13 | 92.7 | — | — | — | — | — | — | — |
| 29X-1 | 266.13 | 10.23 | 85.2 | — | — | — | — | — | — | — |
| 29X-3 | 269.12 | 9.16 | 76.3 | 9.25 | 0.09 | 0.02 | 0.18 | 0.15 | 5.54 | 0.51 |
| 29X-5 | 272.16 | 10.09 | 84.0 | — | — | — | — | — | — | — |
| 30X-1 | 275.81 | 9.01 | 75.1 | 9.15 | 0.14 | 0.02 | 0.21 | 0.27 | 6.99 | 0.67 |
| 30X-3 | 278.74 | 11.32 | 94.3 | — | — | — | — | — | — | — |
| 31X-1 | 285.28 | 10.90 | 90.8 | — | — | — | — | — | — | — |
| 32X-2 | 296.33 | 11.44 | 95.3 | — | — | — | — | — | — | — |
| 33X-1 | 304.58 | 10.49 | 87.4 | — | — | — | — | — | — | — |
| 33X-3 | 307.60 | 8.02 | 67.2 | 8.30 | 0.28 | 0.07 | 0.23 | 0.28 | 4.00 | 1.22 |
| 34X-1 | 314.18 | 9.20 | 76.6 | 9.24 | 0.05 | 0.01 | 0.14 | 0.14 | 3.46 | 0.31 |
| 34X-3 | 317.14 | 10.57 | 88.0 | — | — | — | — | — | — | — |
| 34X-5 | 320.15 | 10.83 | 90.2 | — | — | — | — | — | — | — |
| 35X-1 | 323.80 | 11.26 | 93.8 | — | — | — | — | — | — | — |
| 35X-3 | 326.70 | 9.46 | 78.8 | 9.56 | 0.10 | 0.01 | 1.79 | 0.08 | 11.14 | 0.06 |
| 35X-5 | 329.72 | 8.94 | 74.5 | — | — | — | — | — | — | — |
| 36X-1 | 333.34 | 6.35 | 52.9 | 6.57 | 0.22 | 0.06 | 0.37 | 0.50 | 3.67 | 0.59 |
| 36X-3 | 336.40 | 10.05 | 83.7 | — | — | — | — | — | — | — |
| 37X-1 | 342.94 | 5.92 | 49.3 | 6.31 | 0.40 | 0.02 | 2.22 | 0.31 | 19.75 | 0.18 |
| 37X-3 | 345.94 | 10.46 | 87.2 | — | — | — | — | — | — | — |
| 37X-5 | 348.94 | 11.00 | 91.6 | — | — | — | — | — | — | — |
| 38X-1 | 352.54 | 8.22 | 68.5 | 8.45 | 0.23 | 0.02 | 0.21 | 0.35 | 11.27 | 1.07 |
| 39X-1 | 362.16 | 10.55 | 87.9 | — | — | — | — | — | — | — |
| 39X-3 | 365.27 | 9.35 | 77.9 | — | — | — | — | — | — | — |
| 40X-1 | 371.92 | 10.05 | 83.7 | — | — | — | — | — | — | — |
| 40X-3 | 374.87 | 3.65 | 30.4 | 4.02 | 0.37 | 0.06 | 1.11 | 0.79 | 6.22 | 0.34 |
| 41X-1 | 381.54 | 6.59 | 54.9 | 6.73 | 0.14 | 0.06 | 0.31 | 0.52 | 2.33 | 0.45 |
| 42X-1 | 391.24 | 9.52 | 79.3 | — | — | — | — | — | — | — |
| 42X-3 | 393.96 | 6.90 | 57.5 | 7.09 | 0.19 | 0.06 | 0.28 | 0.53 | 3.19 | 0.68 |
| 43X-1 | 400.94 | 8.80 | 73.3 | — | — | — | — | — | — | — |
| 44X-1 | 410.54 | 8.47 | 70.6 | — | — | — | — | — | — | — |
| 44X-3 | 413.36 | 7.88 | 65.7 | 8.01 | 0.13 | 0.02 | 0.15 | 0.38 | 5.38 | 0.87 |
| 44X-5 | 416.36 | 10.57 | 88.1 | — | — | — | — | — | — | — |
| 45X-1 | 420.14 | 9.69 | 80.7 | — | — | — | — | — | — | — |
| 45X-3 | 423.14 | 9.84 | 81.9 | — | — | — | — | — | — | — |
| 45X-5 | 426.14 | 9.15 | 76.2 | — | — | — | — | — | — | — |
| 46X-1 | 429.74 | 9.23 | 76.9 | — | — | — | — | — | — | — |
| 46X-3 | 432.44 | 8.51 | 70.9 | 8.60 | 0.09 | 0.02 | 0.35 | 0.35 | 4.50 | 0.26 |
| 46X-5 | 435.44 | 8.80 | 73.3 | — | — | — | — | — | — | — |
| 47X-1 | 439.44 | 7.67 | 63.9 | 7.90 | 0.22 | 0.06 | 0.34 | 0.42 | 3.67 | 0.65 |
| 47X-3 | 442.39 | 9.24 | 77.0 | — | — | — | — | — | — | — |
| 47X-5 | 445.21 | 9.06 | 75.5 | — | — | — | — | — | — | — |
| 48X-1 | 449.04 | 7.71 | 64.2 | 7.95 | 0.24 | 0.02 | 0.81 | 0.44 | 12.00 | 0.30 |
| 48X-3 | 452.04 | 10.45 | 87.0 | — | — | — | — | — | — | — |
| 48X-5 | 455.04 | 10.35 | 86.3 | — | — | — | — | — | — | — |
| 49X-1 | 458.64 | 10.55 | 87.9 | — | — | — | — | — | — | — |
| 49X-3 | 461.64 | 10.12 | 84.3 | — | — | — | — | — | — | — |
| 50X-1 | 468.34 | 2.16 | 18.0 | 2.18 | 0.02 | 0.00 | 0.03 | 0.27 | 6.67 | 0.67 |
| 51X-1 | 477.94 | 5.13 | 42.7 | 5.21 | 0.08 | 0.08 | 0.00 | 0.24 | 1.01 | — |
| 52X-1 | 487.54 | 7.25 | 60.4 | — | — | — | — | — | — | — |
| 54X-1 | 506.83 | 8.65 | 72.0 | — | — | — | — | — | — | — |
| 54X-3 | 509.84 | 6.66 | 55.5 | 6.95 | 0.29 | 0.06 | 0.36 | 0.39 | 4.83 | 0.80 |
| 55X-1 | 516.33 | 8.60 | 71.7 | — | — | — | — | — | — | — |

Notes: IC = inorganic carbon, TC = total carbon, TOC = total organic carbon, C/N = carbon/nitrogen, C/S = carbon/sulfur. — = not analyzed.

**Table T13.** Results of Rock-Eval pyrolysis analyses on sediments, Site 1195.

| Core, section | Depth (mbsf) | $T_{max}$ | $S_1$ | $S_2$ | $S_3$ | HI | OI | TOC (wt%) |
|---|---|---|---|---|---|---|---|---|
| 194-1195A- | | | | | | | | |
| 1H-1 | 0.64 | 395 | 0.07 | 0.06 | 21.19 | 150 | 52,980 | 0.04 |
| 1H-3 | 3.64 | 337 | 0.05 | 0.02 | 17.61 | 200 | — | 0.01 |
| 2H-1 | 5.34 | 450 | 0.12 | 0.06 | 31.72 | 300 | — | 0.02 |
| 2H-3 | 8.34 | 392 | 0.12 | 0.14 | 24.71 | 155 | 27,460 | 0.09 |
| 2H-5 | 11.34 | 398 | 0.11 | 0.09 | 15.26 | 180 | 30,520 | 0.05 |
| 3H-1 | 14.84 | 390 | 0.11 | 0.12 | 31.57 | 150 | 39,460 | 0.08 |
| 3H-3 | 17.84 | 365 | 0.05 | 0.07 | 18.69 | 350 | — | 0.02 |
| 3H-5 | 20.84 | 302 | 0.08 | 0.06 | 17.61 | 500 | — | 0.01 |
| 4H-1 | 24.34 | — | 0.11 | 0.04 | 24.81 | 400 | — | 0.01 |
| 4H-3 | 27.34 | 347 | 0.08 | 0.04 | 30.92 | 400 | — | 0.01 |
| 4H-5 | 30.34 | — | 0.14 | 0.06 | 14.37 | 300 | — | 0.02 |
| 5H-1 | 33.84 | — | 0.13 | 0.05 | 25.71 | 500 | — | 0.01 |
| 5H-3 | 36.84 | 384 | 0.15 | 0.07 | 17.92 | 350 | — | 0.01 |
| 5H-5 | 39.84 | 410 | 0.10 | 0.20 | 30.42 | 168 | 27,510 | 0.12 |
| 6H-3 | 46.34 | 340 | 0.20 | 0.11 | 18.41 | 220 | 36,820 | 0.05 |
| 6H-5 | 49.34 | 390 | 0.12 | 0.16 | 21.59 | 177 | 23,990 | 0.09 |
| 7H-1 | 52.84 | 352 | 0.06 | 0.06 | 31.96 | 200 | — | 0.03 |
| 7H-3 | 55.84 | 386 | 0.15 | 0.14 | 19.30 | 233 | 32,170 | 0.06 |
| 7H-5 | 58.84 | 361 | 0.19 | 0.09 | 37.83 | 180 | — | 0.05 |
| 8H-3 | 65.34 | 389 | 0.11 | 0.16 | 35.20 | 200 | 44,000 | 0.08 |
| 8H-5 | 68.34 | 358 | 0.19 | 0.09 | 20.32 | 300 | — | 0.03 |
| 9H-1 | 71.84 | 395 | 0.07 | 0.10 | 30.69 | 125 | 38,360 | 0.08 |
| 9H-3 | 73.76 | 325 | 0.14 | 0.09 | 34.22 | 358 | — | 0.03 |
| 194-1195B- | | | | | | | | |
| 9H-3 | 78.54 | 395 | 0.09 | 0.14 | 16.91 | 116 | 14,090 | 0.12 |
| 9H-5 | 81.54 | 398 | 0.08 | 0.16 | 18.24 | 134 | 15,970 | 0.12 |
| 10H-1 | 85.04 | 393 | 0.09 | 0.14 | 22.93 | 125 | 13,020 | 0.12 |
| 10H-3 | 88.04 | 403 | 0.09 | 0.17 | 28.66 | 113 | 19,110 | 0.15 |
| 10H-5 | 91.04 | 409 | 0.07 | 0.18 | 19.00 | 138 | 14,610 | 0.13 |
| 11H-1 | 94.54 | 409 | 0.08 | 0.30 | 33.50 | 140 | 15,950 | 0.21 |
| 11H-3 | 97.54 | 412 | 0.08 | 0.22 | 25.72 | 169 | 19,780 | 0.13 |
| 11H-5 | 100.50 | 413 | 0.03 | 0.09 | 21.86 | 112 | 27,330 | 0.08 |
| 12H-1 | 104.00 | 408 | 0.09 | 0.18 | 29.42 | 163 | 26,740 | 0.11 |
| 12H-3 | 107.00 | 403 | 0.08 | 0.24 | 23.38 | 160 | 15,590 | 0.15 |
| 12H-5 | 110.00 | 410 | 0.05 | 0.26 | 14.97 | 178 | 10,110 | 0.14 |
| 13H-1 | 113.50 | 410 | 0.09 | 0.31 | 32.82 | 206 | 21,880 | 0.15 |
| 13H-3 | 116.50 | 407 | 0.07 | 0.19 | 29.99 | 211 | 33,320 | 0.09 |
| 13H-5 | 119.50 | 411 | 0.09 | 0.12 | 14.07 | 120 | 14,070 | 0.10 |
| 14H-1 | 123.00 | 402 | 0.15 | 0.21 | 30.31 | 140 | 20,210 | 0.15 |
| 14H-3 | 126.00 | 412 | 0.09 | 0.23 | 26.41 | 209 | 24,010 | 0.11 |
| 14H-5 | 129.00 | 420 | 0.09 | 0.22 | 27.10 | 129 | 15,940 | 0.17 |
| 15H-1 | 132.50 | 407 | 0.06 | 0.18 | 30.29 | 200 | 33,660 | 0.09 |
| 15H-3 | 135.50 | 412 | 0.08 | 0.29 | 30.93 | 181 | 19,330 | 0.16 |
| 15H-5 | 138.50 | 409 | 0.05 | 0.26 | 13.85 | 200 | 10,650 | 0.13 |
| 16H-1 | 142.00 | 407 | 0.14 | 0.22 | 15.68 | 183 | 13,070 | 0.12 |
| 16H-3 | 145.00 | 412 | 0.08 | 0.15 | 19.55 | 128 | 17,137 | 0.12 |
| 16H-5 | 148.00 | 408 | 0.13 | 0.13 | 13.32 | 144 | 14,800 | 0.09 |
| 17H-1 | 151.50 | 412 | 0.05 | 0.17 | 13.48 | 170 | 13,480 | 0.10 |
| 17H-3 | 154.50 | 422 | 0.05 | 0.27 | 12.20 | 207 | 9,384 | 0.13 |
| 17H-5 | 157.50 | 410 | 0.04 | 0.14 | 11.04 | 200 | 15,770 | 0.07 |
| 18H-1 | 161.00 | 412 | 0.05 | 0.17 | 12.91 | 242 | 18,440 | 0.07 |
| 18H-3 | 164.00 | 406 | 0.04 | 0.14 | 5.03 | 175 | 6,287 | 0.08 |
| 18H-5 | 167.00 | 410 | 0.05 | 0.11 | 3.33 | 220 | 6,660 | 0.05 |
| 19H-1 | 170.50 | 407 | 0.06 | 0.15 | 10.38 | 214 | 14,830 | 0.07 |
| 19H-3 | 173.50 | 411 | 0.06 | 0.19 | 4.05 | 211 | 4,500 | 0.09 |
| 19H-5 | 176.50 | 413 | 0.04 | 0.19 | 3.65 | 211 | 4,055 | 0.09 |
| 20H-1 | 180.00 | 412 | 0.06 | 0.23 | 12.77 | 230 | 12,770 | 0.10 |
| 20H-3 | 183.00 | 409 | 0.08 | 0.14 | 3.26 | 175 | 4,075 | 0.08 |
| 20H-5 | 186.00 | 407 | 0.03 | 0.21 | 6.73 | 190 | 6,118 | 0.11 |
| 21H-1 | 189.50 | 409 | 0.06 | 0.25 | 23.30 | 208 | 19,420 | 0.12 |
| 21H-3 | 192.50 | 413 | 0.08 | 0.34 | 6.35 | 231 | 4,442 | 0.15 |
| 21H-5 | 195.50 | 408 | 0.09 | 0.30 | 4.78 | 196 | 6,386 | 0.15 |
| 22H-1 | 199.00 | 410 | 0.06 | 0.15 | 9.95 | 214 | 14,210 | 0.07 |
| 22H-3 | 202.00 | 413 | 0.05 | 0.20 | 3.69 | 222 | 4,100 | 0.09 |
| 22H-5 | 205.00 | 421 | 0.04 | 0.16 | 2.60 | 200 | 3,250 | 0.08 |
| 23H-1 | 208.50 | 415 | 0.28 | 0.28 | 4.35 | 186 | 2,900 | 0.15 |
| 24X-1 | 218.10 | 404 | 0.08 | 0.15 | 12.36 | 166 | 13,730 | 0.09 |
| 24X-3 | 221.10 | 407 | 0.07 | 0.18 | 7.25 | 163 | 6,590 | 0.11 |
| 24X-5 | 224.20 | 417 | 0.13 | 0.41 | 8.63 | 216 | 4,650 | 0.19 |
| 25X-1 | 227.70 | 405 | 0.08 | 0.13 | 4.84 | 216 | 8,066 | 0.06 |
| 25X-3 | 230.70 | 415 | 0.07 | 0.22 | 7.98 | 220 | 7,980 | 0.10 |
| 25X-5 | 233.80 | 404 | 0.10 | 0.11 | 5.33 | 275 | 15,120 | 0.05 |
| 26X-1 | 237.30 | 393 | 0.07 | 0.08 | 6.05 | 160 | 12,100 | 0.05 |
| 26X-3 | 240.30 | 391 | 0.09 | 0.10 | 6.82 | 200 | 13,640 | 0.05 |
| 27X-1 | 246.90 | 406 | 0.09 | 0.09 | 13.82 | 225 | 34,550 | 0.04 |
| 27X-3 | 249.90 | 392 | 0.07 | 0.07 | 6.94 | 316 | 32,930 | 0.02 |
| 27X-5 | 252.90 | 412 | 0.04 | 0.15 | 4.78 | 214 | 6,828 | 0.07 |
| 28X-1 | 256.50 | 385 | 0.18 | 0.07 | 4.44 | 175 | 11,100 | 0.04 |
| 28X-3 | 259.50 | 395 | 0.17 | 0.08 | 1.73 | 200 | 4,325 | 0.04 |
| 28X-5 | 262.60 | 413 | 0.03 | 0.09 | 2.50 | 180 | 5,000 | 0.05 |
| 29X-1 | 266.10 | 406 | 0.10 | 0.12 | 4.78 | 171 | 6,828 | 0.07 |
| 29X-3 | 269.10 | 408 | 0.09 | 0.14 | 2.12 | 175 | 2,650 | 0.08 |
| 29X-5 | 272.20 | 410 | 0.07 | 0.17 | 3.35 | 170 | 3,350 | 0.10 |
| 30X-1 | 275.80 | 401 | 0.11 | 0.20 | 8.21 | 129 | 5,321 | 0.16 |
| 30X-3 | 278.70 | 399 | 0.03 | 0.05 | 0.43 | 167 | 1,416 | 0.03 |
| 31X-1 | 285.30 | 415 | 0.08 | 0.18 | 3.19 | 200 | 3,544 | 0.09 |
| 32X-2 | 296.30 | 418 | 0.13 | 0.17 | 3.26 | 242 | 4,657 | 0.07 |
| 33X-1 | 304.60 | 408 | 0.07 | 0.15 | 3.05 | 250 | 5,083 | 0.06 |
| 33X-3 | 307.60 | 399 | 0.24 | 0.34 | 7.85 | 146 | 3,570 | 0.23 |
| 34X-1 | 314.20 | 402 | 0.08 | 0.13 | 0.73 | 185 | 1,042 | 0.07 |
| 34X-3 | 317.10 | 403 | 0.09 | 0.12 | 2.22 | 200 | 3,700 | 0.06 |
| 34X-5 | 320.10 | 411 | 0.14 | 0.16 | 0.28 | 228 | 400 | 0.07 |
| 35X-1 | 323.80 | 413 | 0.11 | 0.18 | 2.58 | 225 | 3,225 | 0.08 |
| 35X-3 | 326.70 | 398 | 0.09 | 0.07 | 0.00 | 175 | 0 | 0.04 |
| 35X-5 | 329.70 | 403 | 0.13 | 0.24 | 6.78 | 126 | 3,568 | 0.19 |
| 36X-1 | 333.30 | 402 | 0.11 | 0.28 | 13.16 | 87 | 4,802 | 0.33 |
| 36X-3 | 336.40 | 412 | 0.08 | 0.20 | 3.85 | 164 | 4,150 | 0.09 |
| 37X-1 | 342.90 | 411 | 0.10 | 0.36 | 8.51 | 157 | 3,812 | 0.23 |
| 37X-3 | 345.90 | 403 | 0.07 | 0.32 | 9.06 | 228 | 6,471 | 0.14 |
| 37X-5 | 348.90 | 416 | 0.03 | 0.14 | 1.54 | 192 | 2,200 | 0.07 |
| 38X-1 | 352.50 | 416 | 0.09 | 0.41 | 6.55 | 176 | 2,754 | 0.24 |
| 39X-1 | 362.20 | 422 | 0.08 | 0.25 | 4.40 | 232 | 3,938 | 0.11 |
| 39X-3 | 365.30 | 411 | 0.12 | 0.29 | 7.06 | 161 | 3,922 | 0.18 |
| 40X-1 | 371.90 | 417 | 0.04 | 0.35 | 2.55 | 194 | 1,416 | 0.18 |
| 40X-3 | 374.90 | 405 | 0.24 | 0.45 | 29.75 | 81 | 5,441 | 0.55 |
| 41X-1 | 381.50 | 413 | 0.02 | 0.27 | 9.55 | 108 | 3,820 | 0.25 |
| 42X-1 | 391.20 | 406 | 0.17 | 0.17 | 5.45 | 106 | 3,406 | 0.16 |
| 42X-3 | 394.00 | 410 | 0.04 | 0.24 | 15.87 | 114 | 7,557 | 0.21 |
| 43X-1 | 400.90 | 410 | 0.03 | 0.17 | 9.21 | 60 | 3,289 | 0.28 |
| 44X-1 | 410.50 | 410 | 0.02 | 0.14 | 2.74 | 82 | 1,611 | 0.17 |
| 44X-3 | 413.40 | 417 | 0.09 | 0.24 | 11.89 | 126 | 6,257 | 0.19 |
| 44X-5 | 416.40 | 410 | 0.02 | 0.07 | 2.67 | 153 | 5,342 | 0.05 |
| 45X-1 | 420.10 | 412 | 0.07 | 0.17 | 5.66 | 130 | 4,353 | 0.13 |
| 45X-3 | 423.10 | 403 | 0.04 | 0.10 | 7.25 | 111 | 8,055 | 0.09 |
| 45X-5 | 426.10 | 404 | 0.12 | 0.20 | 11.88 | 105 | 6,252 | 0.19 |
| 46X-1 | 429.70 | 415 | 0.06 | 0.27 | 10.70 | 129 | 5,285 | 0.21 |
| 46X-3 | 432.40 | 413 | 0.11 | 0.33 | 12.14 | 126 | 4,669 | 0.26 |
| 46X-5 | 435.40 | 413 | 0.06 | 0.21 | 10.73 | 116 | 5,961 | 0.18 |
| 47X-1 | 439.40 | 413 | 0.04 | 0.21 | 15.02 | 91 | 6,530 | 0.23 |
| 47X-3 | 442.40 | 411 | 0.05 | 0.34 | 15.84 | 117 | 5,462 | 0.29 |
| 47X-5 | 445.20 | 406 | 0.06 | 0.29 | 14.63 | 82 | 4,180 | 0.35 |
| 48X-1 | 449.00 | 408 | 0.23 | 0.27 | 9.42 | 108 | 3,768 | 0.25 |
| 48X-3 | 452.00 | 409 | 0.03 | 0.16 | 3.95 | 123 | 3,038 | 0.13 |
| 48X-5 | 455.00 | 419 | 0.08 | 0.47 | 8.26 | 235 | 4,130 | 0.20 |
| 49X-1 | 458.60 | 409 | 0.08 | 0.19 | 13.33 | 190 | 13,330 | 0.10 |
| 49X-3 | 461.60 | 409 | 0.06 | 0.19 | 8.53 | 211 | 9,477 | 0.09 |
| 50X-1 | 468.30 | 414 | 0.05 | 0.20 | 5.92 | 181 | 5,381 | 0.11 |
| 51X-1 | 477.90 | 377 | 0.09 | 0.05 | 8.50 | 175 | 27,550 | 0.04 |
| 52X-1 | 487.50 | 382 | 0.11 | 0.10 | 8.71 | 145 | 13,415 | 0.07 |
| 54X-1 | 506.80 | 407 | 0.07 | 0.09 | 11.05 | 100 | 12,280 | 0.09 |
| 54X-3 | 509.80 | 398 | 0.12 | 0.15 | 10.96 | 88 | 6,447 | 0.17 |
| 55X-1 | 516.30 | 412 | 0.04 | 0.14 | 7.58 | 233 | 12,630 | 0.06 |

Notes: $T_{max}$ = temperature of maximum hydrocarbon generation during pyrolysis in °C, $S_1$ = milligrams of free hydrocarbons per gram of rock, $S_2$ = milligrams of pyrolyzed hydrocarbons per gram of rock, $S_3$ = milligrams of carbon dioxide per gram of rock, HI = hydrogen index in milligrams of hydrocarbon per gram of TOC, OI = milligrams of carbon dioxide per gram of TOC, TOC = total organic carbon. — = not available.

**Table T14.** Summary of logging operations, Hole 1195B.

| Date (Jan. 2001) | Time (local) | Comments |
|---|---|---|
| 29 | 0305 | Hole preparation complete; rig up wireline. |
| | 0450 | RIH with MGT-HNGS-APS-HLDS-DITE (+TAP). |
| | 0525 | Tools cannot pass bottom of pipe. Pull tools back in pipe; start pumping water through pipe. |
| | 0625 | Tools reach bottom of hole. |
| | 0630 | Uplog with triple combo at 900 ft/hr from 518.5 mbsf to seafloor. |
| | 1030 | Rig up WST. |
| | 1130 | Tool cannot pass bottom of pipe. Tool pulled back on deck; start wiper trip. |
| | 1600 | RIH with WST. |
| | 1640 | Tight spot prevents the tool from going deeper than 121 mbsf. Start check shots. |
| | 1735 | Pull out of hole and rig down. |
| | 1740 | End of logging operations. |

Notes: RIH = run in hole, MGT = multisensor gamma ray tool, HNGS = hostile environment natural gamma ray sonde, APS = accelerator porosity sonde, HLDS = high-temperature lithodensity sonde, DITE = dual induction tool, TAP = high-temperature/acceleration/pressure tool, WST = well seismic tool. Drillers total depth = 520.44 mbsf, water depth = 430.8 mbrf, end of pipe = 98.7 mbsf.

**Table T15.** Time-depth correlation from check shot survey, Hole 1195B.

| Check shot station | Depth (mbsl) | TWT below sea level (ms) | Depth (mbsf) | TWT below seafloor (ms) |
|---|---|---|---|---|
| 1 | 504.6 | 655.12 | 75.6 | 100.12 |
| 2 | 513.7 | 665.54 | 84.7 | 110.54 |
| 3 | 536.9 | 693.13 | 107.9 | 138.13 |

Note: TWT = two-way traveltime.